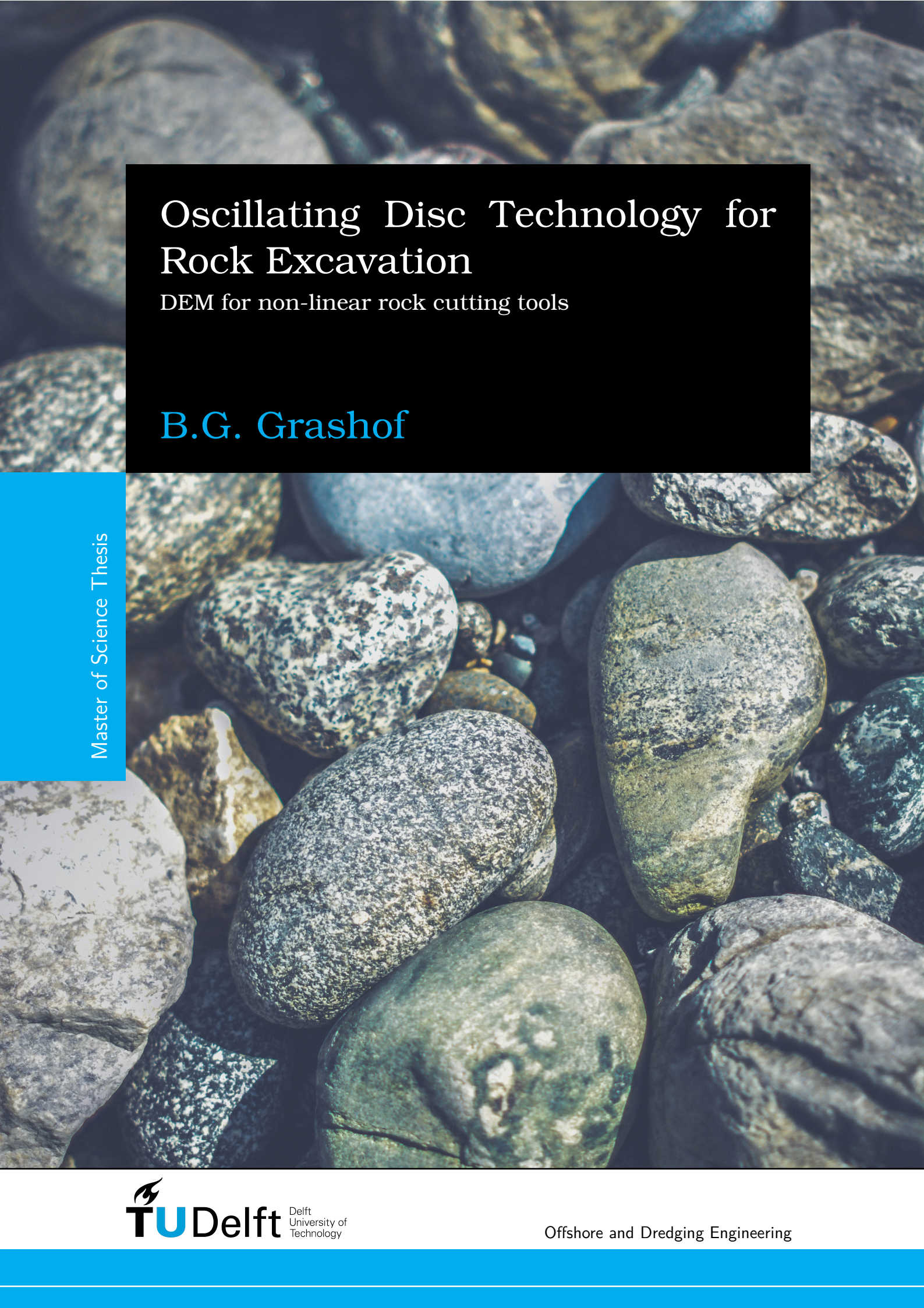

Oscillating Disc Technology for Rock Excavation

DEM for non-linear rock cutting tools

B.G. Grashof

Master of Science Thesis

TU Delft Delft University of Technology

Offshore and Dredging Engineering

Oscillating disc technology for rock excavation

by

B.G. Grashof

to obtain the degree of Master of Science
at the Delft University of Technology,
to be defended publicly on Monday 13 May, 2019.

Thesis committee:	Dr. ir. R.L.J. Helmons,	TU Delft, supervisor
	Dr. ir. S.A. Miedema,	TU Delft
	Dr. ir. M. Alvarez Grima,	Royal IHC
	Ir. C.F. Hofstra,	Royal IHC
	Dr. ir. D.L. Schott	TU Delft

An electronic version of this thesis is available at `http://repository.tudelft.nl/`.

Abstract

Rock cutting is a challenging process. Heavy equipment, large cutting forces, high wear rates and large amounts of required energy are common challenges when cutting rock. Traditionally, rock cutting is based on a linear motion of the cutting tool. However, a significant improvement on the cutting performance is expected when using non-linear cutting techniques. Non-linear cutting can be achieved by using an actuator to create a vibrating or oscillating motion on top of the linear forward motion of the cutting tool. The focus in this paper is on the oscillating undercutting disc cutter. This disc attacks the rock like a chisel or pickpoint, aiming at a cutting process dominated by tensile failures.

Although the discrete element method has been successfully used for various rock cutting processes, all these processes are based on linear rock cutting tools and most of these researches are based on 2D simulations. The use of a 3D approach is necessary to enable the simulation of oscillatory rock cutting tools.

This paper utilizes discrete element method in 3D to investigate non-linear cutting processes, especially the effects of the design parameters such as frequency, velocity and eccentricity of the cutting tool. To resemble rock-like materials the particles are placed in a dense particle assembly and they are bonded together through perfect brittle elastic bonds. The bonds can fail in shear and in tension, allowing the dominant failure mechanisms, i.e. shear and tensile cracks, to occur. After failure of these bonds, particles can still interact through collisions.

The simulation results show the effect of the tested design parameters and are compared with analytical models and actual experiments of oscillating undercutting discs.

B.G. Grashof
Delft, 01-04-2019

Contents

Nomenclature

Acronyms

ADC	Actuated disc cutter
API	Application programming interface
BEM	Boundary element method
BTS	Brazilian tensile strength
FEM	Finite element method
ODC	Oscillating disc cutter
SIF	Stress intensity factor
UCS	Uniaxial compressive strength
XFEM	Extended finite element method

Greek Symbols

α	half wedge angle	deg
α_r	Rake/blade angle	deg
β	Shear angle	deg
δ	External friction angle	deg
ϵ	Entering angle	deg
μ	Rolling friction coefficient	–
ν	Dimensionless ratio speed oscillation	–
ω	Oscillation speed	$\mathrm{rad} \cdot \mathrm{s}^{-1}$
ϕ	Internal friction angle	deg
ϕ_d	Tip angle V-type disc cutter	deg
ρ	Density	$\mathrm{kg} \cdot \mathrm{m}^{-3}$
σ_c	Compressive strength	Pa
σ_n	Normal overlap	m
σ_t	Tensile strength	Pa
τ	Shear strength of bond	Pa
τ_r	Rolling friction torque	$\mathrm{N} \cdot \mathrm{m}^{1}$
$\tilde{\theta}$	Rotation angle disc cutter	deg
φ_L	Contact angle L	deg
φ_R	Contact angle R	deg

Roman Symbols

A	Beam cross section area	m^2
a	Disk radius	m
A_b	Bond cross section area	m^2
c	Damping coefficient(contact model)	–
D	Disc diameter	m
d	Cutting depth	m
E	Young's modulus	Pa
e	Eccentricity	m
E_{sp}	Specific energy	Pa
f	Natural frequency	Hz
h_i	Cutting depth	m
I	Moment of inertia	$\mathrm{kg} \cdot \mathrm{m}^2$
I_i	Particle moment of inertia	$\mathrm{kg} \cdot \mathrm{m}^2$
k	Bond stiffness	$\mathrm{N} \cdot \mathrm{m}^{-1}$
K_{ic}	Mode 1 fracture toughness	$\mathrm{Pa}/\sqrt{\mathrm{m}}$
l	Beam length	m
l_b	Bond length	m
m_i	Particle mass	kg
p	Penetration depth	m
Q	Rock volume removed	m^3
r	Radius of beam	m
r_b	Radius of bond	m
S_s	Shear strength	Pa
T	Torsion	$\mathrm{N} \cdot \mathrm{m}$
t	Assembly cylinder length	m
V	Cutting disc velocity	$\mathrm{m} \cdot \mathrm{s}^{-1}$
v	Poisson's ratio	–
V_i	Particle velocity	$\mathrm{m} \cdot \mathrm{s}^{-1}$
w	Tool width	m

1 Introduction

1.1. Background

The cutting of rock is neccesary, since it is required for many projects, as in for example: construction and maintenance of ports, tunneling, land reclamation, riverbank protection and dredging trenches for pipelines. Nowadays the cutting of (hard) rock is an expensive business due to high wear rates, heavy cutting equipment and the large amount of energy needed to cut rock. Especially for harder rock types these problems are challenging. The forces needed to cut through hard rocks types (UCS 50>MPa) are significantly high, when dredging. Due to this high cutting force and abrasiveness of hard rocks, the wear rate of the cutting tool will increase (figure 1.1). IHC-MTI, which is specialized in dredging and mining equipment, is investigating possible solutions to overcome this challenge. One solution is to improve the material of the cutter to be more wear resistant. This basically means using a tougher material to lower abrasive wear of the cutting tool. The problem is that harder materials tend to be less ductile and can more easily break during cutting. Another solution is to lower cutting forces, which will lower the frictional wear. It is however important to also take the velocity and cutting depth of the cutter into account, since wear rate is influenced by both [1]. Wear can also be reduced by creating a larger cutting tool, since larger cutting tools can withstand larger forces. However, this might not be the most efficient solution.

Figure 1.1: Wear on dredge cutter [2]

The cutting of rock is explained by the chip formation process. A phenomenological model is developed by van Kesteren [3], which explains this process. Van Kesteren describes the failure of rock, by a tensile crack that is created by bifurcation of the shear crack. This shear crack is formed by the crushed zone, that is created when the tool crushes the rock, see figure 1.2.

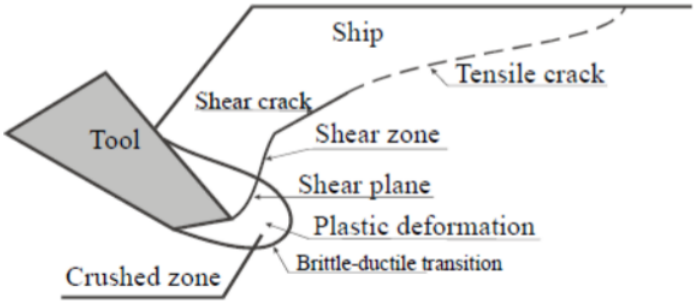

Figure 1.2: Phenomenological model of Verhoef [4]

Reduction of wear rates and improvements to safety and economics might be achieved by developing alternative cutting tools. For rock cutting, different tools exist. The main difference between these tools are their shape and direction of cutting force. Commonly used tools for rock cutting are teeth, pick points, drag tools and indenters.

Teeth, pick points and drag tools

Teeth (figure 1.3) can be used for weaker rock types. The shape of the teeth is like a trapezoidal and is made from steel [4]. Besides teeth there are also pick points (figure 1.4). These are used to cut stronger rock types as they create strong local impacts, which induce tensile cracks. These tensile cracks grow larger, until pieces of rock are removed. Pick points are due to the high forces and low contact area quite susceptible to wear. The wear that occurs on the picks and teeth creates a so called wear flat. This wear flat exists when, due to friction, the cutting tool becomes blunt. Instead of a sharp edge or point the tool will now attack the rock with a flat area (wear flat). To keep the cutting tool deep enough in the rock a force is needed to push the tool down into the rock. This is important, cause if the drag tool is no longer able to penetrate the rock, it will be unable to create tensile fractures. The increase of the normal force (perpendicular of the cutting direction), will increase the specific energy of the cutting process. The material that pick points are made from is mostly steel [1]. For pick points the material hardness is crucial as it affects the wear rate. Materials with higher hardness will be more wear resistant. It should however be noted that in some cases harder materials like tungsten carbide, tend to show more wear than steel, e.g. this occurrs with tungsten carbide, while cutting rocks that contain minerals harder than tungsten carbide. Due to different failure mechanisms of tungsten carbide (fails by micro cracking), abrasive wear increases and the wear rate becomes higher than that of steel, which fails by micro ploughing and micro cutting [1]. Besides abrasiveness, the temperature of the cutting tool is affected by the material to be cut. The size of the crushed zone that appears around the chisel affects the temperature of the cutting tool. Higher temperatures can cause thermal softening of the wear flat, which increases wear rates [4].

Figure 1.3: Cutting teeth (IHC)

Figure 1.4: Pick points (ESCO) [5]

Still, the use of hard materials like tungsten carbide is not possible for pick points, since they tend to become more brittle. As brittle materials are weak against high impact stresses created by the pick point, the pick might break easily. Tungsten carbide has also been used as an insert onto a steel support. The problem however, is that the steel holding the tungsten carbide insert, wears away faster than tungsten carbide. As a result the steel will not be able to hold the tungsten carbide insert in place.

Drag bits are mainly used in petroleum well drilling. A drag cutting tool cuts the rock, while it is positioned with a negative rake angle. An example of a drag tool is a drag bit, see figure 1.5. The drag bit is beneficial for rock with smooth surfaces, since it does not require a surface to grasp underneath. Drag bits are quite susceptible to failure, due to bending stresses in the bit. In practice the use of drag bits are for high strength (UCS <200MPa) and non-abrasive rocks. Abrasive rocks are rocks that contain abrasive (hard) minerals. These hard minerals can increase wear on the cutting tool, since the minerals can be harder than steel [6].

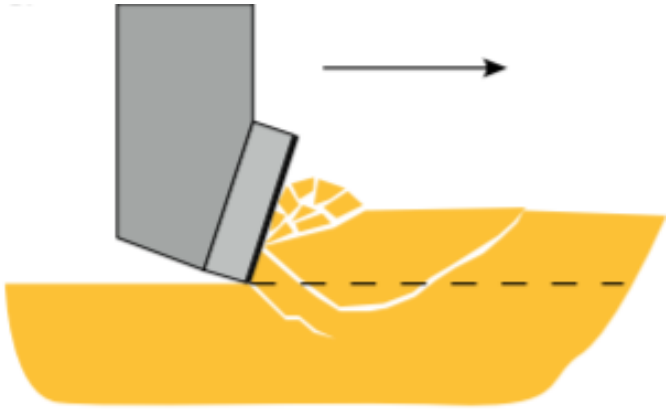

Figure 1.5: Drag bit [7]

Indenters

An indenter applies compressive force into the rock, due to the parallel movement of the indenter over the rock's surface. This compressive force creates a crushed zone underneath the indenter. Due to the widening of the crushed zone, tensile cracks occur. These cracks grow larger until rock chips are formed. These chips are of similar size to the width of the indenter. The use of indenters requires a signifant amount of energy. Most of this energy is used to crush the rock [8]. Indenters are primarily used in tunneling. The indenter can cut through high strength rock (UCS 80>MPa), and therefore requires a significant force to push the indenter down into the rock. To push the tool into the rock, it requires a strong support. In tunneling the drilling machine can clamp itself onto the tunnel and push itself forward, making it possible to use the indenter to cut high strength (UCS <200MPa) rocks.

Since most cutting tools are made of brittle materials, they are weak when loaded in tension. Since, indenters are dominantly loaded in compression (in contrast to drag tools), they are more resistant to brittle failure. Therefore, tougher materials can be selected for the indenter, which reduces the wear rate in most cases. Another factor that decreases the wear of indenters, is the rotating area of the disc, which can cool off and therefore reduce heat load. Lower heat means the material is harder, since hardness is influenced by temperature. Higher temperatures yield lower material hardness [6].

There are different types of indenters. They mostly differ by cutting edge, which can be sharp (V-type disc cutter figure 1.6) or rounded (figure 1.7). The different shapes are governed by the material that is to be cut. There are also indenters which, instead of a equipped edge, are cutting with buttons. The buttons consist of hardened materials, e.g. tungsten carbide. They create local failure due to the high local stresses. The button cutters are mainly used for high strength rock (80>MPa) cutting and create mainly fines.

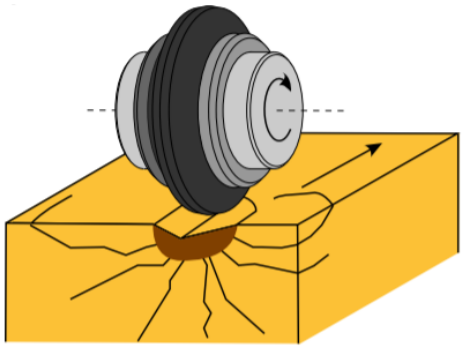

Figure 1.6: V-type disc cutter [7]

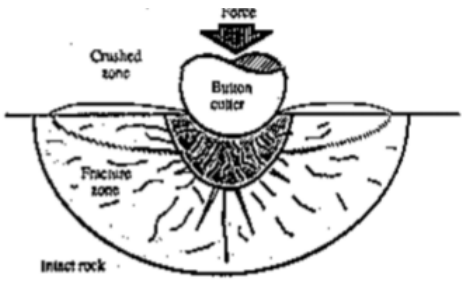

Figure 1.7: Button cutter [6]

Oscillating cutting

Besides linear cutting tools, there are also tools that cut non-linear by oscillating the cutting tool. One promising non-linear cutting tool is the oscillating disc cutter. This type of cutting tool basically is quite similar to a chisel. The only difference is that the edges of the chisel are rounded, so that it looks like a disc. Recent models and experiments suggest, that lower cutting forces can be achieved in case the disc is oscillated by means of an actuator or kinematics [8]. These lower cutting forces only occur for an actuator that creates an eccentric oscillatory movement. This eccentric movement affects the contact area between the cutting tool and the rock. In figure 1.8 this eccentric oscillated movement is shown. The disc moves around an eccentricity. By adding a forward movement to the center of the disc, its center moves over a path that looks like a helix.

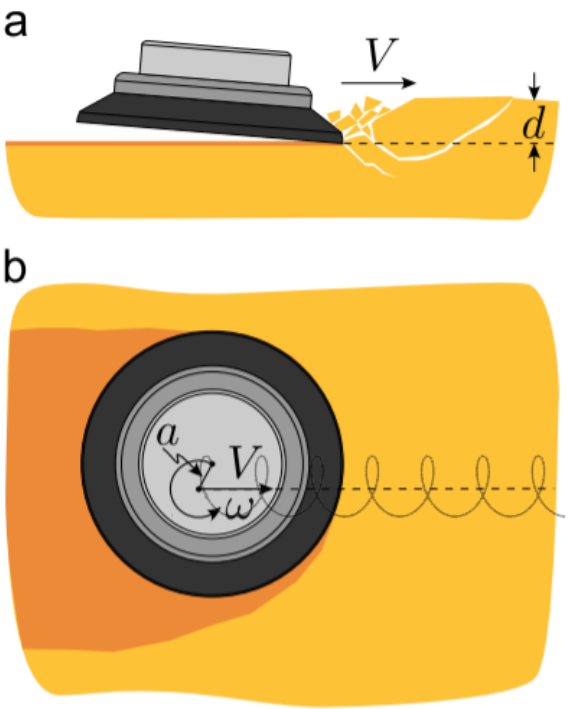

Figure 1.8: Oscillated disc cutter, with forward speed V, eccentricity a and oscillation speed ω [7]

1.2. Research purpose

The purpose of this research is providing a better understanding of the oscillating disc cutter. In literature information is found on the kinematics of the ODC, however this information is mostly limited to the oscillation speed of the disc. Therefore, results of cutting forces on the oscillating disc cutter, by adjusting oscillation frequency, disc forward velocity, clearance angle and eccentricity, will be studied to provide more knowledge about the working principle of an oscillating disc cutter. The corresponding research questions are as following:

- What are the effects of the kinematic parameters of an oscillatory disc cutter on the cutting forces?
- How can eccentric oscillations help to improve the cutting equipment?

The oscillating disc cutter is investigated using a mathematical model. This is chosen since, the experimental testing of an ODC is complex and expensive. The mathematical model is built using discrete element modelling (DEM). In literature no research is found, whether DEM can describe oscillatory cutting. Therefore, another goal is to investigate the possibilities for the use of DEM to simulate an oscillatory disc cutter. In the end the forces of the ODC simulations are compared to values found in literature. In short the research goals are:

- Is DEM suitable to simulate oscillatory cutting methods on rock?
- Do the forces found in oscillating disc cutter simulations agree with those from literature?

1.3. Approach

The research starts with a literature review in chapter 2, on linear and non-linear cutting. The state of the art on linear rock cutting models and oscillating disc cutters (non-linear) is discussed in this chapter. In chapter 3 the mathematical model chosen to simulate the oscillating disc cutter is discussed. Furthermore, the implementation and requirements for this mathematical model to simulate the oscillating disc cutter is studied. At the end of chapter 3 the performance of the model is tested, in order to prove that it works and calculates the correct results. In chapter 4 the micro-macro properties are validated. The model is calibrated in order to create a material, which represents a rock with chosen UCS and BTS values. After material calibration, the oscillating disc cutter simulations will be performed in chapter 5. The chapter will start with a list of simulations and parameters, which are chosen based on the research goals and available computation time. Afterwards, in the same chapter, the results are given, which will be compared to findings in literature. At last in chapter 6, the conclusions and recommendation are given.

2

Rock cutting theory

In this chapter different rock cutting tools are described. The first part of this chapter explains theories for linear rock cutting. In the second half non-linear rock cutting for the oscillating disc cutter is explained. The chapter ends, with a discussion in which the difference between linear and non-linear rock cutting model is discussed. Furthermore, the theories for ODC's are compared in this discussion.

2.1. Linear rock cutting theory

2.1.1. Introduction linear rock cutting models

Van Kesteren [3] states, that rock failure is to be described by a phenomenological model. One reason for a phenomenological model is that the theoretical models of Nishimatsu, Evans and Miedema all assume homogeneous materials. In practice however, rocks are a product of nature that consist of chemical bonds and therefore are inhomogeneous and anisotropic. Failure will differ by rock specimen and influence cutting forces. Van Kesteren [3] describes the failure of rock by a tensile crack that is created by bifurcation of the shear crack. This shear crack is formed by the crushed zone that is created when the tool crushes the rock. See figure 2.1.

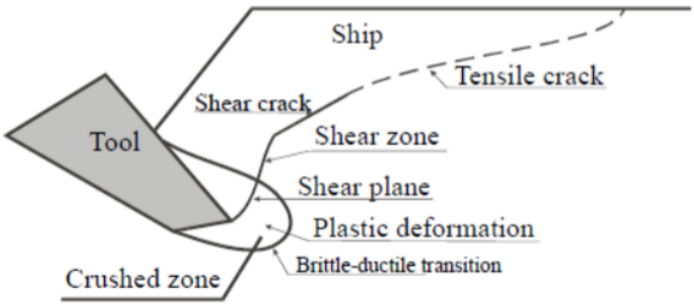

Figure 2.1: Rock failure mode by Verhoef [4].

To quantify cutting forces and get more knowledge about the parameters effecting these forces analytical models are required. There are many different models describing the failure of rock. In this chapter the following models are described:

- Tensile failure model by Evans [9]
- Brittle shear failure by Nishimatsu [10]
- Combined tensile and shear failure by Miedema [11]

These models describe different failure mechanism. The last model from Miedema combines both failure mechanism. All models explained in this section make use of a chisel.

2.1.2. Evans coal cutting theory

Tensile failure for brittle rock/coal is described by the theory of Evans [9]. With the tensile strength and geometrical properties of a chisel the cutting forces can be calculated. Evans claims that instantaneously an circular tensile failure path is created due to the (small)indentation of the wedge, see figure 2.2. The model is not influenced by velocity and is two dimensional. In figure 2.2 an equilibrium be-

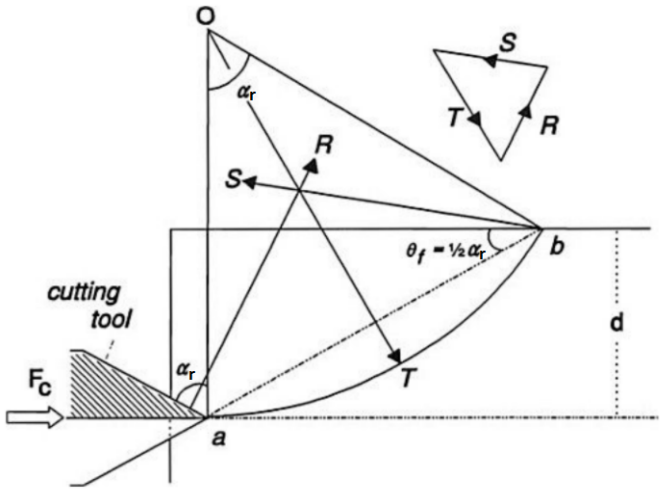

Figure 2.2: Evans tensile rock cutting theory [9].

tween forces is shown. R is the resultant force as a result of the chip pushing on the wedge. T describes the tensile forces on the curved failure plane. S is the force needed to achieve equilibrium and acts on point b(hinge). The peak cutting force is formulated as following:

$$F_{c_E vans} = \frac{2\sigma_t h_i w sin\frac{1}{2}(\frac{\pi}{2} - \alpha_r)}{1 - sin\frac{1}{2}(\frac{\pi}{2} - \alpha_r)} \tag{2.1}$$

with, tensile strength σ_t, cutting depth h_i, chisel width w and rake angle α_r. Later, the model of Evans was extended for chisels that enter the rock under an angle[11]. This model is shown in figure 2.3.

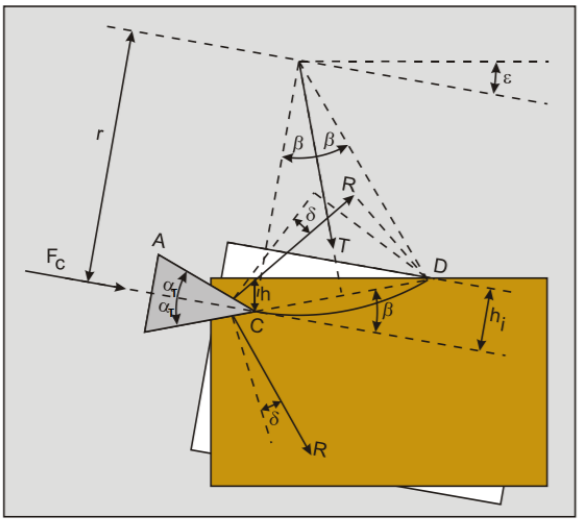

Figure 2.3: Evans extended theory for chisels that enter under an angle [11].

The horizontal and vertical forces for the chisel, which attacks the rock under an angle are as following:

$$F_{hor_Evans} = \sigma_t h_i w \frac{sin(\alpha_T + \delta)}{sin(\beta - \epsilon) * cos(\alpha_T + \beta + \delta)} * cos(\epsilon) \tag{2.2}$$

$$F_{vert_Evans} = \sigma_t h_i w \frac{sin(\alpha_T + \delta)}{sin(\beta - \epsilon) * cos(\alpha_T + \beta + \delta)} * sin(\epsilon) \tag{2.3}$$

with, shear angle β, external friction angle δ, entering angle ϵ and half tool angle α_T.

2.1.3. Nishimatsu's theory

Nishimatsu's theory states that rock fails in a brittle shear manner due to the non-plastic behavior of rock cutting. Nishimatsu assumes a stress distribution over the line AB, as is shown in figure 2.4. The brittle failure condition is given by a linear envelope of the Mohr circle [10]. Nishimatsu's model is quite similar to that of merchant, which describes a model for ductile cutting of steel.

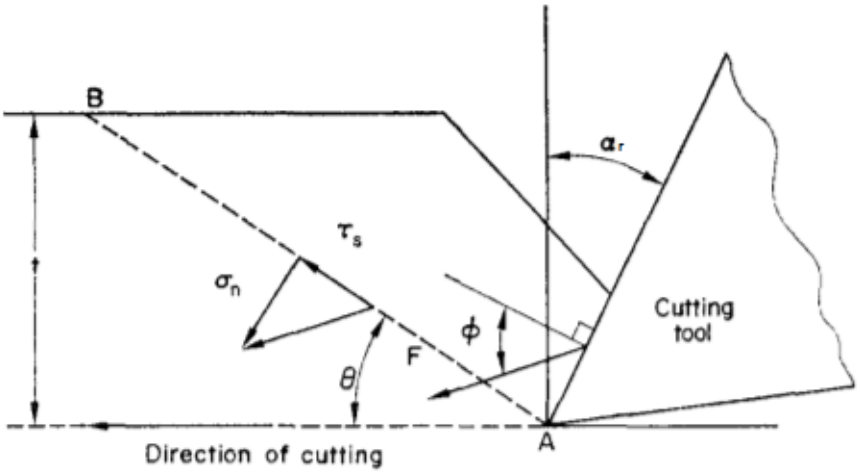

Figure 2.4: Stress distribution while cutting [10].

The resultant cutting force is described by the following equation.

$$F_{c_Nish} = \frac{1}{n+1} S_s h_i \frac{cos(\varphi)}{1 - sin(\varphi - \alpha_r + \delta)} \tag{2.4}$$

with, stress distribution factor n, shear strength of specimen rock S_s, angle of internal friction φ and external friction angle δ.

2.1.4. Miedema's rock cutting theory

Miedema created an extension of the model of Merchant. Miedema's model is based on the Mohr-Coulomb failure criterion. This extended model includes the effects of adhesion, gravity, inertia and pore pressures. The theory assumes that the cutting depth is significantly smaller than the width of the cutting tool. Furthermore, the cutting depth and velocity are kept constant and failure occurs instantaneous.

The theory of Miedema is also applicable for dredging, since pore pressure is taken into account. In normal dredging, rock failure is dominated by the internal shear strength and internal and external friction angle. Under hyperbaric conditions, the pore pressure influences failure mechanism as well (crushing vs. brittle behavior) [11].

Miedema's theory describes rock failure by two different types. The chip type and the crushed type. The chip type is more common and appears at larger cutting depths. Chipping occurs when crushing of the rock creates shear cracks. The bifurcation of this shear cracks will lead to a tensile crack that

creates a chip [3]. At smaller cutting depths, the crushed zone reaches the surface destroying the rock by shear strength(scratching), Miedema calls this the crushed type. Both types are shown in the figures below.

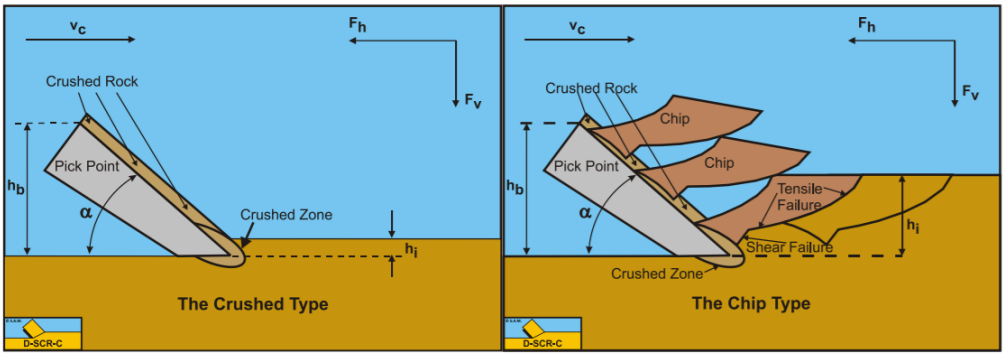

Figure 2.5: Crush type(left) and Chip failure type(right) [11].

To determine the cutting forces, first the failure mode needs to be identified according to figure 2.6.

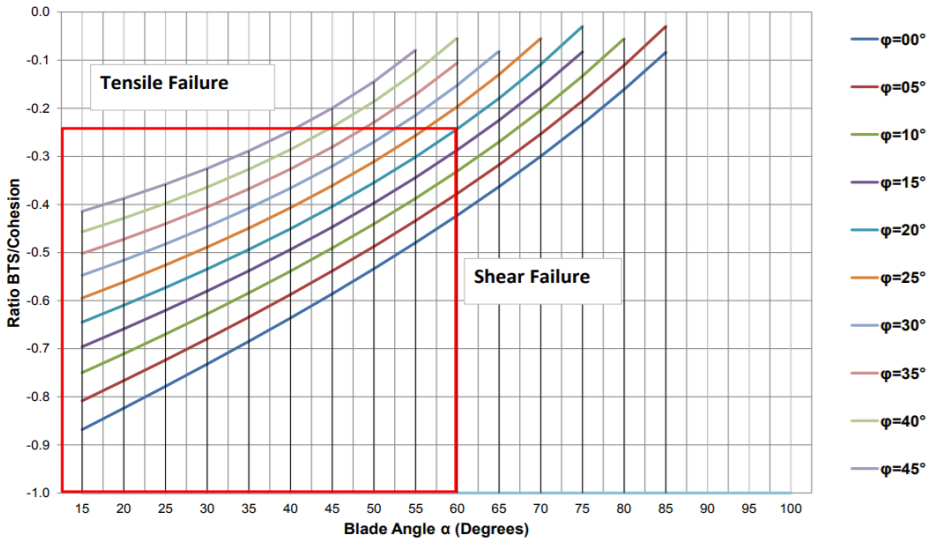

Figure 2.6: Determine tensile(tear) or shear(flow) failure [11].

After identification failure mode, the values for λ can be determined from figure 2.7 and 2.8. The cutting forces for atmospheric conditions can then be determined according to the following formula. A factor of 0.3 till 0.5 can be applied to get the average cutting forces.

Formula's chip (tear) type:

$$F_h = \frac{2c_m dwcos(\varphi)sin(\alpha+\delta)}{1+cos(\alpha+\delta+\varphi)} = \lambda_{HF} cdw \tag{2.5}$$

$$F_v = \frac{2c_m dwcos(\varphi)cos(\alpha+\delta)}{1+cos(\alpha+\delta+\varphi)} = \lambda_{VF} cdw \tag{2.6}$$

Formula's crushed (flow) type:

$$F_h = \frac{2cdwcos(\varphi)sin(\alpha+\delta)}{1+cos(\alpha+\delta+\varphi)} = \lambda_{HT}\sigma_t cdw \tag{2.7}$$

$$F_v = \frac{2cdwcos(\varphi)cos(\alpha+\delta)}{1+cos(\alpha+\delta+\varphi)} = \lambda_{VT}\sigma_t cdw \tag{2.8}$$

with, cohesion c, mobilized cohesive shear strength c_m and σ_t tensile strength.

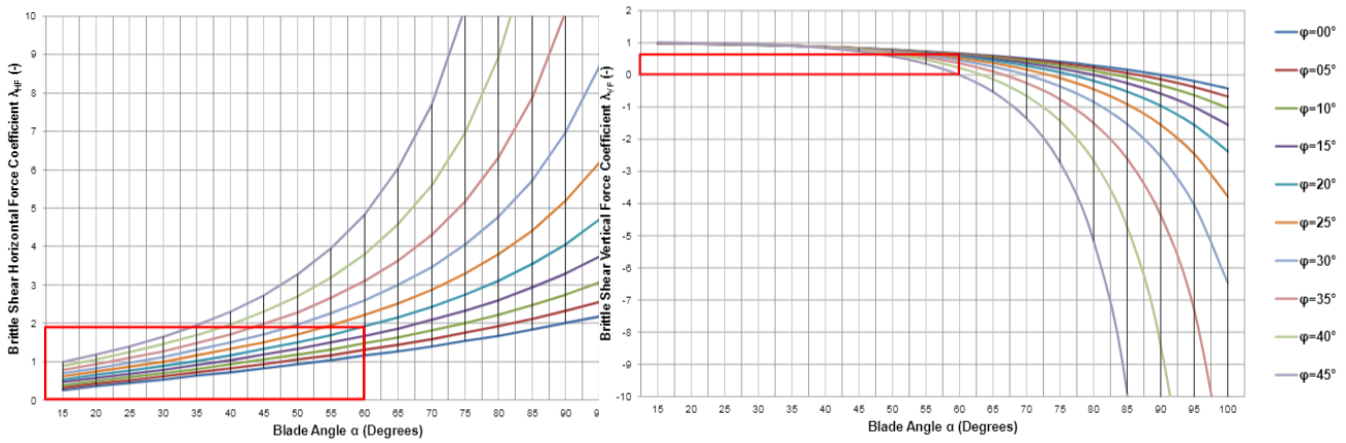

Figure 2.7: The brittle tensile horizontal and vertical force coefficient λ_{HT} and λ_{VT} respectively.

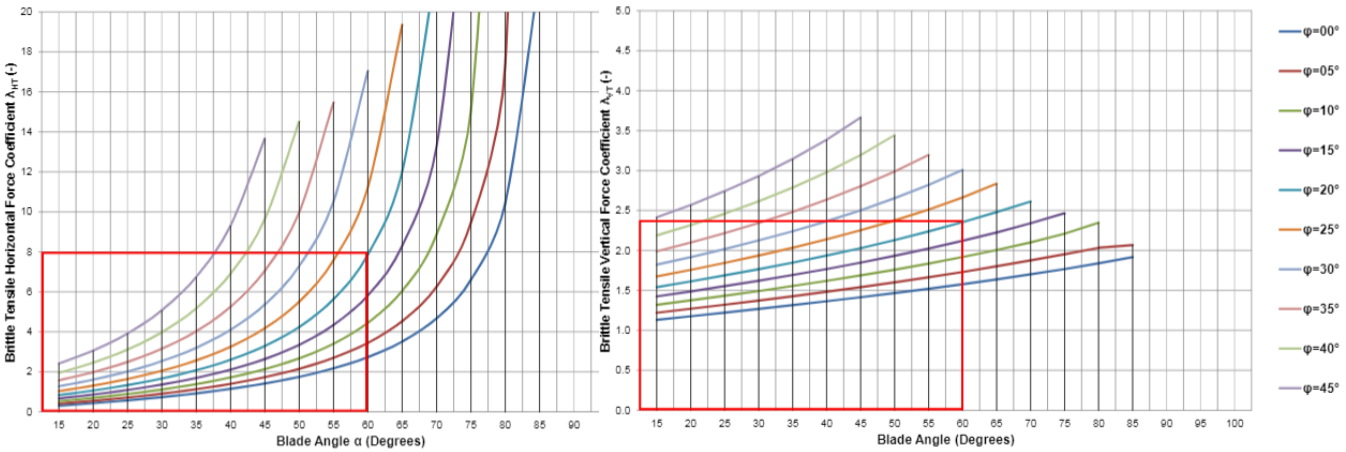

Figure 2.8: The brittle shear horizontal and vertical force coefficient λ_{HF} and λ_{VF} respectively.

The specific energy during cutting can be calculated as following:

$$E_{sp} = \frac{P_c}{Q} \tag{2.9}$$

It should be noted, that specific energy is taken as the ratio of the power and production. This notation is common for dredging.

2.2. Non-linear rock cutting

In this section literature findings on the ODC, which is a non-linear cutting are explained. The ODC is a non-linear rock cutting tool, since an oscillating eccentric rotation is applied on the cutter. The section will start with an introduction on ODC. Afterwards the kinematics of the ODC are explained. At the end of this section the mathematical models and experimental findings from literature are explained.

Introduction to oscillating disc cutters

By placing the indenting disc cutter under an angle, the cutting mechanism of the disc becomes like a chisel with rounded edges. The advantage of this method is that the cutting force and wear decreases [7]. This decrease in wear occurs due to the lower cutting forces and the larger rotating contact area, which reduces heat load. in figures 2.8 a comparison is shown between the cutting forces of the indentation disc cutter and the ODC(for similar conditions). The failure mode for undercutting disc is similar to the the-

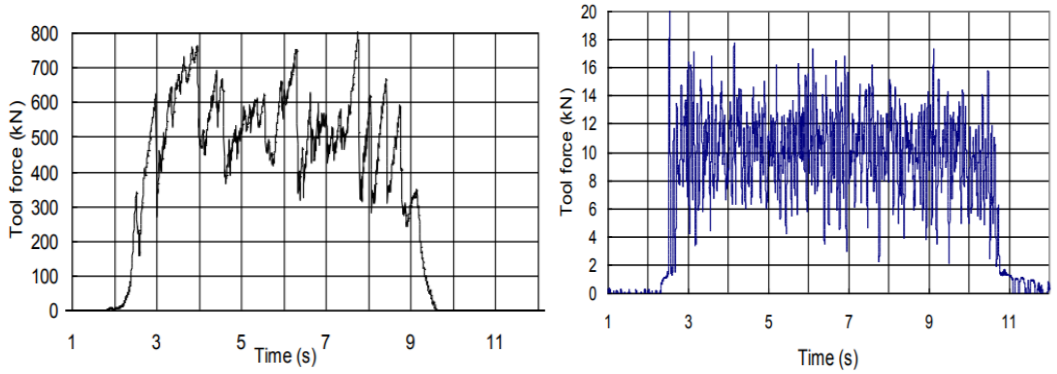

(a) Force(magnitude) in indentation disc cutter for Harcourt granite. (160MPa UCS; Steel cutter 311 mm diameter; cutting speed 100 mm/s; penetration 15 mm; groove width 35 mm) [6]

(b) Force(magnitude) in ODC for Harcourt granite (150MPa UCS; WC 50 mm diameter disc cutter; oscillating frequency 45 Hz; cutting speed 100 mm/s; eccentricity 1.4mm ;depth of cut 15 mm; groove width 55 mm) [8]

Figure 2.9: Comparison indenter force and oscillated disc cutter force in similar conditions.

ory of van Kesteren [3]. A crushed zone near the tip's contact area is created. Due to high stresses near the contact area tensile cracks occur. These cracks grow towards the rock surface creating chips of rock.

Recent models/experiments show that oscillating the disc in an eccentric motion leads to significant lower cutting forces. In figure 2.10 a comparison is shown. It can be seen that cutting forces drop significantly, due to the higher oscillation frequency. A difficulty in calculating the forces of an oscillatory disc cutter is that the kinematic behavior complicates the use of conventional models from Evans and Nitshimatsu. The eccentric motion creates fluctuating forces and velocities, which differ in direction during an actuation cycle. This behavior is not described by the conventional models. Furthermore, for calculations of the forces on an ODC one more dimension is to be taken into account, because of the eccentric rotation of the ODC.

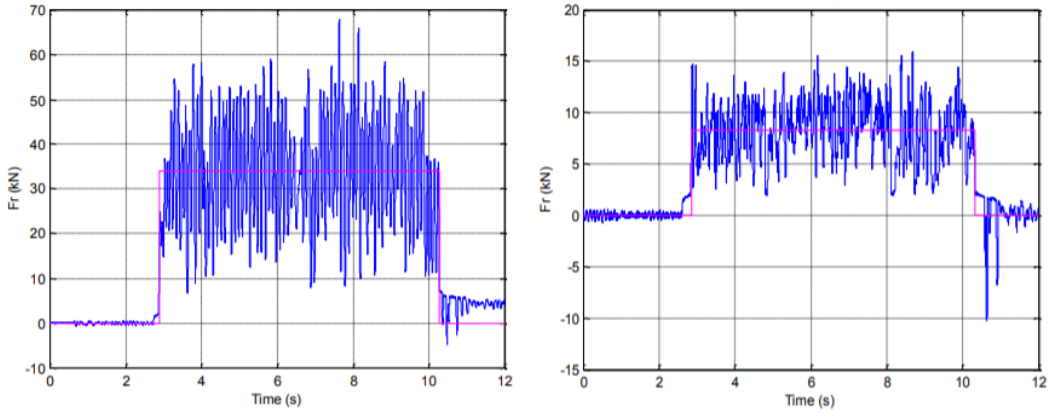

(a) Zero oscillation frequency

(b) 45 Hz oscillation frequency. in this case the groove created by the ODC is slightly wider, due to the eccentricity

Figure 2.10: marble UCS 87MPa; diameter 50mm, cutting speed 100mm/s; eccentricity 1.4mm; cutting depth 10mm [8].

Kinematics of ODC

The kinematics of the disc can be adjusted by varying eccentricity, oscillation speed and forward speed. It should be noted that two different situations can occur depending on the input parameters. The input can be varied to create a situation where the cutter loses contact with the rock. This mainly occurs when the oscillation speed multiplied by the distance of the eccentricity is higher than the forward speed of the cutter. It is found that the forces on the oscillating disc are reduced when the disc loses contact with the rock during a cycle [7].

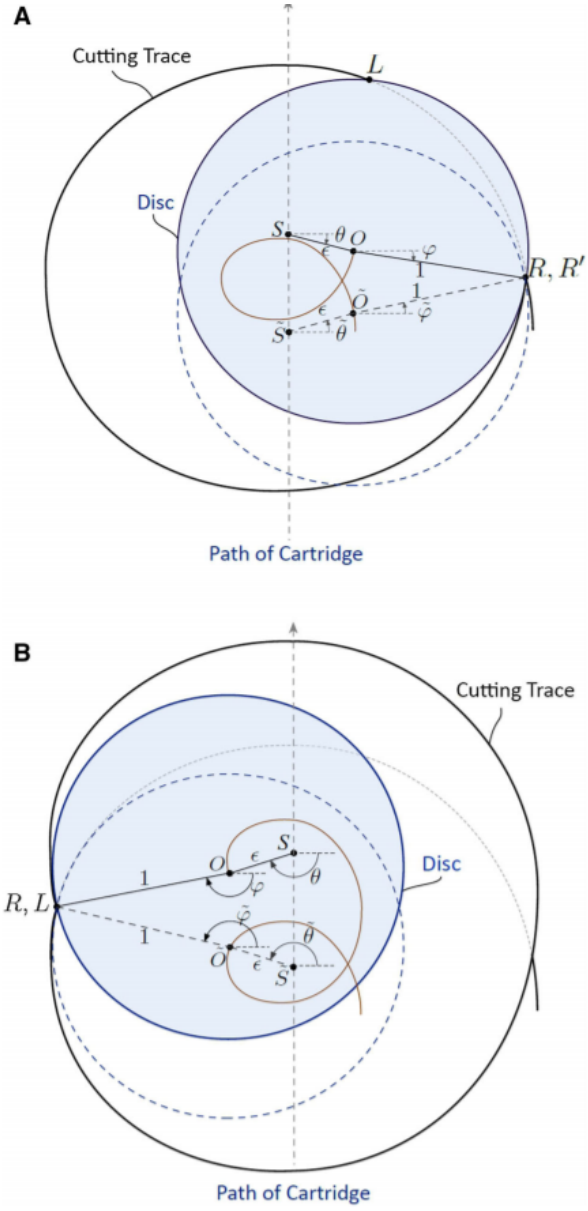

Figure 2.11: Oscillating disc cutter which, periodically loses contacts with rock [12].

Some experiments are already done with oscillating disc cutters(ODC) and show that the forces are significantly lower for ODC compared to indenting disc cutters. This reduction in force was found in various rock types. For example in: sandstone(UCS 35MPa), marble(UCS 100MPa), granite(UCS 160MPa) and norite(UCS 240MPa) significant force reduction were found [8]. One reason for this reduction in force is the angle at which the disc is positioned. Like drag tools the disc cuts the rock in a direct tensile manner. Because the tensile strength of rock is significantly lower than the compressive strength rock will fail more easy. However this does still not explain why the slightly eccentric oscillatory movement reduces the forces even more.

It is important to note that during this report a rotation cycle of the disc is defines as parameter $\tilde{\theta}$, as seen in figure 3.13, which ranges from $-\pi$ to π.

2.2.1. Kinematic model of ODC by Kovalyshen

Kovalyshen developed an analytical model to estimate the cutting forces for an oscillating disc cutter. The kinematics are chosen as the main input for this analytical model [7]. The model makes the following assumptions:

- The energy to destroy a volume of rock is constant
- The velocity and cutting depth of the disc is not affected by the cutting process (cutting mechanism is stiff)
- The direction of the force is determined only by kinematics
- The model is only valid for oscillations with small eccentricity. The eccentricity divided by the radius of the disc needs to be smaller than 0.1

Doubt still exist, whether the second assumption is applicable. The cutting tool might not be rigid. Furthermore, the oscillation speed is hard to keep constant because of the friction between the rock and the tool.

Kovalyshen based the calculation of the cutting force on energy theorem. The area of contact between the disc and the rock is approximated. The force is then, determined by multiplying the cutting area with, the UCS and a dimensionless number, which comes from the cutting tool geometry. Beside the analytical model Kovalyshen, also did experimental test to investigate the ODC. The practical results obtained by Kovalyshen describe the model quite well. He researched and tested the effects of the oscillating frequency of the disc cutter on the cutting force. The results of the experiments are shown in figure 2.12.

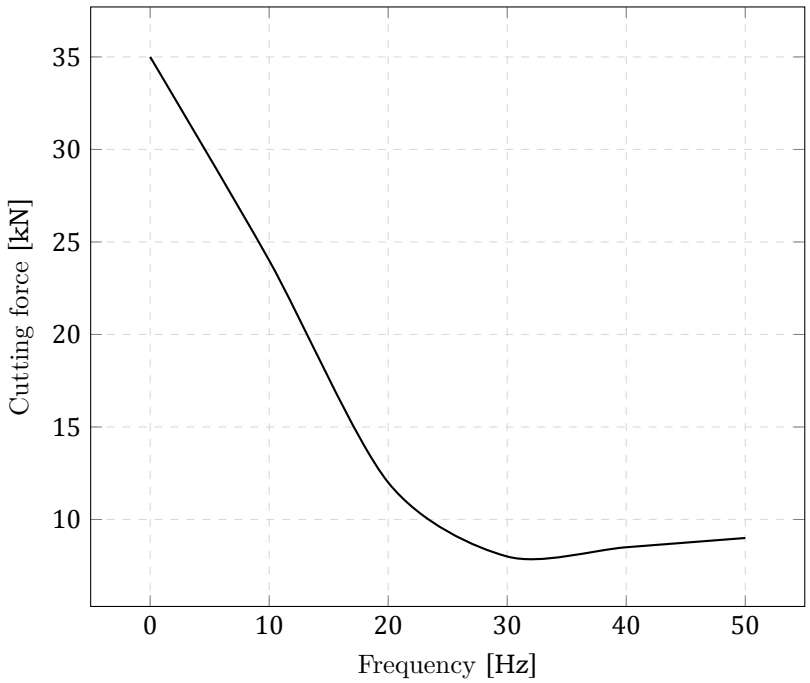

Figure 2.12: Effect of oscillation frequency disc cutter on cutting force(UCS 87MPa; diameter 50mm, cutting speed 100mm/s; eccentricity 1.4mm; cutting depth 10mm) [7].

Kovalyshen found a significant decrease in cutting forces due to the actuated eccentric movement of the disc. Therefore, the kinematic energy is lower for an ODC. However, Kovalyshen states that the total energy required is still comparable to a disc without oscillation, since the oscillatory movement also requires energy. This energy is needed to provide the torsion on the rotating axis.

2.2.2. ODC model by Detournay and Dehkhoda

In 2017 Dehkhoda and Detournay [12] extended and increased accuracy of the model of Kovalyshen [7]. It is less restrictive and can be used for all motions. The kinematics are shown in figure 2.13. The paper from Dehkhoda and Detournay describes a mathematical model to determine the cutting forces, volume of removed rock and specific energy during an actuation cycle of the disc.

Detournay and Dehkhoda did experiments from which a relation is found between the cutting depth and failure type. At small cutting depths failure occurs quasi-continuous and the rock fails primarily due to crushing. At larger cutting depths failure will be discontinuous and chips of rock will be visible at failure. The transition depth between both cutting types is found proportional to a characteristic length scale calculated from material properties. This characteristic length scale for an oscillatory disc cutter is calculated as the ratio between the mode I fracture toughness and the uni-axial compressive strength. This relation is as following:

$$\lambda \sim \left(\frac{K_{ic}}{\sigma_c}\right)^2 \tag{2.10}$$

However, it should be noted that limited tests are conducted to approve this theory for an ODC. The tests suggest that such a transition exists, but more tests are to be done to be certain [12]. Still it is important to make a distinction between the mode of failure, because the specific energy determination differs for grinding or chipping failure. The forces depend on the type of failure since they are calculated from rock volume removed and its required energy. Chipping failure is preferred, since less energy is needed to create chips. The intrinsic specific energy for chipping is determined by using the mode 1 fracture toughness, since the mode 1 fracture toughness represents the opening of the rock and is correlated with the tensile failure of rock. For crushing failure at low cutting depths the UCS value is taken to determine the intrinsic specific energy. The UCS corresponds with the energy needed to crush rock. For scratching failure at low cutting depths, the cutting force scales linearly with the cutting depth. At larger cutting depths at which chipping failure occurs, the force scales with the square root of the cutting depth. Therefore it might be beneficial to cut at larger cutting depths. However the cutting process might be limited to high cutting forces, because of force and wear limitations of the cutting tool.

In the model specific energy is used, along with the angle of contact and cutting depth, to determine the directional cutting force. The angle of contact can be determined as the angle between L and R as seen in figure 2.13. Distinction has to be made whether the disc stays in contact with the rock or loses contact within a single oscillation cycle. If the disc loses contact an implicit equation is to be solved numerically to find the angle R, at which the disc initiates and loses contact with the rock. Therefore, numerical calculations together with boundary conditions(since sinusoidal function gives multiple solutions) are needed to calculate the contact angle. It should be noted that the model only calculates forces in X and Y direction.

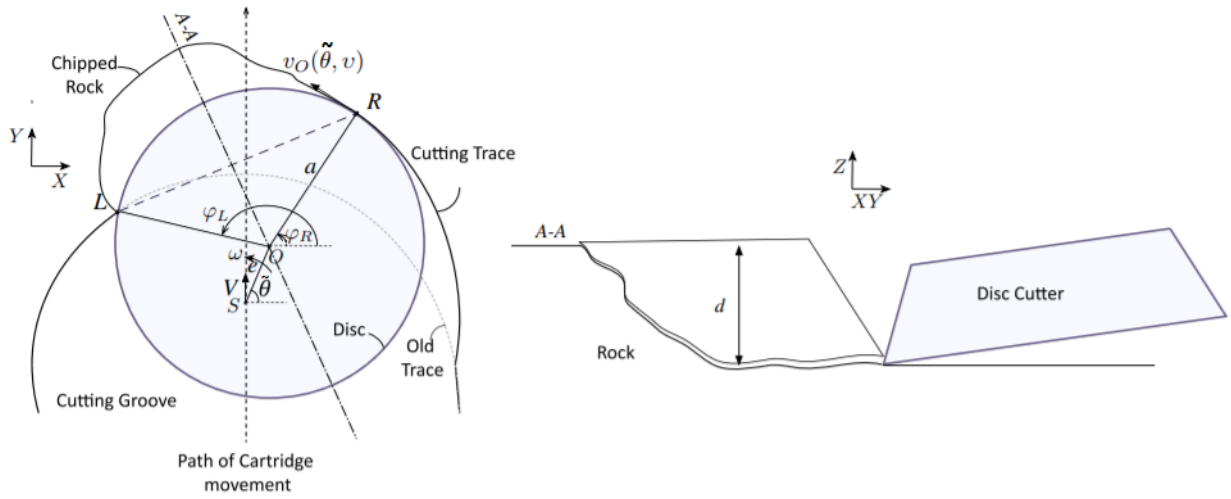

Figure 2.13: Model of Dehkhoda and Detournay. With disk radius a, eccentricity e, cutting depth d, rotation angle disc $\tilde{\theta}$, forward speed V, oscillation speed ω and contact angles φ_l and φ_r [12].

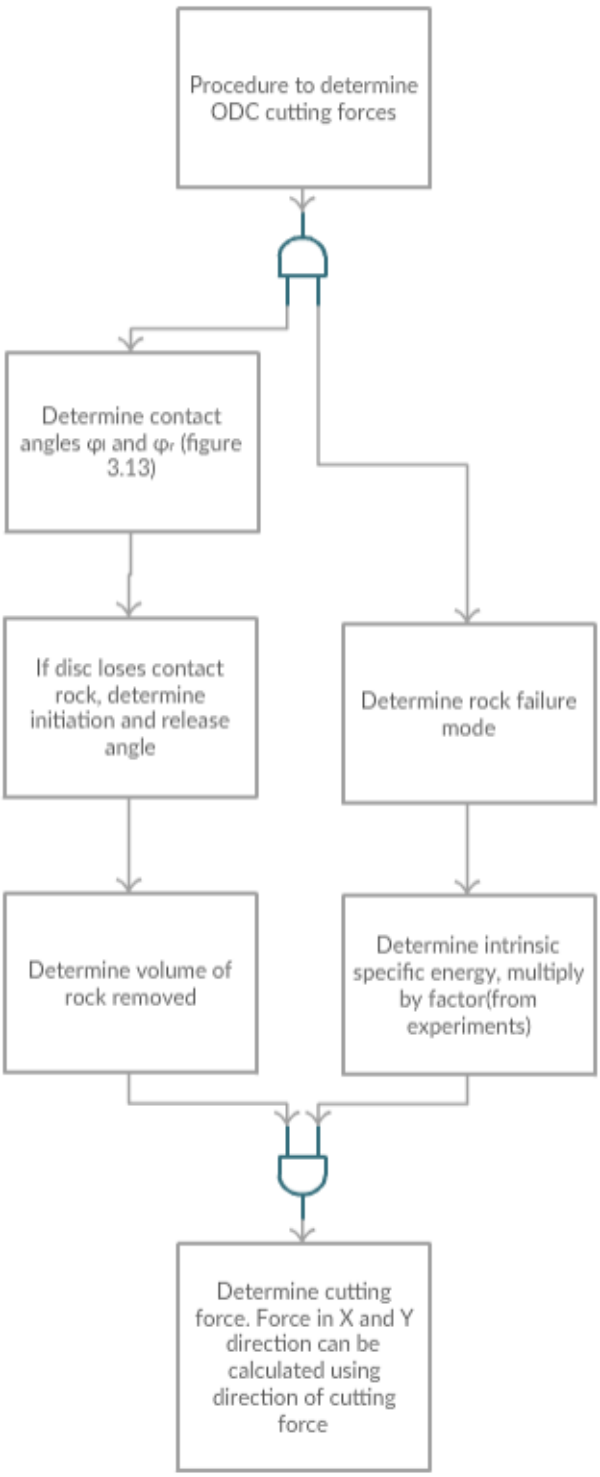

Figure 2.14: Determination procedure of forces. The contact angles are to be determined numerically(implicit equation). After [12].

2.2.3. Fracture model for ODC's

Hood et al. [6] describe the failure of rock when using an ODC from a different view. Instead of looking at kinematics the theory describes failure due to crack propagation only. They describe an analytical model to calculate the forces on an ODC.

The fracturing in rock is explained by the model of Thouless et al [13]. Fracturing occurs in 3 stages as seen in the picture below. The first stage is the crack initiation. In the second stage the crack propagates parallel to the surface of the rock. When the crack deviates towards the surface of the rock the last stage is initiated until the rock is chipped. With the model of Hood, the force needed to cut the rock for a certain depth can be calculated. Furthermore, the maximum cutting depth can be calculated. This occurs when the stress intensity factor (SIF) becomes positive and the crack can't propagate towards the surface.

The method of Hood describes the model of Thouless et al. for rocks. It should be noted that the model assumes a homogeneous material. Furthermore, the model does not allow rotation of the material. For rock this implies that the model should not be used in case of crushing failure, because it can neglect effects due to lateral loading. Furthermore, the model uses strong assumptions. Setting an initial crack length that is perpendicular to the surface of the rock seems unrealistic. Also, the maximum cutting force and initial crack length are linearly dependent.

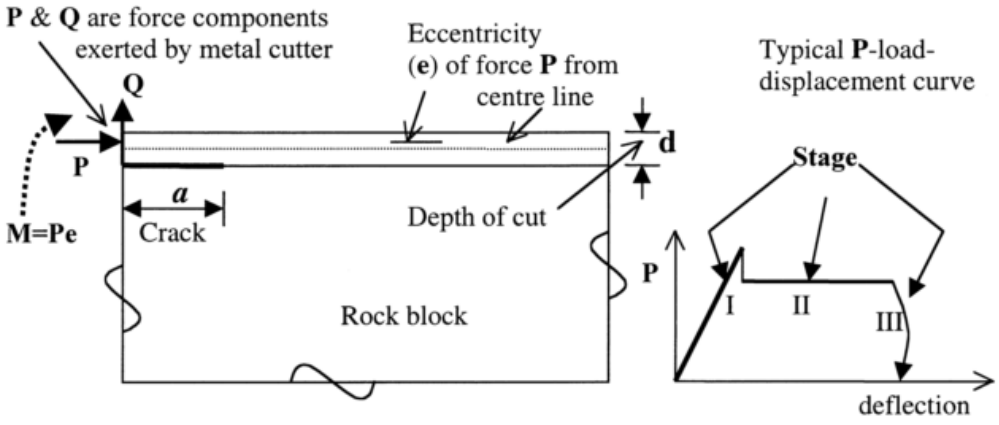

Figure 2.15: Crack propagation in 3 stages [6].

2.2.4. Experimental ODC tests

Karekal [8] explains the ODC in a more practical manner, his research is focused on experiments. He states that the ODC does not require large support against the reaction forces in comparison to other cutting techniques. However the system uses inertial effects to dampen the peak forces that are transmitted to the support structure (figure 2.16). Karekal explains the failure as a result of repeated loading (pre-cracking).

To improve cooling of the cutter and remove crushed rock a high pressure water jet is added. The cooling is beneficiary, because it will result in lower wear rates of the disc cutter. Furthermore the water jet also supports the initiating and propagation of cracks in the rock [8]. There is no explanation, why the jet helps lowering cutting forces. But presumably the jet pre-stresses the rock, which helps the initiating of cracks. However, the drawing suggests that the jet also helps in preventing the crack to propagate towards the surface

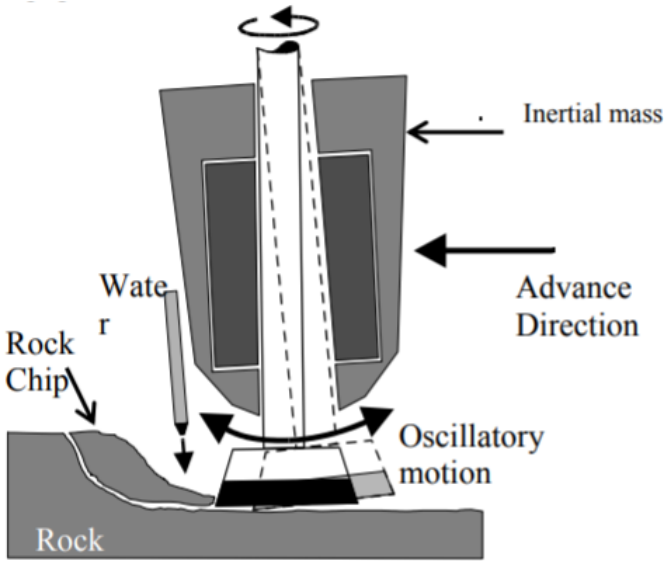

Figure 2.16: Schematics ODC set-up [8].

The rake angle and clearance angle of the cutter are kept at 10 degrees. For harder rocks tungsten carbide discs were used. Soft and medium strength(20-50MPa) rocks where cut using heat treated alloy steels. The rate of wear was found to be lower in the case of tungsten carbide discs. Karekal only investigates the ODC with an amplitude of oscillation, set at 1.5-2.5 mm.

From the experiments Karekal did the following observations:

- Unlike drag tools the mean cutting forces tend to increase for higher cutter velocities
- An correlation occurs between the frequency of oscillation and linear forward speed of the cutter
- The water jet helps by decreasing cutting forces
- The cutting force does not relate linearly with the UCS value of the rock
- Oscillation strongly reduces cutting forces

2.3. Discussion

In this chapter different models for linear and non-linear rock cutting were evaluated. It is found that the linear cutting models presented in this research can't be used to calculate forces on the ODC. The fluctuation of the force and velocity in magnitude and direction are not captured in the linear cutting models. However, the specific energy of an ODC can be calculated, with the formula 2.9. The only difference is that for the ODC in comparison to linear rock cutting torsion is needed. This can be added to the total power by multiplying the torsion with the angular velocity.

For the ODC, the experimental assessments from literature agree that oscillating helps to reduce cutting forces. However, experiments did not give good insight on the effect of the eccentricity of the ODC. The mathematical models for the ODC differ strongly. Kovalyshen and Hood et al. both agree on a transition in cutting depth from crushing to tensile failure. Both models however, don't take this transition into account. The model of Detournay and Dehkhoda takes this transition into account. Furthermore, the model of Detournay and Dehkhoda is the only one that fully defines the kinematic equations. The model of Detournay and Dehkhoda is not restricted to small eccentricity, and is more accurate in determining the contact area between the disc and the rock than the model of Kovalyshen. Still there is no mathematical model for the ODC found, that calculates forces in all three dimensions.

3

Modelling approach

Due to the eccentric movement of the disc a three-dimensional mathematical model is needed to simulate the forces on the ODC. An ODC cuts in an oscillatory manner, therefore the model must be able to simulate this eccentric oscillatory motion. Discrete element modelling (DEM) is able to simulate the cracking of rock by using bonds between particles and is selected to model the ODC. As one particle usually forms more than one bond, particles allow for damage accumulation during the cutting cycles of the ODC. In this chapter, the state of the art on numerical rock cutting methods and the discrete element model with bonding between particles is explained and calibrated. An analysis is done to check bond breakage. In this analysis the failure types between two bonded particles are checked. Furthermore, the transition from the bonded model to the contact model is verified. At the end of the chapter the requirements and method for creating the particle assembly is discussed.

3.1. State-of-the-art numerical rock cutting simulations

There are different numerical methods to simulate rock cutting. The methods can be distinguished as continuum or discontinuum cutting techniques. Continuum methods are methods driven by equations, which need to describe the physical problem. One example of a continuum model is the finite element method (FEM). To describe the physics of rock cutting with FEM's, different problems are encountered. These difficulties occur when simulating fracture and fragmentation of rock material [14]. FEM can not handle large deformations, therefore the cracking of the rock is difficult to model. A solution is to remove elements when cracks appear during the modelling [15]. However, due to the removal of elements mass is lost and effects of cutting debris are neglected [16]. To solve the negative impact of removing mesh elements an adapted finite element model called XFEM can be used [17]. XFEM is able to simulate cracks without re-meshing. It extends the finite element model by applying differential equations with discontinuous functions to the solution space. However, the model is not able to simulate multi crack propagation [18].

Another numerical method capable to simulate fracture is the boundary element method (BEM). BEM is commonly used in fracture mechanics. It is a numerical computational method, which solves linear partial differential equations, which are formulated as integral equations. With BEM discretization is only needed at the boundary of the domain. The solution found on the boundary is used to calculate the solution within the domain by use of an integral equation. This method reduced the dimensions of the model by one and thus reduces input parameters [19]. The drawback of the numerical model is, that it can only simulate homogenous linear elastic material [18].

Besides continuous methods, which are driven on equations, discrete element methods (DEM) can be used. DEM is often used for rock cutting processes. DEM is based on a collection of particles, which represent the granular material. In DEM for solid granular materials it is most common that particles are shaped as spheres (3D) or circles (2D). The particles can be bonded together and create an assembly capable of representing solid granular material, like rock. Using particles is beneficial as a particle can lose contact between other particles and therefore cracks can be simulated. The difficulty however of

using DEM is that, it requires a significant amount of particles and therefore requires more computation compared to FEM. Another disadvantage is that the coupling between micro and macro properties requires more effort to be obtained, due to the less simplistic geometry and calibration procedures.

It is also possible to use multiple numerical methods at once. This is commonly done for DEM's and FEM's [18]. In this case coupling is needed between the FEM and the DEM. The reason to use both is to reduce computation time. In these simulations the part of the geometry at which cracks occur is simulated with DEM [14]. The other part, which lies far away from the cracks is simulated using FEM. Since FEM's, are faster than DEM's computation time is saved. However, to do this the geometry where cracks occur must be known beforehand, otherwise it is difficult to find out in which part of the geometry to apply DEM and/or FEM. Another difficulty is the need for a contact model between the DEM and the FEM part of the solution.

Since, the goal of this research is to simulate a three dimensional rock cutting process using an ODC, it requires the possibility to simulate damage done towards the rock specimen at every rotation of the disc. At every rotation cycle of the disc cracks can initiate and grow through the rock. DEM is quite capable to simulate this, since a particle is connected to surrounding particles using bonds. These bonds can fail and this damage can be accumulated at every rotational cycle of the disc cutter. Therefore, DEM is selected to simulate the ODC. In this research EDEM 2018 is selected to create a DEM, since EDEM offers a easy user interface for simulation setup.

3.2. Discrete element method

To describe such a system of particles the motion of particles are to be calculated. The translational and rotational motion are calculated using the Newton-Euler equations for rigid body dynamics. These laws, describe the motion of the center of gravity by adding up the forces and torques acting on a particle.

Equations of motion:

$$F_i = m_i \dot{V}_i \tag{3.1}$$

$$T_i = I_i \dot{\omega}_i \tag{3.2}$$

with, particle mass m_i, particle velocity V_i, angular velocity ω_i and particle inertia I_i. In the end, all the contributing forces are added and the motion of the particles can be calculated. The force on the particles is calculated by adding the numerical damping, external and contact forces.

$$F_i = \sum F_i^d + F_i^{ext} + F_i^{ct} \tag{3.3}$$

$$T_i = \sum T_i^d + T_i^{ext} + T_i^{ct} \tag{3.4}$$

Damping term

The system is affected by a numerical damping term (α_d) of 0.7. This number is well accepted in DEM's for rock cutting theory. The damping is needed to acquire more realistic behaviour of the particle assembly. It can be seen as a simplification to the simulation in order to simulate the energy lost to heat generation and wave scattering. Furthermore, damping is needed to reduce the energy peaks in the simulation when the brittle bonds suddenly break. Damping affects the angular and translational accelerations of the particles in the simulation.

Damping equations:

$$F_i^d = -\alpha_d |F_i| sign(V_i) \tag{3.5}$$

$$T_i^d = -\alpha_d |T_i| sign(\omega_i) \tag{3.6}$$

3.2.1. Contact model

In case no bond exists between two particles, a contact model is needed to model the contact forces. EDEM 2018 [20] offers several contact models. From literature many bonded model simulations use the linear spring contact model. However in EDEM the linear contact model applies equal stiffness to the normal and tangential direction[1]. Using this model will result in non-physical force changes in case of bond breakage. The Hertz-Mindlin (no slip) model accounts for differences in normal and tangential contact forces and is therefore used in this research. The Hertz-Mindlin contact model can be seen in figure 3.1. The contact model accounts for tangential and normal and rolling friction. Further information of the implementation of the Hertz-Mindlin contact model is given in Appendix A. It should be noted that the contact model exist between particles if one or both particles are disconnected from all bonds. Therefore two bonded particles can have a Hertz-Mindlin contact force with a loose particle.

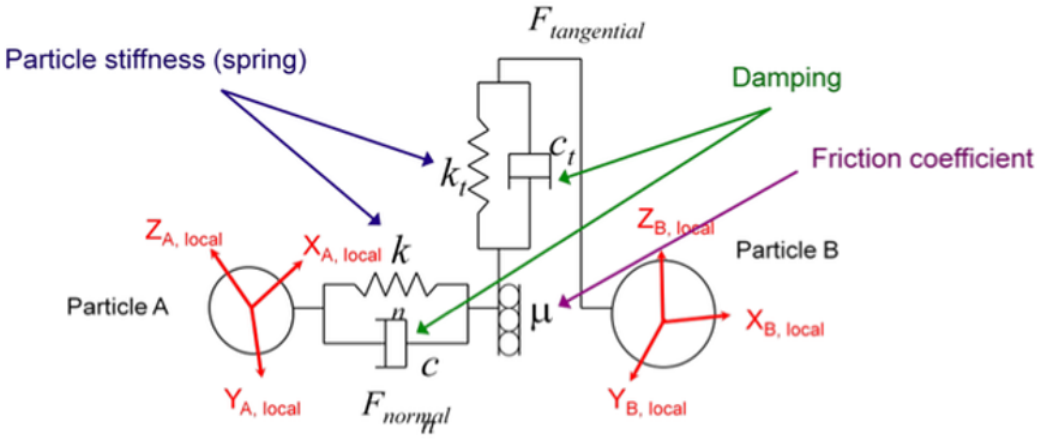

Figure 3.1: Hertz-Mindlin contact model [21].

[1]It is possible to change the linear contact model in EDEM trough the API, however an increase in simulation time (5x) can be expected in case API is used to change linear contact models.

3.2.2. Bonded particle model

To achieve an assembly that reproduces a rock sample in DEM bonding between particles is required. These bonds offer the possibility to reproduce properties of solid granular material. The bond is placed between the 2 centers of the particles. The radius of the bond is equal to the radius of the smallest of 2 particles (figure 3.2). For a bond to be created between 2 neighboring particles, EDEM 2018 searches whether particles contact radius overlap. If overlapping occurs a bond is created. The contact radius is an imaginary shell around the particle, which size is determined by a input factor times the particle radius. This factor should be chosen carefully. If it is chosen too large the particle can bond with a particle behind a neighboring particle. The particle distribution is therefore important when choosing the contact radius. N.J. Brown [22] studied the effect of the contact radius on the particle assembly. The average number of bonds per particles increases when the contact radius is increased. The strength of the particle assembly for UCS simulations also increased slightly when this occurs. In the simulations done in chapter 4 and 5 a particle assembly, with UCS 16.7 and BTS 1.8MPa is targeted.

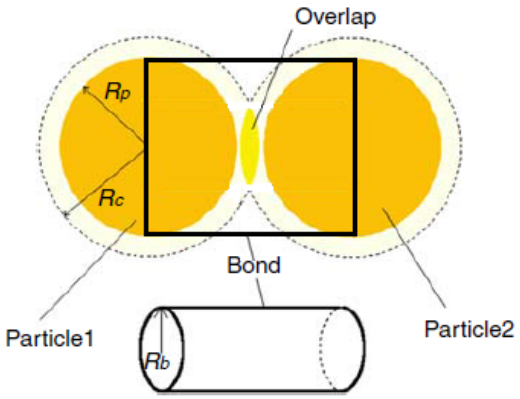

Figure 3.2: Bond between 2 particles [23].

The bond is described by a stiffness matrix, according to the Timoshenko beam theory. If stresses reach a certain criterion the bond fails and the bonded connection between the two particles is lost. The stiffness matrix is used as proposed by J.S. Przemieniecki [24]. The matrix uses thin-walled beam theory. Therefore, it assumes that only small bond displacements/rotations are allowed. The stiffness matrix is shown by matrix 6.9. The matrix calculates the forces, moments and displacements of the both particles centers. These results are needed to solve the Newton-Euler equations.

$$\begin{bmatrix} S1 \\ S2 \\ S3 \\ S4 \\ S5 \\ S6 \end{bmatrix} = \begin{bmatrix} \frac{EA}{l} & & & & & \\ 0 & \frac{12EI_z}{l^3(1+\phi_y)} & & & & \\ 0 & 0 & \frac{12EI_y}{l^3(1+\phi_z)} & Symmetric & & \\ 0 & 0 & 0 & \frac{GJ}{l} & & \\ 0 & 0 & \frac{-6EI_y}{l^2(1+\phi_z)} & 0 & \frac{EI_y(4+\phi_z)}{l(1+\phi_z)} & \\ 0 & \frac{6EI_z}{l^2(1+\phi_y)} & 0 & 0 & 0 & \frac{EI_z(4+\phi_y)}{l(1+\phi_y)} \end{bmatrix} \begin{bmatrix} u1 \\ u2 \\ u3 \\ u4 \\ u5 \\ u6 \end{bmatrix} + \begin{bmatrix} P_{T_z} \\ 0 \\ 0 \\ 0 \\ M_{T_y} \\ -M_{T_z} \end{bmatrix} \tag{3.7}$$

Where,

$$\phi_y = 24(1+v)\frac{A}{A_{s_y}}\left(\frac{r_z}{l}\right) \tag{3.8}$$

and,

$$\phi_z = 24(1+v)\frac{A}{A_{s_z}}(\frac{r_y}{l}) \tag{3.9}$$

with, E the Young's modulus of the bond, v the Poisson's ratio of the bond, the cross-sectional bond area A, and the second moment area of the bond I, bond length l and bond radius r.

S1-S6 are the forces and moments relating to one of the particles.

- 1 is the axial force
- 2 is the shearing force (upwards)
- 3 is the shearing force
- 4 is the twisting moment
- 5 is the bending moment (around upwards axis)
- 6 is the bending moment

Failure occurs if the ultimate stress of the bonds in tensile or shear direction is exceeded. The stresses in these directions are computed by using beam theory [22].

$$\sigma_t \leq \left(\frac{S1}{A_b} - \frac{r_b\sqrt{(S5)^2+(S6)^2}}{I_b}\right) \tag{3.10}$$

$$\tau \leq \left(\frac{|S1| * r_b}{2I_b} + \frac{4\sqrt{(S5)^2+(S6)^2}}{3A_b}\right) \tag{3.11}$$

To avoid re-bonding after bond failure in EDEM, the bonding determination procedure must be set during one time step. This can be done in the EDEM API. The API is the application programming interface, which basically is a back-door to change contact, bonded models and particle properties in EDEM.

Time step

The time step is calculated based on the highest natural frequency of the system. For a mass spring system the natural frequency can be calculated according to:

$$f = \sqrt{\frac{k}{m_p}} \tag{3.12}$$

with, stiffness k, particle mass m_p and natural frequency f. In case of the highest natural frequency the natural frequency needs to be calculated for all bonds by selecting the highest stiffness component of the bond and the corresponding particle mass. The critical time step is then easily calculated.

$$t_{crit} = \frac{2}{f_{crit}} \tag{3.13}$$

In this research only spherical particles are used for sake of simplicity and to make use of EDEM. The effect of the particle shape cannot be neglected. Especially in case all bonds connected to a particle fail the shape can affect the motion and thus forces on the particle. In case of spherical particles rotational motion is not obstructed, because no interlocking between particles occurs. For the model particles will therefore, rotate more easily. However the rolling friction of the contact model helps slightly to prevent the rotation of particles.

3.3. Particle model verification

In the following sub sections different failure mechanics of the bond between particles is verified. First the tensile and shear failure of the bonds are checked. Afterwards, the transfer of forces to the contact model is checked, in case a bonded connection between two particles fails.

3.3.1. Tensile bond failure

To investigate the effects of failure on the particles different situations are verified, to see if the failure response is as it should be. First two particles are pulled in opposite direction to test tensile failure, see figure 3.3. When the tensile stress of the bond reaches the tensile strength limit the bond is supposed to fail in a brittle manner. The tensile strength and stiffness of the bond are input parameters of the bonded model.

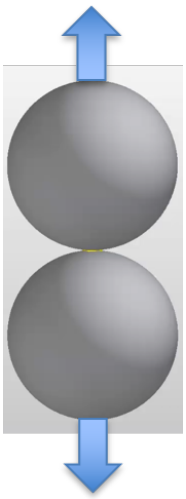

Figure 3.3: Testing tensile failure of bond.

In this test both particles are pulled out of each other at low speeds. Only the first component from the stiffness matrix is used in the simulation. The first component of the stiffness matrix:

$$k_{11} = \frac{E_b A_b}{L_b} \tag{3.14}$$

with, normal stiffness k_{11} [N/m], Elastic modulus bond E_b [GPa], Bond length L_b [m] and Bond area A_b $[m^2]$

The relevant bond parameters are:

E_b [GPa]	72
σ_t [MPa]	175
R_p- Particle radius [mm]	0.76
L_b- bond length [mm]	1.52

Table 3.1: Relevant parameters tension test.

After a small displacement the bond fails. The displacement of the bond and the tensile bond stress are shown in figure 3.4. It can be seen that the bond fails at the indicated stress level as expected. At failure the bond is removed. By using Eq. 3.14, it can be shown that the strain to failure is as expected.

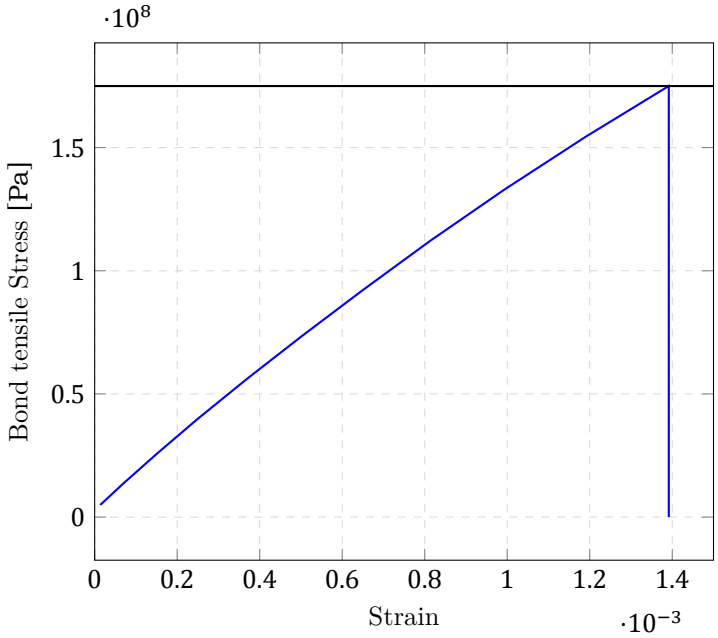

Figure 3.4: Tensile bond stress versus strain. Horizontal line shows tensile strength limit of bond.

3.3.2. Shear bond failure

The failure of the bond in shear direction is verified by setting the normal stiffness to zero and pulling the particles sideways in opposite direction of each other. The reason the normal stiffness is set to zero is that the bond length will increase, due to the shearing of the particles. Because only shear failure is verified, the effect of the normal stiffness needs to be excluded. In figure 3.5 the shear bond stress and elongation is shown. The bond shear strength is set to be 175MPa.

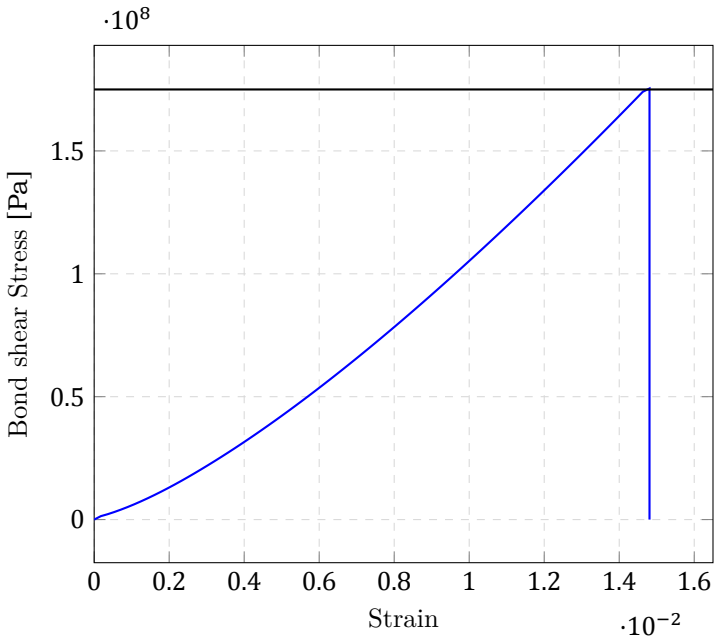

Figure 3.5: Shear bond stress versus strain. Horizontal line shows shear strength limit of bond.

3.3.3. Bond breakage calibration

When a particle breaks looses a bond between another particle it still affects each other. The influence of a loose particle is described by the previously explained Hertz-Mindlin contact model. The breakage of bonds releases energy, which in case of a loose particle is transferred to the contact model. Since, the contact model is described by a spring-damper system, it needs calibration. The particle Young's modulus is calibrated by trial and error, until almost no energy gets lost when the bonds break and the contact model comes into place. The energy transfer is validated by running two simulations where two particles are compressed into each other. In one simulation the particle is bonded, in the other the particle uses the Hertz-Mindlin contact model. It can be seen in figure 3.6 that the energy transfer is quite accurate when the bond is removed. However when transferring to the contact model the particle looses a little bit of energy (around 4%). The damper in the Hertz-Mindlin model is not needed and therefore a low damping constant is used.

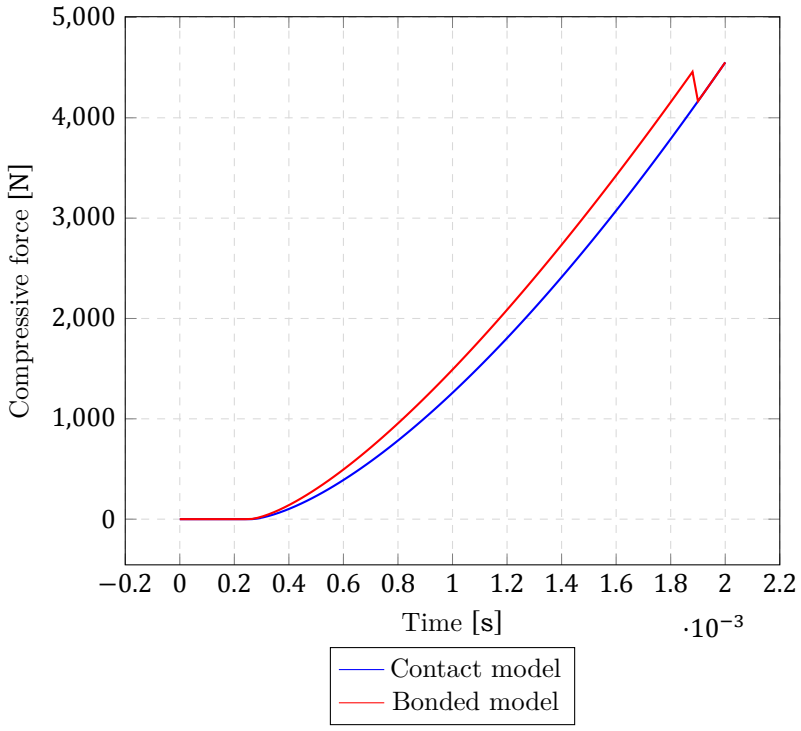

Figure 3.6: Force drop during bond breakage.

The small loss of force after a particle looses all it's bonds, could be avoided by using a linear contact model. However, the linear contact model in EDEM creates a normal stiffness component, which is equal to the shear stiffness component. This will result in non-physical behaviour if a bond is broken.

3.4. Particle assembly generation

The particle assembly is important because the DEM solution is driven by geometry. Simulated materials are affected by the particle assembly properties. The particles assembly is generated using external software, since EDEM does not offer functionality to make a dense particle assembly able to represent solid granular material. GID 14.0 [25] is used to generate an assembly. Several aspect are taken into account when creating an assembly. Those aspects are:

- Particle size and distribution
- Number of particles
- Porosity
- Number of Neighboring particles
- Particle position error

Particle size and distribution

The size of the particle is important as it affects the simulation time and behaviour of the assembly. The geometry and particle size are related for low strength rock as shown by Yenigül and Alvarez Grima [26]. Furthermore, simulation time is affected by the size of the particles. Smaller particles increase simulation time. More particles will give more interactions, besides, the time step is affected by the smallest particle, and therefore more time steps are to be calculated.
Using smaller particles results in more bonds, this effects the Young's modulus and BTS/UCS strength of the assembly. The distributions of the particles is a parameter for consistency of the assembly (isotropy). A dense particle assembly can be created when using a distribution with large standard deviation of the radii. This will however, create an anisotropic material, since the smaller particles will fill up voids around larger particles.

Porosity

Porosity is important, because it it related to the strength of the rock. A material with gaps can fail more easily, since particles will have less support from neighboring particles. In literature the porosity in 3d is lower than 2d. A minimum porosity of 0.3 is defined as a requirement for this research. This value is chosen, since in literature the porosity for 3 dimensional assemblies resembling rock specimens is mostly below 0.3, as seen in [14]. For rock it is important to avoid high porosity, since the cracking in the UCS/BTS test will become non-physical (too large deflections) because of the intern mobility of the particles.

Number of particles and neighbors

Particles need multiple neighboring particles in order to simulate a solid material like rock. If there are few particle neighbors the assembly can become weak and less stiff. The number of particles is crucial for assembly behaviour. There is a relation between particles and geometry size which should be accounted for. For example the cutting depth should be larger than at least several particles for cracks to initiate. Of course more particles is beneficial, but this is limited by simulation time.

Particle position tolerance

The fast creation of the assembly in GID, can give problems when the input parameters are not chosen carefully. Small rounding errors in position can create overlapping particles. When exporting such an assembly into EDEM 2018 the solution becomes unstable.

3.4.1. Particle assembly generation

There are different methods for creating a particle assembly in this research the particle assembly genertation of PFC [27] and GID [28] are discussed. In PFC particles are randomly placed inside a rectangular geometry and expanded until their preferred size is achieved. Then the radii of all particles are reduced until a specified isotropic stress is reached. Now the floating particles with less than three contacts are removed followed by the removal of the rectangular geometry [27]. This method takes quite some computation time. A much quicker method is the one created by GID. In GID particles are generated by creating a mesh at which spheres are placed at the nodes. The size of the spheres is affected by the distance to the neighboring nodes and a random factor. These spheres can be allowed to overlap. The overlapping is corrected by solving an algorithm that optimizes the distance between particles [28]. The difference is that in GID the particle assembly is completely relaxed, there are no internal stresses in the assembly. Since, the computation time by using GID is fast it is used in this research.

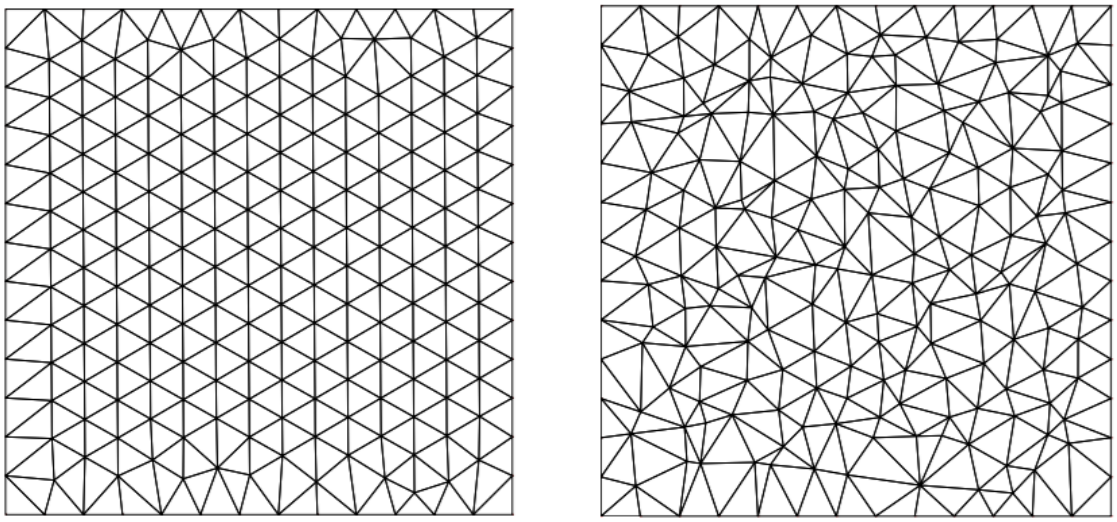

Figure 3.7: Structured (left) and non-structured (right) mesh [28].

To create more randomness in the assembly a random mesh generator is applied in GID. The differences between the types of mesh can be seen in figure 3.7. By using this non-structured mesh a less uniformly stacked assembly will be achieved. In GID this will result in a more dense material. The downside is that the generation is more random, and therefore more simulations are to be done to visualize the effects of the random mesh generation. At the end of the mesh generation the assembly can be improved using boundary treatment, as seen in figure 3.8. The boundary treatment uses a different algorithm to fill up the space left on the outside of the meshed volume. By doing this, denser particle assemblies can be created. During particle assembly creation it was seen that the stacking of particles near the boundaries is more uniform.

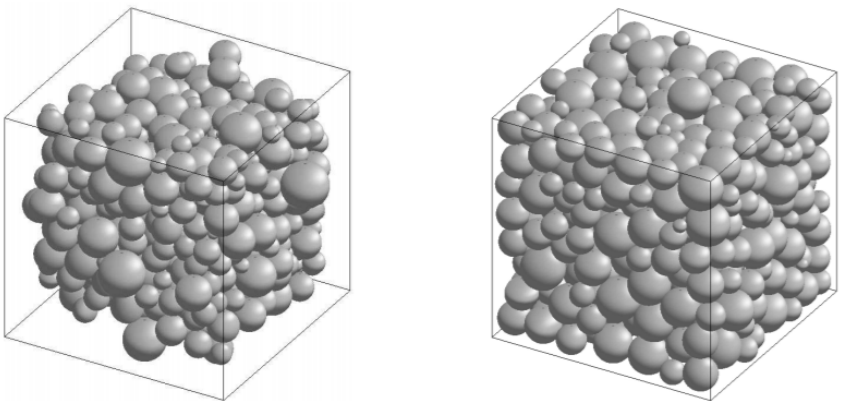

Figure 3.8: No boundary treatment (left), boundary treatment (right) [28].

The solution can now be exported from GID. The assembly data can be imported into EDEM 2018 by using the API. A custom dll is created to load the assembly into EDEM 2018. It is important to import the solution into EDEM before the bonding is applied, since bonding is applied in a single time step.

3.5. Random particle assembly generation

The particle assembly is created through GiD. This process is random and therefore the effect of this random particle stacking needs to be taken into account. Eight different assemblies are generated and tested by doing simulations with the ODC. The kinematic properties of the ODC were as following: oscillation speed is 1350 rpm, linear velocity is 0.5m/s and eccentricity is 0.4. The BTS of the assembly is 1.8 MPa. The average of the cutting force (magnitude) found is 636N. Below different boxplots are shown where the effect of the random assembly generation on the forces in all directions and the peak force can be seen. The randomness in the assembly affects the peak force significantly. Smaller particles might help for a less diverting peak force.

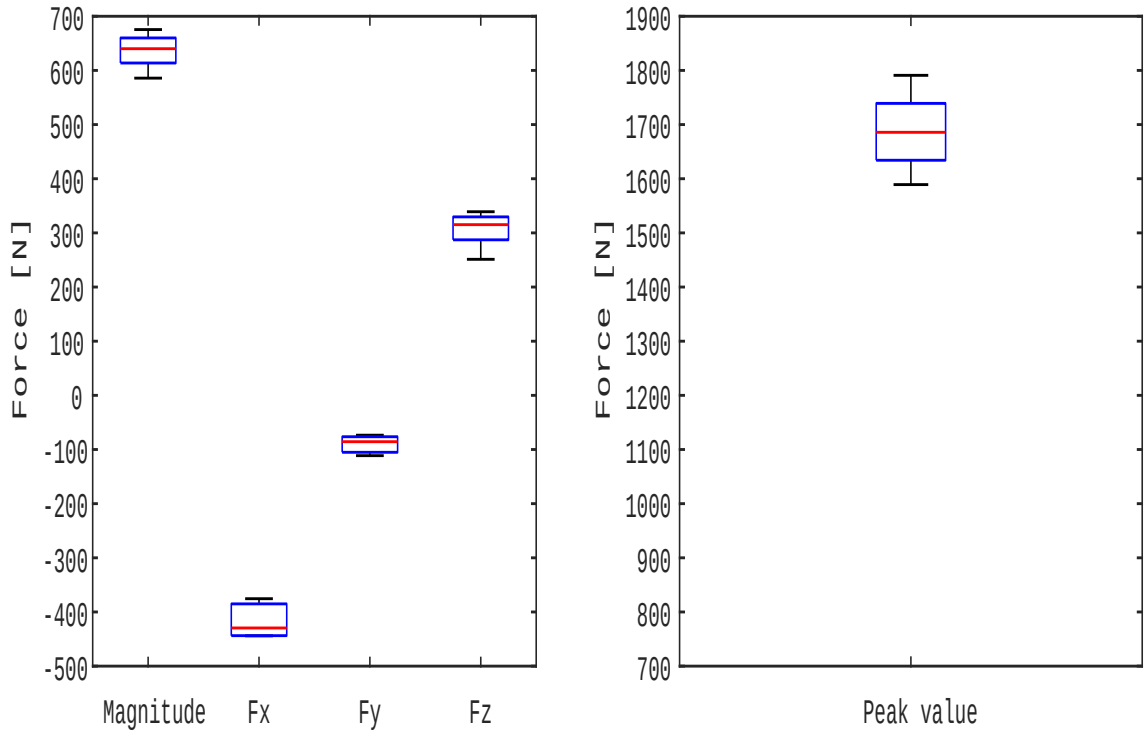

Figure 3.9: Boxplots forces for random particle assembly generation.

The inaccuracy due to the randomness in the particle generation, seems to increase a lot more than for the BTS and UCS test, where it was found to be almost negligible. This difference probably comes from the positioning of the particles on the disc edge. A particle that hits the cutting edge on the lower half of the sphere is more likely to create tensile fracture than a particle that is hit in the upper half of the sphere. A solution to this would be a smaller particle size and/or create a wearflat on the disc edge. However as said before computation time increases significantly, when using smaller particles.

4

Material calibration

In this chapter the main focus is to calibrate the particle assembly. Since, the assembly is supposed to model rock, UCS and BTS simulations are done to verify the assembly behavior and calibrate the micro-macro properties.

4.1. Material tests

The BTS and UCS of the particle assembly will be calibrated until a strength of 1.8 and 16.5MPa respectively is found. Besides the strength values, also the strain and failure type of the assembly will be checked. To reach a certain particle assembly strength (BTS/UCS) is not difficult. This can be done mainly by adjusting the tensile and shear bond strength. However, by focusing only on these two parameters, the visual failure of the particle assembly is not representative of a UCS or BTS test representing solid granular material. Also, the strain of the bulk material might not yet be acceptable. Both the visual failure mode and bulk modulus of elasticity can be calibrated by changing the bond Young's modulus. Increasing the bond Young's modulus will lower strain at failure and increase the bulk Young's modulus. However, increasing the Young's modulus too much will change failure like shear failure for a UCS simulation to non-physical failure.

The method in this research used is as following, first find the bulk strength (UCS/BTS) by changing the tensile and shear bond strength. Then adjust the bond Young's modulus until failure patterns like a shear failure plane for UCS is found. Beside the failure pattern, the bulk material's strain at failure needs to be in range. If this is achieved the whole calibration procedure is to be repeated, due to the change of the bond Young's modulus, which also changes the UCS and BTS. The process is iterated until the preferred UCS and BTS values are found. It should be noted, that this method does not work for all preferred UCS and/or BTS values. In this research higher strength rocks (UCS 90>MPa) were approached as well. However the strain response for the BTS test was incorrect as strain at failure is too high and the bulk material stress-strain response is found to be non-linear.
In this research the sensitivity of the input parameters for calibrating the material is not carried out, since the focus is more on the simulations of the ODC. Furthermore, this is chosen since, it is difficult to quantify the failure plane of the UCS and BTS simulations.

4.1.1. Brazilian tensile strength test

To create a three dimensional bonded particle assembly that behaves like a rock a Brazilian tensile strength and uniaxial compressive strength test are done. Since in literature experimental tests for the ODC are done by Dehkhoda and Detournay, the same rock properties are taken in this research to allow for comparison between simulations and practical tests. Dehkhoda and Detournay used limestone Savonnière with UCS 16.5 MPa and BTS 1.8 MPa.

To investigate whether the resemblance between limestone Savonnière and the particle assembly is sufficient, different criteria of the assembly are analyzed. For both the UCS and BTS test these criteria are the strength and fracturing of the assembly. In case of the BTS test the cracks are most likely to occur parallel to the loading direction. This happens due to the compression, which induces tensile stresses perpendicular to the compressive direction. There are a number of parameters which influence the two criteria mentioned above. These parameters can be categorized in three categories: assembly generation parameters, bond parameters and contact parameters. For the following parameters the two criteria are met.

Delta radius factor	0.2
Min. Radius factor	0.7
max. radius factor	1.3
Max. iterations	1000
Max. local iterations	4
Delta position factor	0.3
Filter iteration	10
Search iteration	10
Factor contact	1.25
Factor overlap	0.6
Delta position factor	0.3
Cylinder radius	15[mm]
Cylinder height	55[mm]
Number of particles	12.3k
Coordination number average	8
Particle radius average	1.67[mm]
porosity	0.255

Table 4.1: GiD assembly parameters.

ν	0.3
ρ	$2730 kg/m^3$
Shear Modulus	29[MPa]
Coefficient of restitution	0.5
Coefficient of static friction	0.5
Coefficient of rolling friction	0.5
Time step	$6.3e^{-7}$

Table 4.2: Contact/EDEM 2018 parameters.

E_{bond}	15[GPa]
ν	0.3
σ_{bond}	23[MPa]
τ_{bond}	23[MPa]
bond radius ratio	1
contact radius	1.1

Table 4.3: Bonded parameters.

The BTS test is done by compressing 2 plates together at a total velocity of 0.1m/s. Both plates can be seen in figure 4.1. The figure also shows the damage property of particles. The damage property describes the number of bonds that failed for a single particle. It is a ratio between initial bonds and failed bonds. A damage parameter of one means all the bonds are failed.

$$Damage_{parameter} = \frac{failed_{bonds}}{initial_{bonds}} \tag{4.1}$$

In the figure it can be seen that there is little crushing failure near the compressive plate. The failure is found to be a fracture splitting the two halves of the cylinder apart. The figure only shows a slice (2d), but the same type of failure is found throughout the whole material (3d).

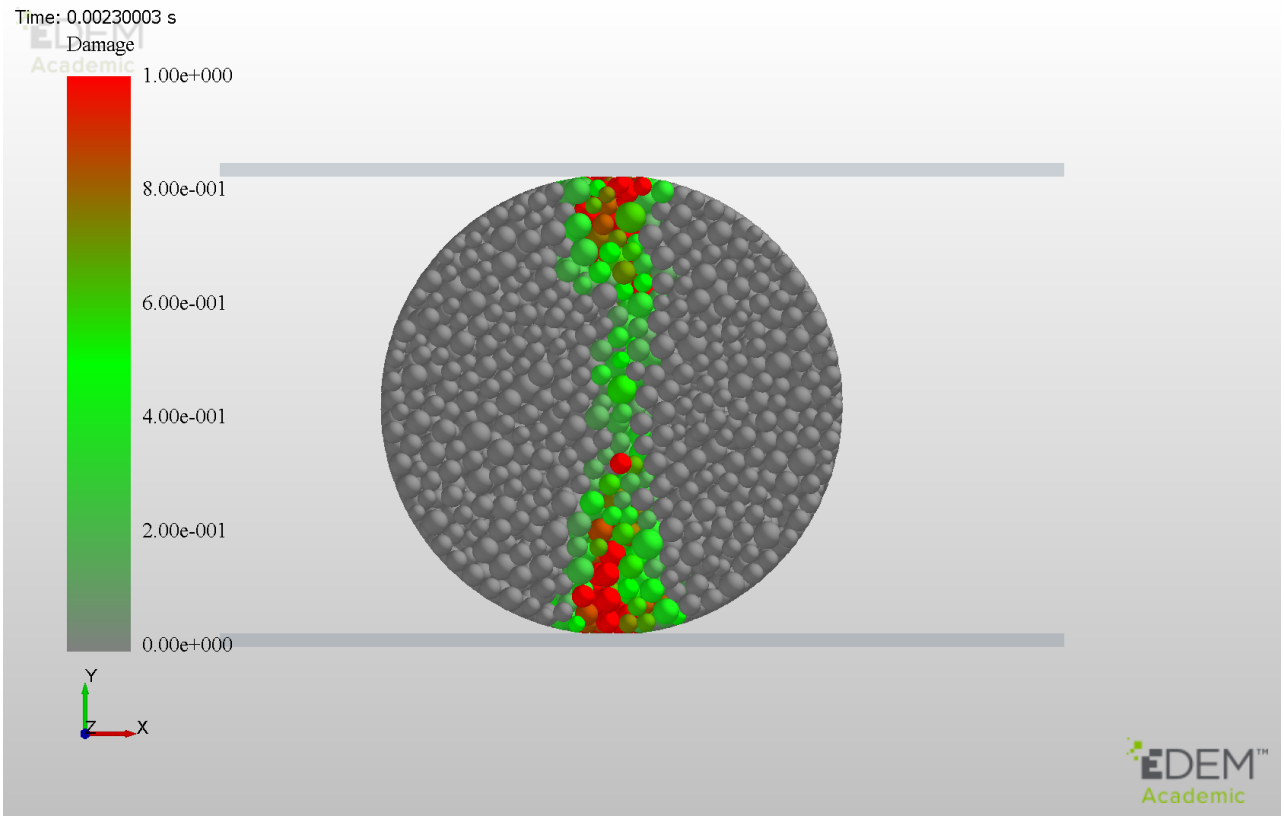

Figure 4.1: Damage property of particles in BTS test.

The Brazilian tensile strength is calculated as following:

$$BTS = \frac{F_{max}}{\pi R t} \tag{4.2}$$

with, R is cylinder radius and t is cylinder height The stress strain response is shown in figure 4.2. The BTS value found is 1.81 MPa at a strain of 0.0049. The strain is in range with BTS tests for rock in literature, but more information is needed to see if it is comparable to the strain response of Savonnière limestone.

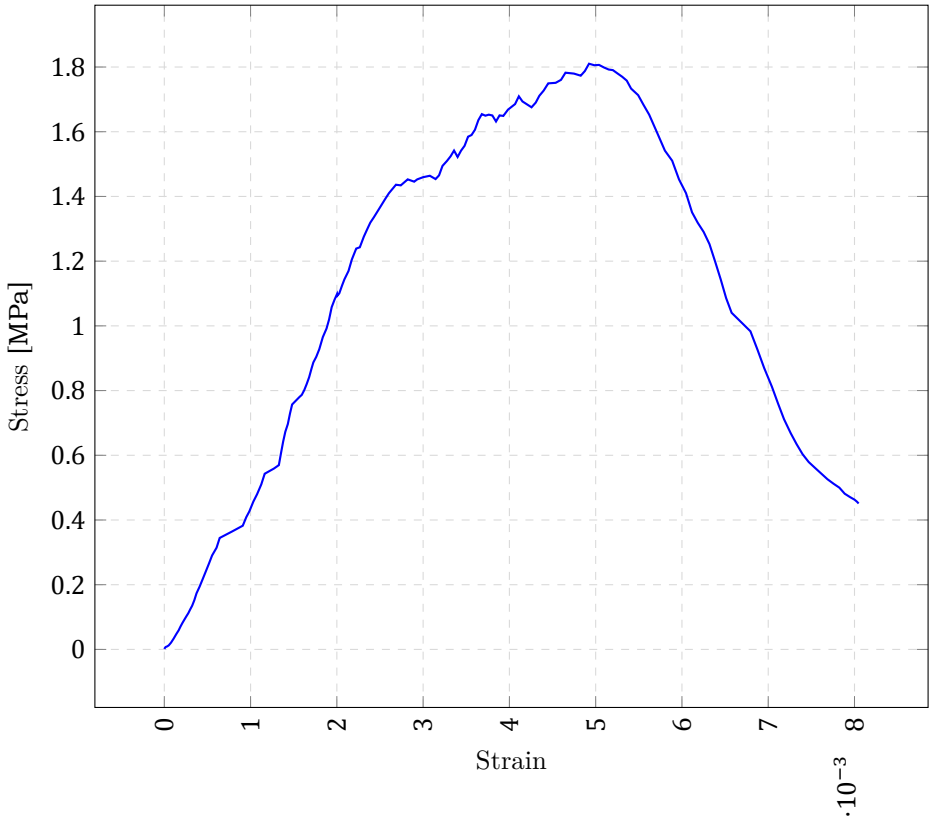

Figure 4.2: Stress versus strain for Brazilian disc assembly.

Since the generation of the particle assembly is random multiple tests are required to find an average BTS value. The effect of this randomness is found to deviate 5 percent towards the BTS value. This probably occurs due to the boundary treatment GiD uses. Boundary treatment affects the edges of the cylinder which become more homogeneous. Therefore randomness affects the outer layer of the cylinder less. Since as seen in figure 4.1, most damage occurs in the outer layers, the BTS will be significantly affected by the particles near the compressive plate. This is probably due to the assembly generation. Particles, which are generated on the outside of the cylinder will have less bonds, and therefore are more susceptible to damage.

BTS	1.79 [MPa]
Standard deviation	0.04 [MPa]
Number of tests	10

Table 4.4: Effect assembly generation randomness on BTS value.

4.1.2. Uniaxial compressive strength test

In a uniaxial test two plates are compressed until the rock specimen fails. For the uniaxial compressive strength simulation the same two criteria as the BTS simulation are taken. The UCS stress aimed for is 16.5 MPa (Savionnière). For the fracturing it is critical to find a typical failure of rock. This could be for example a shear plane failure or axial splitting. While running simulations to accomplish both criteria it is found that the ratio of the elastic modulus of the bond and the bond critical stress affects the fracturing significantly. If the bond critical stress is set too high in comparison to the elastic bond modulus the shear fracture plane will disappears and mostly crushing failure near the compressing plates is seen. This is not preferred and therefore avoided in this study. The parameters below give the solution for which the UCS is 16.6 MPa.

Delta radius factor	0.2
Min. Radius factor	0.7
max. radius factor	1.3
Max. iterations	1000
Max. local iterations	4
Delta position factor	0.3
Filter iteration	10
Search iteration	10
Factor contact	1.25
Factor overlap	0.6
Delta position factor	0.3
Cylinder radius	15[mm]
Cylinder height	55[mm]
Number of particles	12.3k
Coordination number average	8
Particle radius average	1.67[mm]
porosity	0.255

Table 4.5: GID assembly parameters.

ν	0.3
ρ	$2730 kg/m^3$
Shear Modulus	29[MPa]
Coefficient of restitution	0.5
Coefficient of static friction	0.5
Coefficient of rolling friction	0.5
Time step	$5.2e^{-7}$

Table 4.6: Contact/EDEM 2018 parameters.

E_{bond}	15[GPa]
ν	0.3
σ_{bond}	34[MPa]
τ_{bond}	34[MPa]
bond radius ratio	1
contact radius	1.1

Table 4.7: Bonded parameters.

The plates are compressed at a total velocity of 0.1 m/s. The plates can be seen in figure 4.3. Here the damage property also shows a clear crack. In the UCS simulations the crack propagates over the shear plane. Along the main crack some minor cracks exist as seen in figure 4.3.

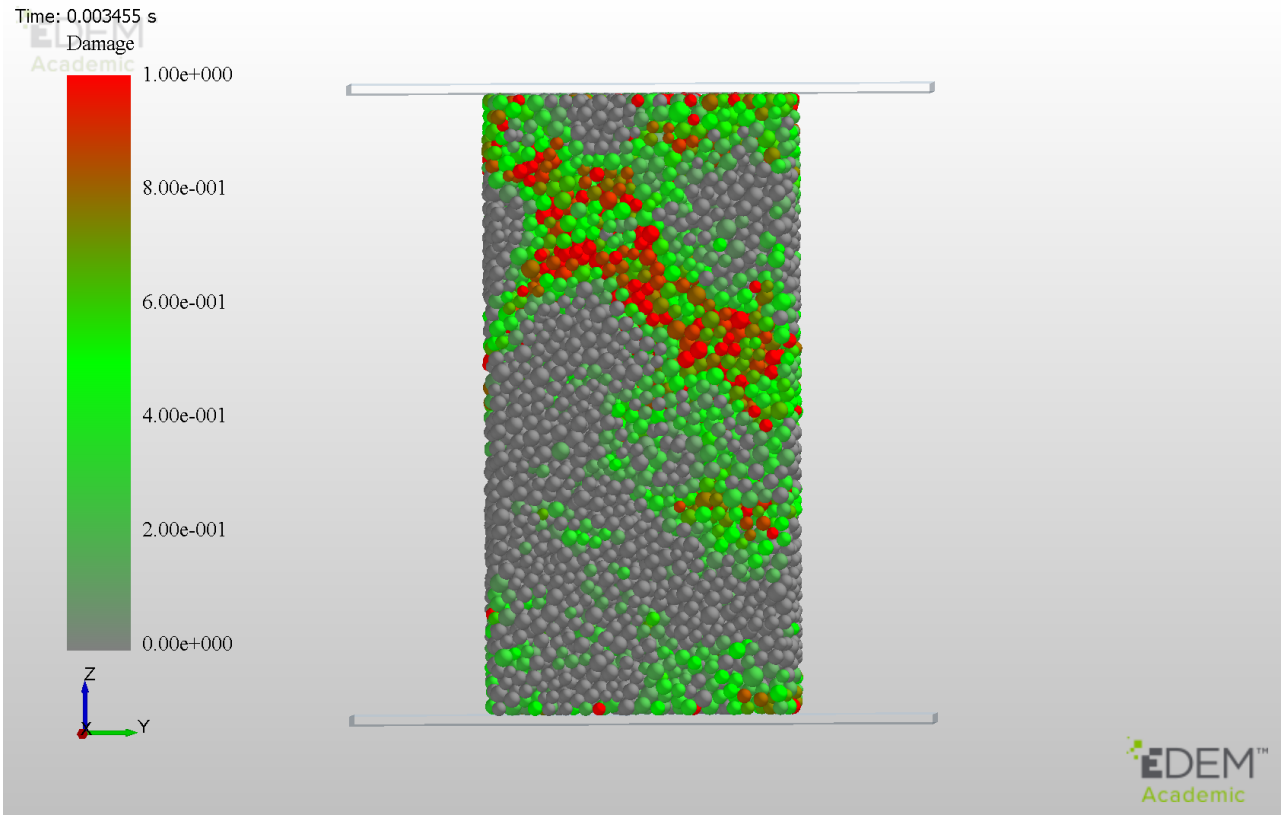

Figure 4.3: Damage property of particles in UCS test.

The stress strain response for a single simulation is shown in figure 4.4. The UCS value found is 16.7 MPa at a strain of 0.0024. The stress is calculated as following:

$$UCS = \frac{F_{max}}{\pi R^2} \tag{4.3}$$

The strain is in range with UCS tests for rock in literature. The elastic modulus is however found to be a bit lower in comparison with the value for savionnere limestone found from literature (12MPa) [29].

UCS	16.7 [MPa]
E	7.5 [GPa]
Standard deviation	0.52 [MPa]
Number of tests	10

Table 4.8: Effect assembly generation randomness on UCS value.

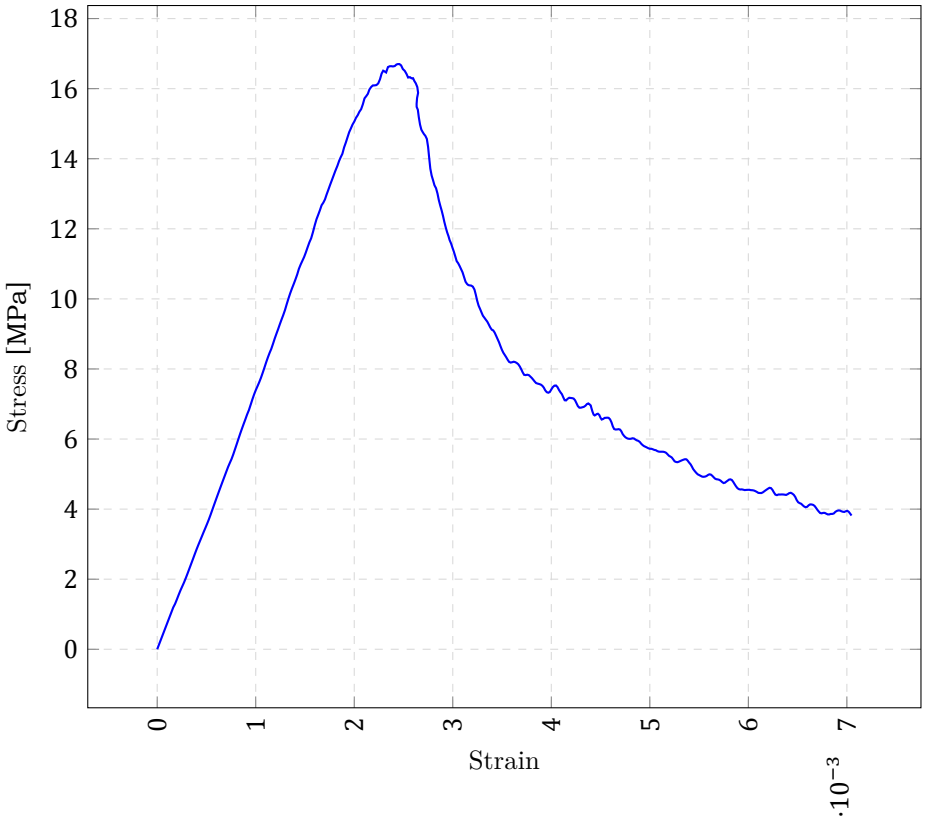

Figure 4.4: Stress versus strain for UCS simulation.

4.2. Conclusion

The BTS test and UCS test are to be fitted separately. Fitting them both with one parameter set was not possible since the UCS/BTS ratio resulting from simulations was to low to reach an exact fit. The rock type which is approached (limestone Savionnière) is a low strength rock (20<MPa). In this research higher strength rocks (UCS 90MPa) were approached as well. However the strain response for the BTS test was incorrect as strain at failure is too high and the bulk material stress-strain response is non-linear. Therefore this model cannot be used to simulate higher strength rocks.

5

Numerical simulation of ODC

In the beginning of this chapter the simulation properties and assumptions of the ODC simulations will be discussed. Afterwards the effects of the kinematics of the ODC and particle size on the cutting force is studied. Furthermore, the results of those simulations and corresponding discussion will be given. The chapter will end with a discussion of the DEM results.

5.1. Modelling approach

To model the oscillatory disc cutter it is important to make decisions based on simulation time. The ODC is supposed to simulate for a far longer time (between 2.5 and 13 days) than the UCS/BTS test. Because of this reason only few simulations are done. The parameters, which affect the computation time are the particle radius, the forward velocity of the disc and the radius of the oscillating disc cutter. The particle size affects the number of particles and the time step. Smaller particles will result in a smaller time step and more particles required to fill the geometry. Both results will affect the computation time significantly. The disc radius and forward velocity is important, since they affect the simulation time. A smaller disc forward velocity or smaller disc radius will increase simulation time, since it takes longer for the disc to penetrate the particle assembly. It is however important to check whether velocities in the simulation are not too high. Too high velocities can result in an unstable simulation. This instability is created, since the phenomena that occur at speed of sound of the particle assembly are not captured in this model. Simulation results will be compared with experiments done by Detournay and Dehkhoda [29]. Only comparison is made to simulations with the highest cutter velocity. In the experiments the disc radius is small (1cm).

Since this model is not fully able to simulate reality as an effect of computational time limits and model limitations, assumptions and simplification are needed for the ODC simulation, these assumptions are discussed below:

Tensile fracture is dominating

The value for the BTS and UCS for the particle assembly could not be calibrated simultaneously. The UCS and BTS were therefore calibrated separately. This resulted in two bonded parameter set, one for the UCS simulation and one for the BTS simulation. The ratio between the UCS and BTS for each bonded parameter set is found to be respectively 6.2 and 6.3. Doing the ODC simulation tests for both UCS and BTS will therefore, probably only result in a shift in cutting forces. This assumption will be checked in this chapter. Furthermore, the cutting depth is large enough to give mainly tensile failure. Therefore, it is chosen to take the BTS bonded parameter set for simulating the ODC in order to reduce the number of simulations.

No gravity

Gravity is neglected in the ODC simulation. Gravity only affect the simulation slightly since particle mass is quite small. The forces on the disc are significantly higher than the forces resulting from gravity, therefore gravity can be neglected as its impact to simulation outputs is negligible. It is found that

removing gravity is also beneficial for the visualization of the particles, since loose particles are less likely to stay near the disc cutter.

Global damping

In reality motions are damped due to internal friction and wave scattering [27]. However in this model motions are only damped by the contact model. The contact model exist between particles and between the disc and the particles. Since the total damping of the contact model only covers a small portion of realistic damping a numerical damping term is introduced. This numerical damping term only affects the particle accelerations. The coefficient of numerical damping used during this thesis is 0.7. This value is well accepted in DEM rock cutting.

Slip on disc cutter

In literature the disc is able to rotate freely around the disc centre axis. To simulate this multi-body dynamics is to be added to the model. Due to complicity this is not implemented in the simulations. The model therefore creates an extra moment T_2 around the disc centre, as can be seen in figure 5.1. The friction, which creates the extra moment is mostly caused by particles, which are pushed against the edge of the disc. This occurs, due to the point contact between the spherical particles and the disc. Loose debris on top of the disc cutter, will loose contact between the disc easily and therefore not create large frictional forces. The significance of the moment T_2 is to be checked.

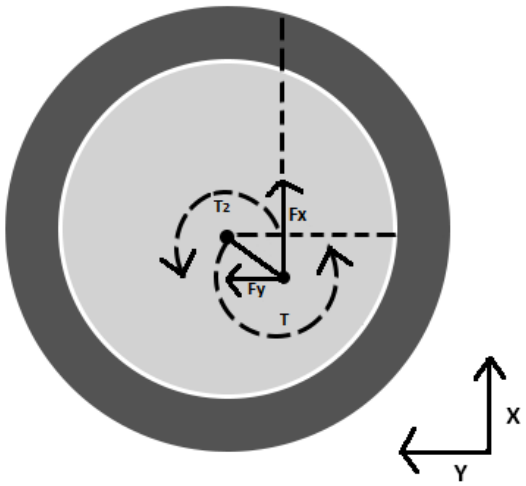

Figure 5.1: Free body diagram (during ODC simulation).

5.2. Geometry ODC simulation

The simulation for the ODC is done by creating an assembly of 32k particles. The assembly consist of a box of 7x7x2cm with porosity 0.25. This small size is selected, since larger sizes require more computation time. The cutting depth is 4mm. This is approximately three particles of cutting depth. The disc cutter consist of a cone with two diameters of 1 and 2 cm. The corresponding time step is $6.3e^{-7}$. When the clearance angle is 0 degrees the rake angle is 30 degrees. The tool will not change shape in all the simulations. For the rotation an eccentric oscillation is applied to the cone.

The dimensions of the assembly are determined by trial and error. Different assembly sizes are tried until the cracks no longer come near the sides of the assembly. Therefore, simulations are also needed to achieve a balance between kinematics, geometry and simulation time. Damage is taken as a parameter to control whether a simulation is acceptable. Simulations where, too much damage toward the

boundary layers or breakage of the assembly into multiple pieces occurred are disregarded. In figure 5.2 the plates holding the assembly in place can be seen. These plates are necessary as boundary condition, since the assembly will be pushed in the bottom right corner of the boundary, as seen in figure 5.2. Instead of using plates it is also possible to fix certain particles. In EDEM this can be done through the API called particle-body force.

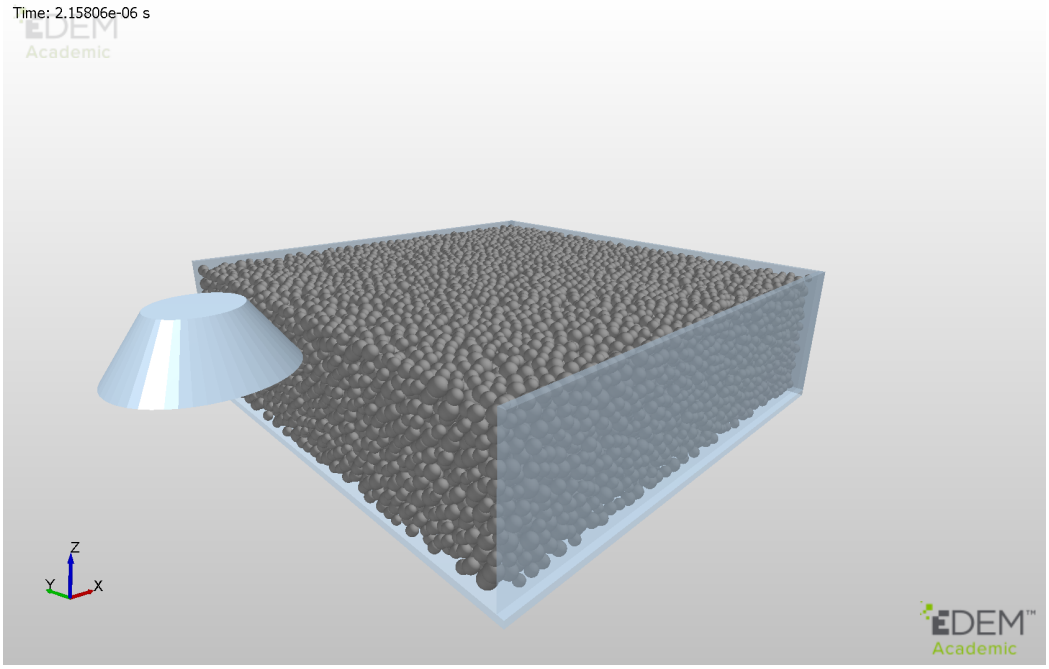

Figure 5.2: ODC simulation set-up [20].

The contact model between the geometry and particles is the Herz-Mindlin contact model shown in Appendix A.

5.3. Simulation test matrix

The need for the simulations is to study the effects of different kinematics of the ODC on the cutting forces in X,Y,Z direction. In table 5.1 the simulation matrix for the ODC is shown. To give a better view on the kinematics and properties studied in these simulations, they will be explained with corresponding simulation number below. Simulations 1 up to and including 7 and 12 are done to give more insight in the effect of the randomly generated assembly. Eight different particle assemblies are generated and tested, the results are presented in chapter 3.5. Afterwards, one of the simulation properties studied is the clearance angle of the tool. Simulations 8 an 9 will be done to investigate the clearance angle, one without a clearance angle and another one with a clearance angle of 9 degrees, as can be seen in figure 5.3. Secondly, the effect of the oscillation frequency will be simulated. From literature it is seen that for higher oscillation speeds the average force on the disc can be reduced [7]. This statement will be checked by doing simulations 10 up to and including 14. Another kinematic input parameter is the eccentricity. The eccentricity is defined as the ratio of the distance between the oscillation center and disc center divided by the disc radius. The disc cutter rotates slightly out of its center. By adjusting this distance to the center (eccentricity) different movement paths of the disc can be created. The disc can for example, move backwards during a rotation cycle. The effect of the eccentricity and backwards movement is studies by comparing simulations 11,15 and 16. Also the linear cutting test without oscillation can be compared for two different forward velocities. This is done by comparing simulations 9 and 10, the forward velocities are 0.1 and 0.5m/s respectively. Simulation number 17 is done to investigate the effect of the UCS calibrated bond input parameters instead of the BTS input parameters. The effect of the size of the particles is done in simulation number 18. To do this a smaller particle radius is chosen. After recalibrating the material parameters, the ODC is simulated with same kinematic parameters as in simulation 14. In the last simulation, number 19 parameters are chosen to be similar to practical tests done by Dehkhoda and Detournay [29]. This is done as a means to compare the bonded particle simulation to experimental values found in literature.

#	Eccentricity	Rotation speed $[2\pi/s]$	Forward speed $[m/s]$	Clearance angle $[deg]$	Computation time $[days]$
1-7	0.4	22.5	0.5	9	2.5
8	0.0	0	0.1	0	12.5
9	0.0	0	0.1	9	12.5
10	0.0	0	0.5	9	2.5
11	0.4	22.5	0.5	9	2.5
12	0.4	45	0.5	9	2.5
13	0.4	60	0.5	9	2.5
14	0.4	67.5	0.5	9	2.5
15	0.2	22.5	0.5	9	2.5
16	0.1	22.5	0.5	9	2.5
17(UCS)	0.4	22.5	0.5	9	2.5
18($< R_p$)	0.4	67.5	0.5	9	5.5
19	0.4	4.5	0.1	9	12.5

Table 5.1: List of simulations and their parameters.

5.4. Results of kinematics on cutting forces

As discussed in chapter 5.3, the effects of clearance angle, linear cutter velocity, eccentricity and oscillation frequency on cutting forces are simulated. In this chapter the results of those simulations are presented. The same bonded particle properties and assembly generation procedure is used as in the previous chapter. This means that, the assembly has a BTS of 1.79 MPa and a UCS of 11.1 MPa. After the kinematic results the effect of the UCS calibrated material and the size of the particle is presented. It should be noted, that at the beginning of the simulation the disc needs to penetrate the rock and therefore forces are different. In this section this start-up phase is shown in the graphs as a shaded area.

5.4.1. Clearance angle

The placement of the tool can affect the simulation significantly, as seen in the theory of chapter 2.1. Two simulations were done, one with a clearance angle of zero degrees and one with a clearance angle of 9 degrees. It is important to note that the whole tool is rotated, so that the rake angle is 30 and 21 degrees respectively. In figure 5.3 the rake and clearance angle are described by angle 1 and 2 respectively. The XYZ axis are the same as mentioned before in figure 5.2.

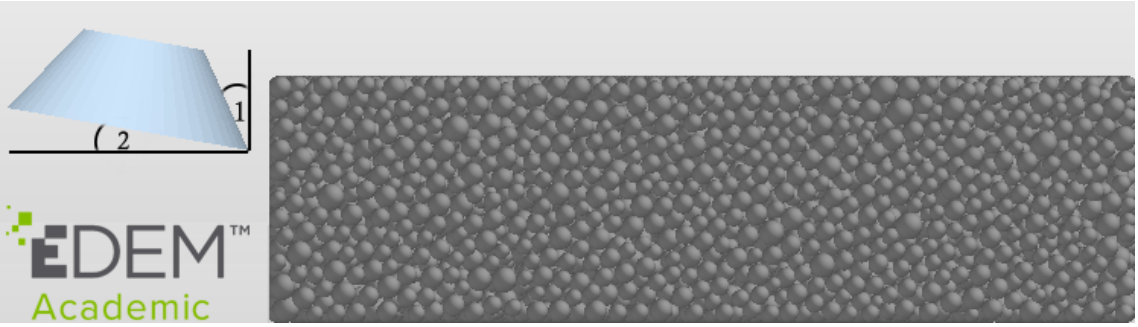

Figure 5.3: xz view (parallel to positive y axis) [20].

The normal force is in positive Z-direction (perpendicular to the cutting direction) for both clearance angles shown in the figure 5.4. The simulations are done by linear cutting (no disc oscillation).

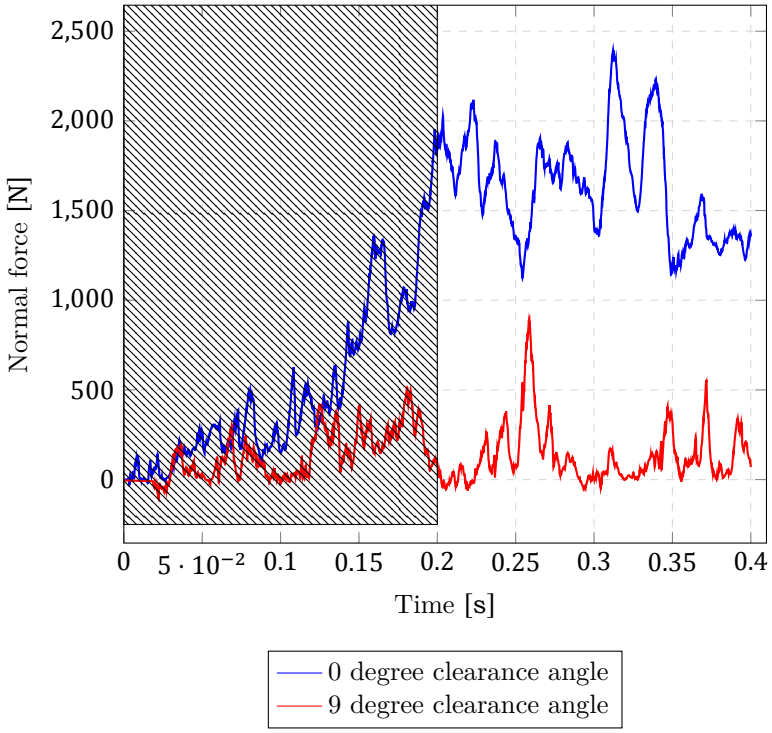

Figure 5.4: Normal force at different clearance angles. Disc radius is 10mm, disc forward velocity is 0.1m/s.

Since particles can be compressed underneath the tool, the contact model will be able to create large forces if this occurs. In case of a clearance angle of zero degrees this effect increases significantly. Furthermore, it can be seen that for an angle of zero degrees, forces in the normal direction gradually increase before reaching an almost stable force. This occurs due to the particles being stuck beneath the tool and therefore particles are less likely to flow away from the cutter. with a clearance angle of 9 degrees the particles have more space and are less likely to be stuck. The main difference in normal force is therefore depended on the contact area. At 9 degrees clearance angle the contact area exists of a edge instead of the contact plane, which exist at 0 degrees clearance angle.

At 0.26m for the 9 degree clearance angle, a high peak force can be seen. in the simulation peaks exist when tensile cracks are created. At this peak the tensile crack is quite big, resulting in a large chip. in figure 5.5 and 5.6 the damage parameter (damaged bonds over initial bonds) is shown before and after the peak. Other particle debris/chips is removed in the figures to give better view on the creation of the chip and cracks.

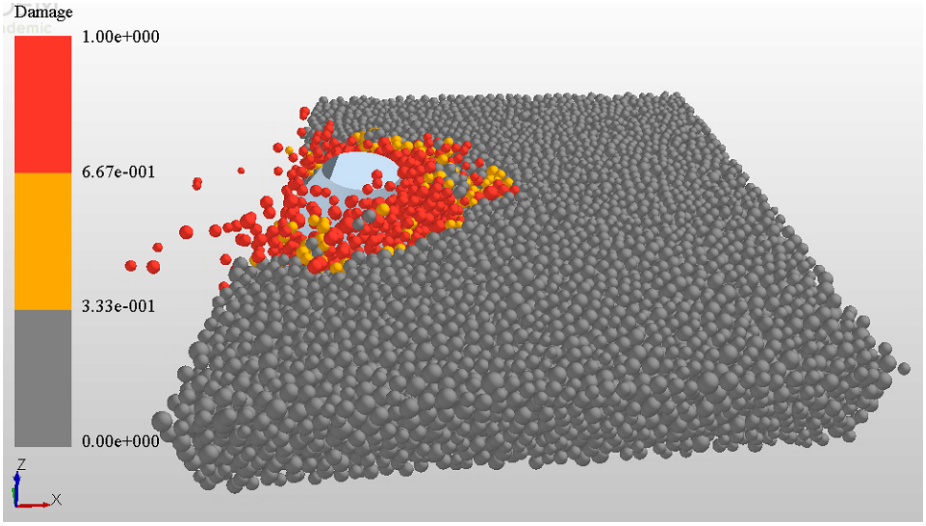

Figure 5.5: Damage before force peak at 0.26m, 9 degree clearance angle, time 0.2591s [20].

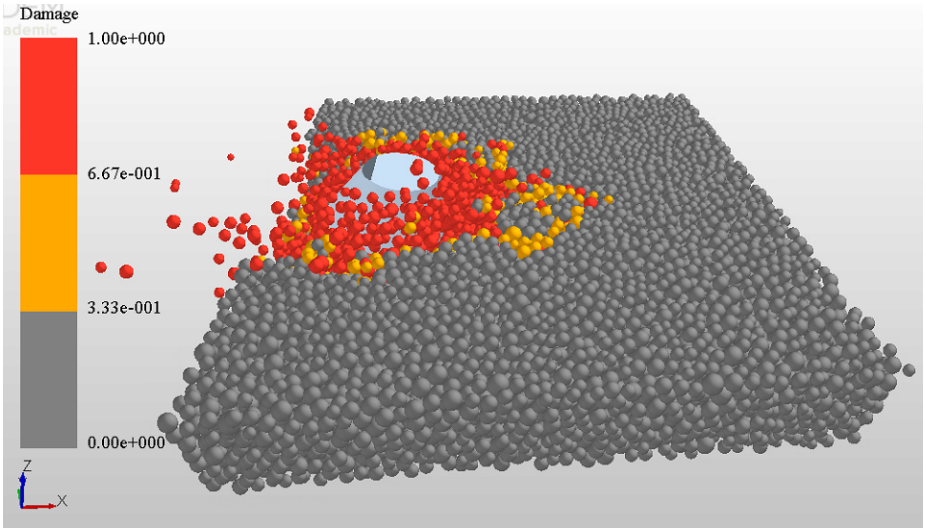

Figure 5.6: Damage after force peak at 0.26m, 9 degree clearance angle, time 0.2611s [20].

5.4.2. Oscillation frequency

Oscillation speed is one of the most important parameters for the ODC. Different oscillation speeds are tested at a linear velocity of 0.5m/s, disc radius 10mm, eccentricity 4mm and cutting depth 4mm. Figure 5.7 shows the average cutting force at different oscillation speeds. A force reduction can be found by increasing oscillation speed. Figure 5.7 suggests an asymptote which, can be found for rotation speeds higher than 3500 rotations per minute.

It was not possible to confirm the asymptote doing simulations. Higher oscillation speeds than 4050 rotations per minute are not possible in these simulations, since the velocities in the model will go near the speed of sound of the DEM assembly. Effect of velocities higher than the speed of sound are not included in this bonded particle model and should therefore be avoided. At 4050 rpm the speed around the disc edge is approximately 4.2m/s.

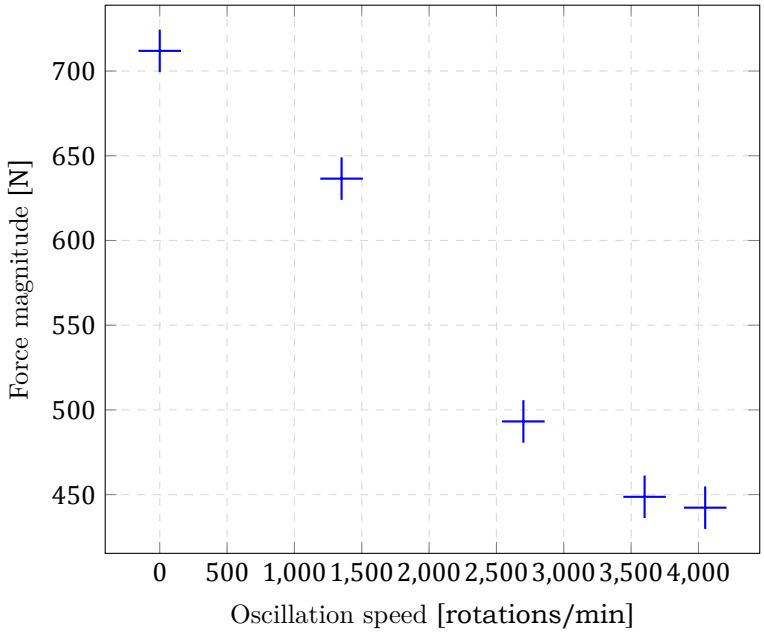

Figure 5.7: Force (magnitude) for different oscillation speed. Disc radius is 10mm, disc forward velocity is 0.5m/s, and eccentricity is 0.4.

In chapter 2.2 a similar graph can be found from experimental data shown by Kovalyshen [7]. The difference between the simulation results and those of Kovalyshen is that the simulations show a larger oscillation speed before the asymptote is reached. Kovalyshen found the asymptote at 30Hz and the simulations found the asymptote at 50Hz. However this comparison is not valid since different disc radius and linear velocities of the disc are used. To compare them the following dimensionless value is investigated.

$$\nu = \frac{V}{e * \omega} \tag{5.1}$$

with, distance between disc center and rotation axis e. ν gives a ratio between the forward velocity and linear velocity of the eccentric rotation of the disc [7]. This dimensionless value can be used to distinguish regimes in the contact between the rock and the disc. A value below 1 suggest that the disc loses contact with the rock during a cycle. The value of ν when the asymptote is reached for the simulations is 0.66 approximately in the simulations. Kovalyshen found ν to be 0.67 when reaching an asymptote. This suggest that an optimum between cutting forces and kinematics can be found using the dimensionless number ν.

In the figures 5.8 and 5.9 the force (magnitude) for different oscillation speeds are shown. In the graphs a horizontal line is added to show the average force. Also an area in the graph is highlighted. This area is, where the disc still needs to penetrate the rock until the full diameter of the disc is in the rock. It can be seen throughout the simulations that the forces are higher for an ODC when initially penetrating an undamaged assembly. This might be explained by the ODC creating pre cracks, which lower cutting forces for the next cutting cycle.

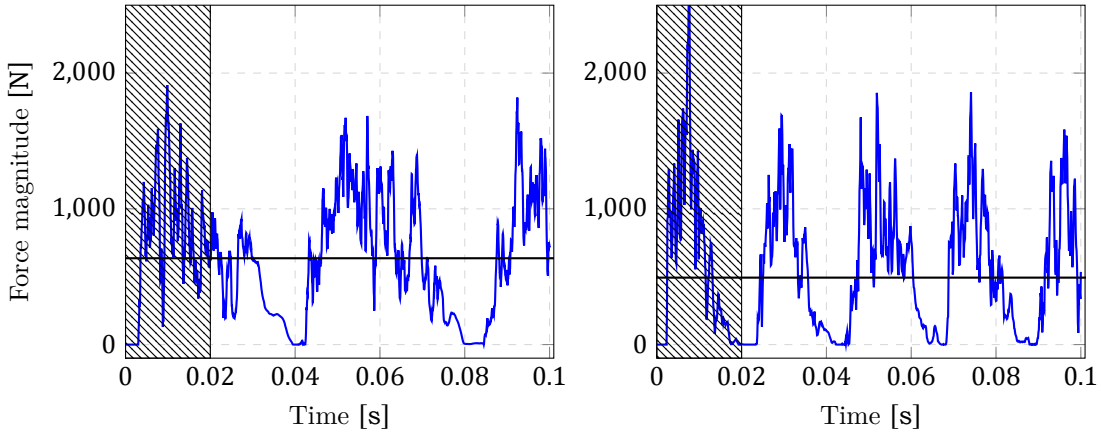

(a) 1350 rotations/min. Average force is 636N. (b) 2700 rotations/min. Average force is 493.2N.

Figure 5.8: Force (magnitude) for different oscillation speeds. (Disc radius is 10mm, disc forward velocity is 0.5m/s, and eccentricity is 0.4)

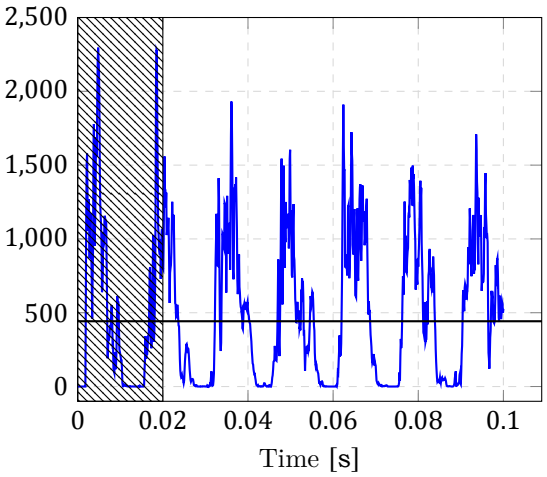

Figure 5.9: Force (magnitude) over simulation time for 4050 rotations/min. Average force is 442.3N. (Disc radius is 10mm, disc forward velocity is 0.5m/s, and eccentricity is 0.4)

The highest oscillation speed gives a reduction of 38% of the average force magnitude. The force drop is found to be approximately equal in X,Y and Z direction as can be seen in Appendix C. It is more important, to investigate where this force reduction comes from. Peak forces stay the same when oscillating speed increases, while the average force drop. This is however counter intuitive, since a lower average force suggest, that less energy is needed for the cutting process. However the ODC also need to provide torsion which will also require energy.

To get more information about the cracks that occur in the particle assembly during cutting, the broken bonds are to be investigated. The broken bonds can occur due to shear or tensile failure. For the ODC the failure is mainly tensile (around 99%). Figure 5.10 shows the tensile failure at low oscillation speed and at high oscillation speed. It can be seen that most failure occurs when the slope in the graph gets steep, afterwards there is a moment where almost no failure occurs. These steep lines at which failure occurs, occur when the forces are highest as seen at the peaks in the figures 5.8 and 5.9. These high peak forces therefore, initiate many tensile cracks.

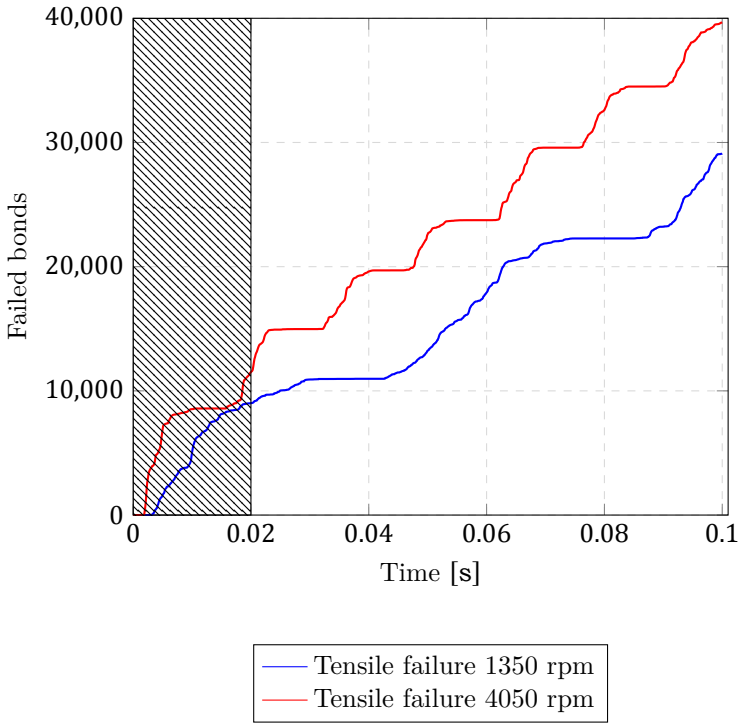

Figure 5.10: Bond failure at 1350 and 4050 rotations/min. (Disc radius is 10mm, disc forward velocity is 0.5m/s, and eccentricity is 0.4)

5.4.3. Eccentricity

Another parameter that is investigated is the eccentricity. This parameter affects the center of rotation for the disc cutter. Since the disc cutter is rotated off center it's motion will change depending on the distance between the center of the disc and the point of rotation. The eccentricity is described as the distance between the center of the disc and the point of rotation divided by the disc radius (for these simulations 10mm). In figures 5.11 and 5.12 the movement of the disc center with small eccentricity and large eccentricity is shown.

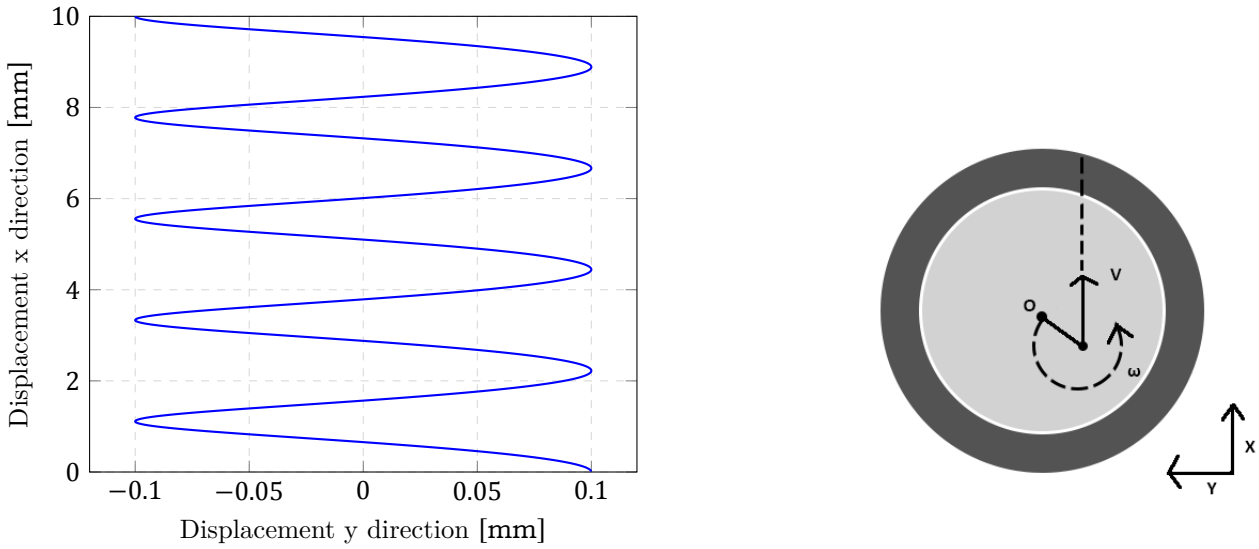

Figure 5.11: Disc center position (Disc radius is 10mm, disc forward velocity is 0.5m/s, oscillation speed is 1350 rpm and eccentricity is 0.1)

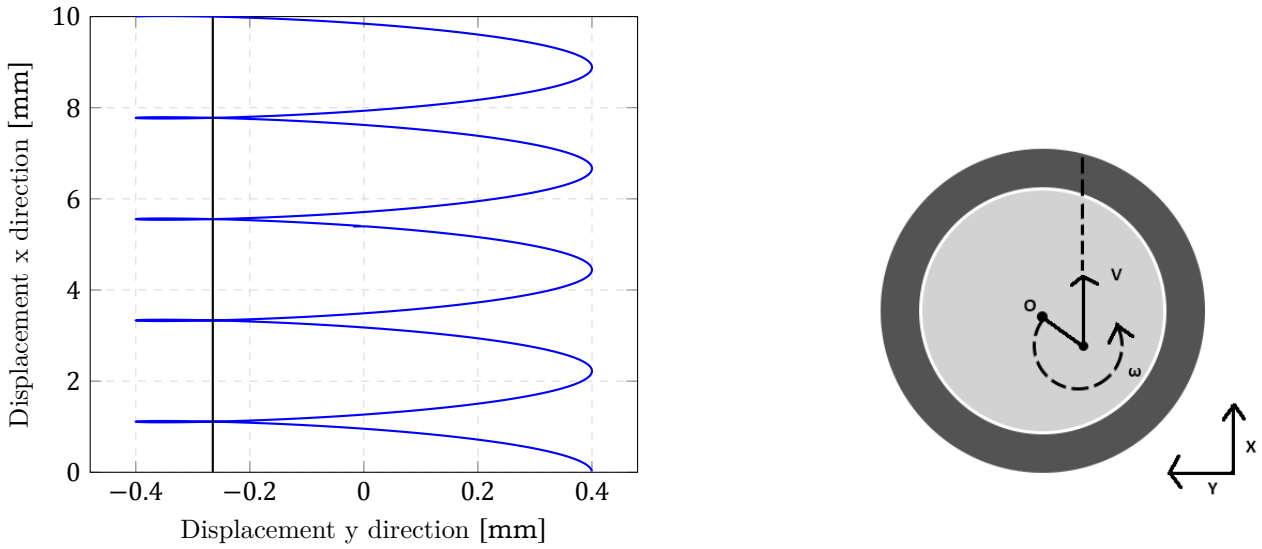

Figure 5.12: Disc center position. Vertical line shows discontinuous contact rock and disc. (Disc radius is 10mm, disc forward velocity is 0.5m/s, oscillation speed is 1350 rpm and eccentricity is 0.4)

Here different movements can be seen. In figure 5.11 the disc is always in contact with the rock. in figure 5.12 the eccentricity is larger and the disc moves backwards when the horizontal displacement reaches -0.265mm till -0.4mm. This backwards movement is necessary to achieve force reduction when using an ODC according to literature [7].

It is found that the force (magnitude) only decreases when backwards movement exist. This effect can be seen in figures 5.13 and 5.14. At 0.1 eccentricity the average force are slightly higher than normal linear cutting with no oscillation. At 0.2 eccentricity the average force rises even more. This is normal since the eccentric movement removes more rock in comparison to linear cutting with no oscillation. When the backwards movement exists at an eccentricity of 0.4 the average force lowers at the cost of slightly higher peak forces.

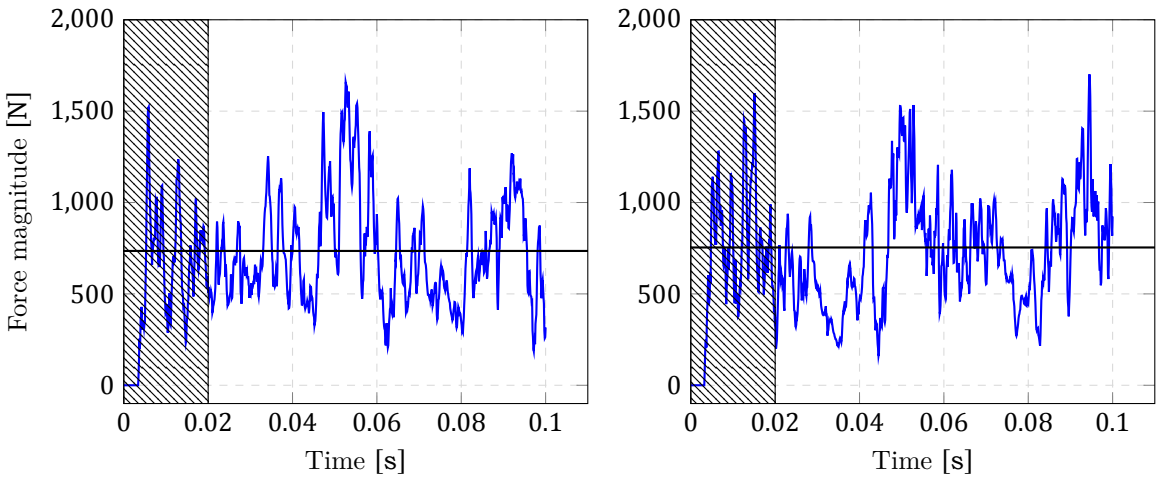

(a) Eccentricity is 0.1. Average force 735N.

(b) Eccentricity is 0.2. Average force 754N.

Figure 5.13: Force (magnitude) during cutting for different eccentricity. Disc radius is 10mm and disc forward speed is 0.5m/s.

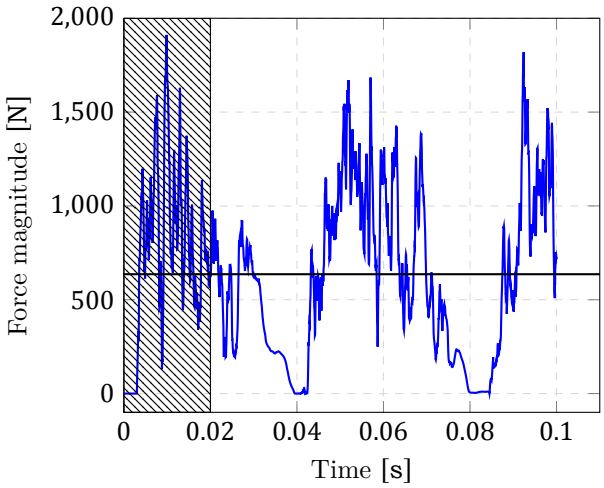

Figure 5.14: Force (magnitude) during cutting, eccentricity is 0.4. Disc radius is 10mm, disc forward speed is 0.5m/s and oscillation speed is 1350 rpm. Average force 636N.

Figure 5.14 shows the minimum eccentricity needed in order to get a decrease in force(magnitude). The disc periodically loses contact with the rock. The average force for 0.1, 0.2 and 0.4 eccentricity is 735N, 754N and 636N respectively. For linear cutting with no oscillation the average force is 712N, this is reasonable since less rock is removed by linear cutting. In appendix B the failure of the bonds can be seen for different eccentricities. Here it is visible that the slope is steeper when backwards movement exists at 0.4 eccentricity. This means more tensile fractures occurs in the assembly. Bond failure will increase significantly. This increase is not due to the increased rock removal rate, because of the larger rotations. In figure 1 and 2 from appendix B this does not occur as well. The increase of failure, which occurs when backward motion exist is probably due to the contact area between the rock. The contact area during an oscillation cycle becomes smaller if backward motion occurs. The smaller contact area increases stress in the bonds near the ODC, which is beneficial for creating tensile failure.

5.4.4. Linear cutter velocity

The linear velocity is found to have a significant effect on the cutting forces. The linear velocity is tested without oscillation, so it is similar to linear cutting theory presented in section 2.1. The only difference is the shape of the tool, which is still quite similar to a chisel. In figure 5.15 the magnitude of the force is shown for 0.1m/s and 0.5m/s. For the disc it is found that increasing the linear velocity five times from 0.1m/s to 0.5m/s effects the forces significantly. The forces in all direction are multiplied by approximately a factor 2.2. This is contrary to the theory of section 2.1, where velocity does not affect the cutting force. However, in practice it is found that increasing the velocity increases cutting forces. The increase found in the simulations is however too significant. The inertial forces in the simulation are probably too high. Still, there are simulations done with 0.5m/s, since the total computation time for this research is limited.

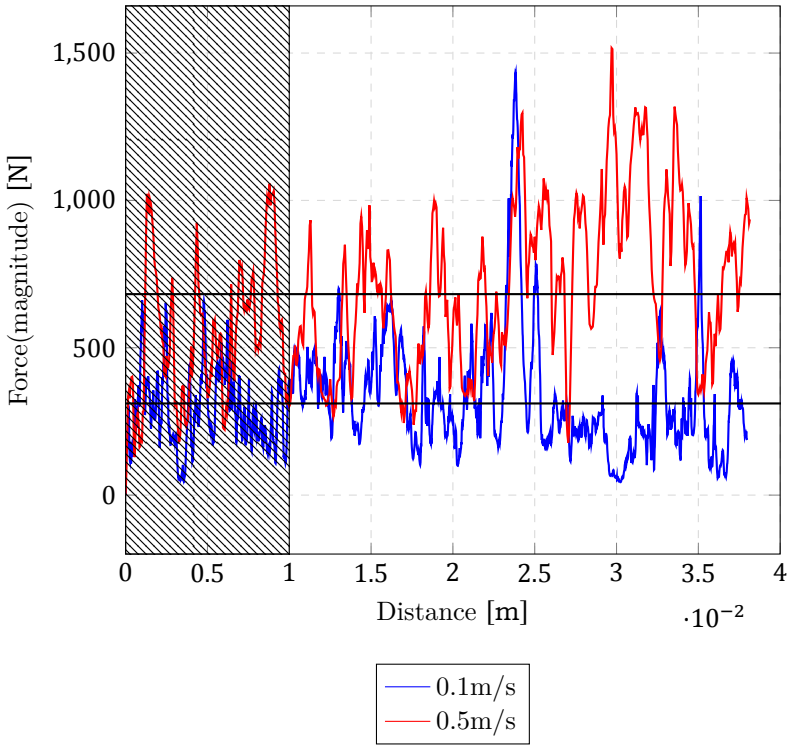

Figure 5.15: Force (magnitude) for linear cutting at 0.1m/s (average is 311N) and 0.5m/s (average is 3682N), disc radius is 10mm.

5.4.5. UCS calibrated material

As mentioned before the UCS of the particle assembly was not equal to that of Detournay and Dehkhoda's rock samples. Matching both the UCS and BTS was not possible since the bonded model could not achieve these properties. However since tensile fracture is dominant in case of ODC the BTS was used. It is still important to check what the effect of a lower UCS for the particle assembly will have on the forces. Therefore an assembly is created where the UCS is matched instead of the BTS. The BTS in this case is also higher and is 2.65 MPa. To achieve this assembly properties both the tensile and shear bond strength was increased to 34MPa. For this test the forces increase, which can be expected since the BTS value also increased and tensile cracks require higher forces to initiate. The average force found was 942.9N for the ODC test with UCS calibrated bonded parameters. For the BTS bonded parameter set the average force is found to be 636N. For the UCS bonded parameter set it is found that the peaks of the force increase significantly (factor 1.8).

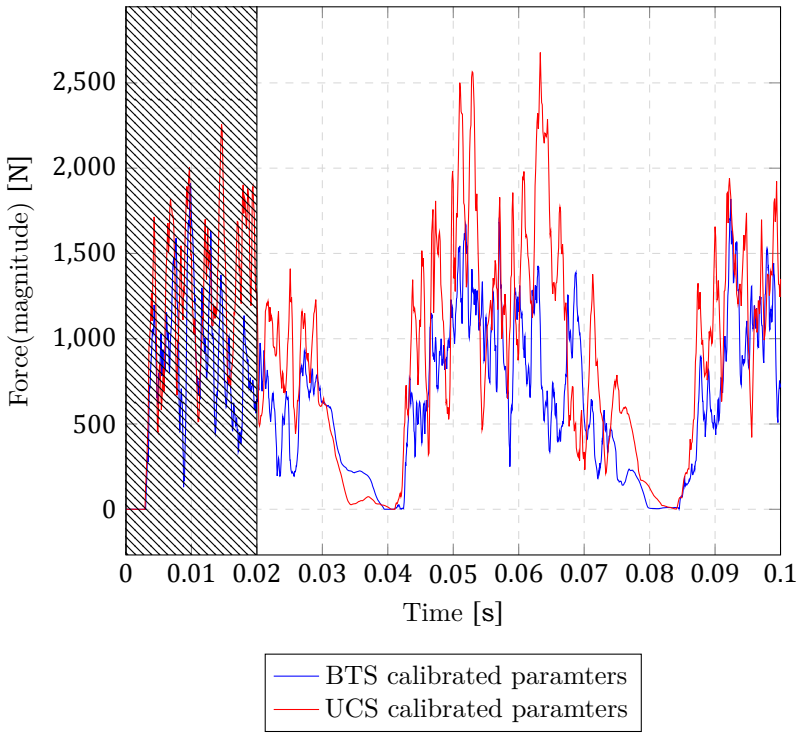

Figure 5.16: Total force for BTS and UCS bonded parameter set. (Disc radius is 10mm, eccentricity is 0.4, forward velocity 0.5m/s and oscillation speed 1350rpm)

5.4.6. Effect of particle size

To get a better understanding of the particle size, one simulation is done with a smaller particle radius. In this simulation the average cutting depth of three particles is increased to four particles. In order to do cutting experiments the BTS value is to be recalibrated. The number of particles increased from 32k to 71k. It is found that the BTS is 1.8MPa, when the shear and tensile bond strength is 19MPa. The bond elastic modulus is 15GPa. The bond strength is therefore almost decreased by 21%. The UCS found is 10.0 MPa, which is slightly lower. After recalibrating the BTS, an ODC simulation is done. The results can be seen in figure 5.17. The force (magnitude) is still quite similar. More tests at different particle sizes are needed to confirm this. However, doing those tests is quite time consuming, since the material is to be recalibrated. The peaks seen in the figure seem to be less extreme for the 71k particle assembly. This suggests, that the accuracy of the data can be increased by decreasing particles size. However, the limitation is still the computation time, which increases significantly, when reducing the particle radius.

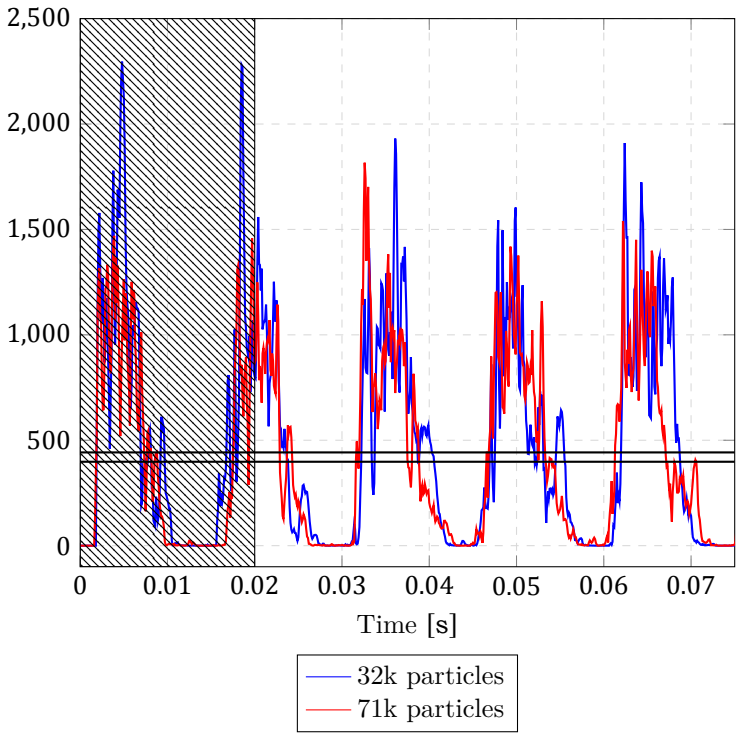

Figure 5.17: Force (magnitude) over simulation time for 4050 rotations/min, 32k particles (average 442N) and 71k particles particles (average 398N). (Disc radius is 10mm, disc forward velocity is 0.5m/s, and eccentricity is 0.4)

5.5. Comparison simulations and model of Dehkhoda & Detournay

Dehkhoda and Detournay did experiments to validate their ODC model [29]. The model fits well with their experimental data, as can be seen in appendix D. There is however a limitation to the model. The model can not predict forces normal to the cutting direction (Z-direction). One of the experiments performed by Dehkhoda and Detournay is simulated with the bonded particle model in order to compare the results with the model of Dehkhoda and Detournay. For the simulation the particle assembly will have the same BTS value as the experiment. Due to difficult calibration of the bonded particle model the UCS value will be slightly lower as mentioned in chapter 4. In figure 5.18 and 5.19 a comparison between the model and simulation data can be seen for forces in the direction of the cutter (X-direction) and lateral forces (Y-direction). It is chosen to compare with the model of Detournay and Dekhoda, since the experimental data is not available and in their paper it is already shown that the experimental data follows the data of the model.

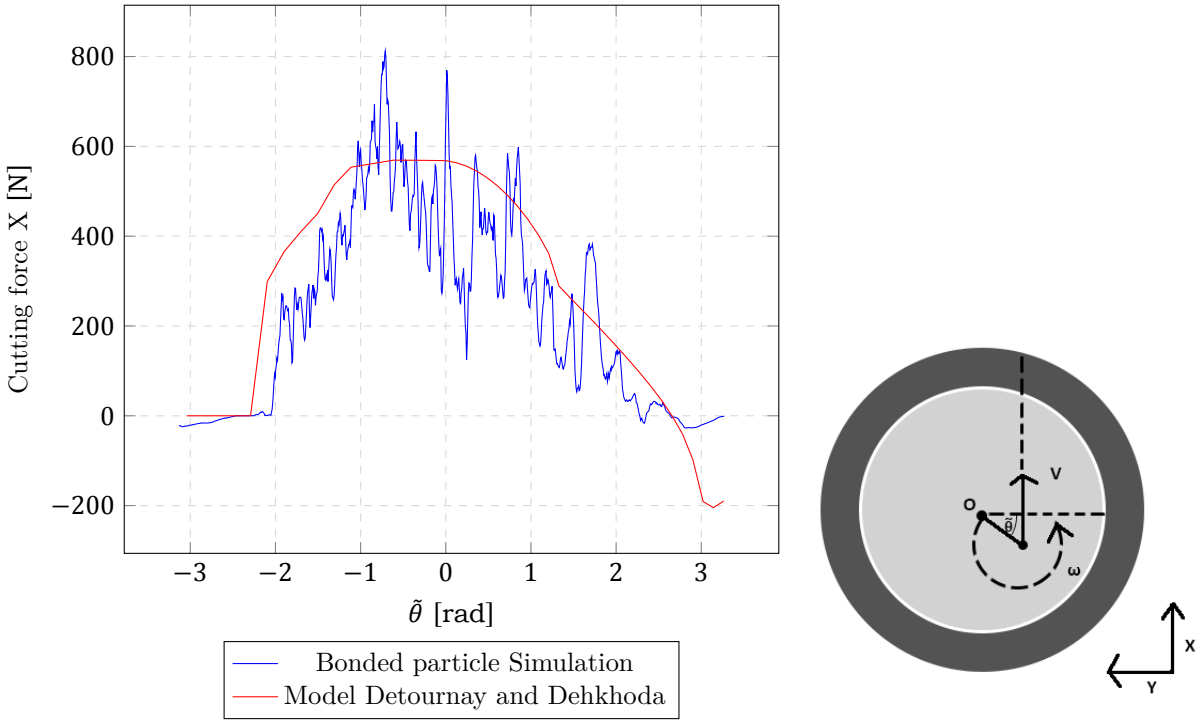

Figure 5.18: Comparison between model of Detournay and Dehkhoda and simulation results. Cutting forces (in X direction) are displayed over one actuation cycle. (Eccentricity is 0.4, forward velocity, oscillation speed 0.1 m/s and 4.5 rotations/s)

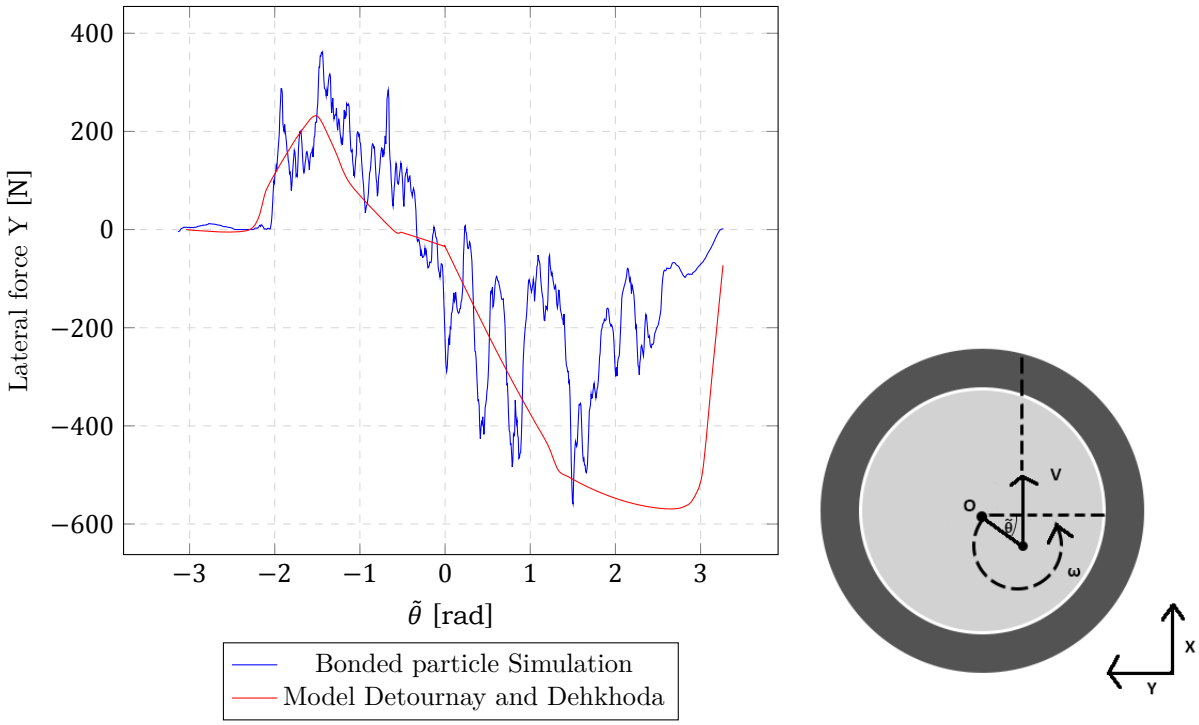

Figure 5.19: Comparison between model of Detournay and Dehkhoda and simulation results. Cutting forces (in Y direction) are displayed over one actuation cycle. (Eccentricity is 0.4, forward velocity, oscillation speed 0.1 m/s and 4.5 rotations/s)

The data is noisy but the trend is followed by the data of the simulations. It can however be seen, that on the end the force in the simulations flattens out faster. This could also be seen in the experimental data from Dehkhoda and Detournay. The model assumes that the rock only will be removed at the position of the disc cutter. In the simulations chips of rock are removed and therefore the contact time during a cycle between the rock and the disc cutter can be shorter. For this reason the force in the simulation flattens out faster at the end of the actuation cycle. The same can be said of the beginning of the cycle, here due to the same reason the disc in the simulation can contact the rock at a later time step.

It should be noted that the model does not allow rotation around the disc centre, as mentioned before in section 5.1. The influence of the extra (slip)moment T_2 therefore is to be checked. This is done by running a simulation, where the friction coefficient of the disc's contact model is set to be zero. By doing this the moment T_2 is removed. However, it should be noted that the rotation and inertia of the disc is still not taken into account. This will require multi-body dynamics, to simulate the dynamics between the disc and the particles. From the simulation data it is found that the magnitude of the force is decreased by 29%. Furthermore, the trend does not change.

5.6. Specific energy for ODC

As stated in chapter 2.1 the specific energy is described as the ratio of power over production [11]. In case of an ODC the specific energy differs, since an oscillation is added and the rock volume removed is more complicated. Below the formula for specific energy of an ODC is explained:

$$E_{sp} = \frac{F_x * V + T * \omega}{Q} \tag{5.2}$$

with, specific energy E_{sp}, rock volume removed Q and Torsion T. The formula is different for an ODC, since torsion is needed to rotate the disc. For the simulations the determination of the specific energy is complicated. The torque signal is extremely noisy, which prevents accurate determination of the specific energy. Furthermore, the torque often drops to zero. This probably occurs, since frictional forces are not yet correctly implemented in the model. Torsion is mainly needed to overcome frictional forces in this model, since particles are spherical. The spherical particles create a point contact and therefore are more likely to lose contact between the disc cutter. To improve the determination of torsion, smaller particles and non-spherical particle are required. However from the formula, it can be seen that increasing oscillation speed increases specific energy. Since forces in the cutting direction can drop for higher oscillation speeds there is presumably an optimum setting for the specific energy of the ODC.

Still, it is possible to make a guess about the change of specific energy by dividing the volume of rock removed by the amount of broken bonds. This is a rough method that, specifies the removed cubic meter of rock per broken bond. A lower value means less specific energy is required. The volume of rock removed is approximated by the ODC kinematics only, due to simplicity. In figure 5.20 this ratio is shown for the different oscillation frequencies and eccentricities, presented in section 5.4.2. It can be seen that, the specific energy drops slightly by increasing oscillation speed for the chosen kinematic parameters. Still, it is to be noted that only few tests are done to give this insight. The eccentricity is also, found to influence the specific energy. However, an optimum is seen at low (0.0) and high (0.4) eccentricity. Which suggests, that using high eccentricity might be beneficial (combined with the results from section 5.4.3).

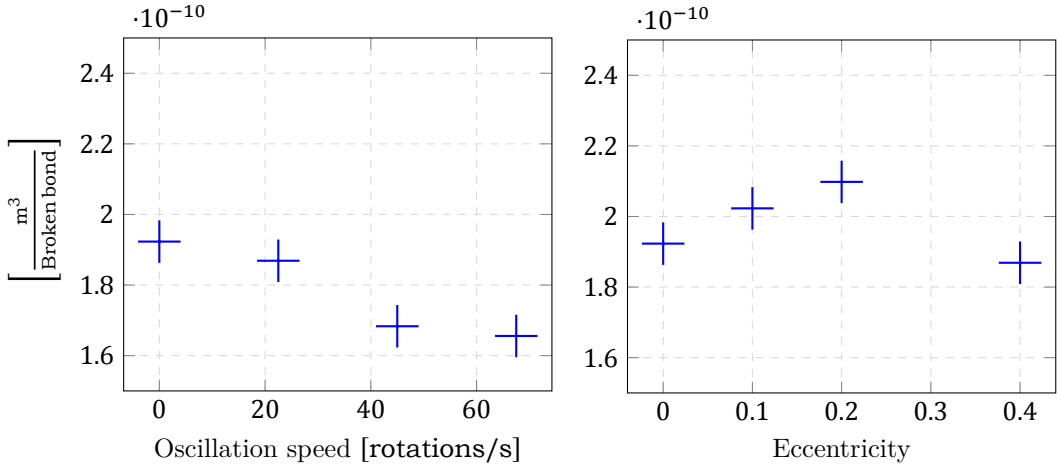

(a) For different oscillation speed. Eccentricity is 0.4.

(b) For different eccentricity. Oscillation speeds is 1350rpm.

Figure 5.20: Removed cubic meter of rock per broken bond. (Disc radius is 10mm, disc forward velocity is 0.5m/s)

5.6.1. Rock removal rate

Because of the eccentricity and oscillation more rock is removed by an ODC in comparison to a disc without oscillation. The rock removal rate is ratio between the volume of rock removed without and with oscillation. It is calculated from kinematics and assumes rock only fails at the positions at which the disc passes. In reality due to chips this number might be different. Some examples of the rock removal rates for are given in table 6.2. The cutting depth and disc radius are equal to those of section 5.4.2.

	Eccentricity	Rotation speed [2π/s]	Forward speed [m/s]	Rock removal rate
1	0.4	22.5	0.5	1.1889
2	0.4	45	0.5	1.371
3	0.4	67.5	0.5	1.397
4	0.2	67.5	0.5	1.184

Table 5.2: Rock removal rate for different type of kinematics.

5.7. Discussion

The bonded particle model generates data, which is noisys. The bonded particle model however, still gives good insight in the effect of the kinematics on the cutting process. Furthermore the bonded model gives the possibility to investigate bond failure. This property is linked to the fracturing in the assembly and gives more insight in why an ODC can lower cutting forces. It is found that most fractures appear when high peak forces occur together with a small contact area between the disc and the rock. The average cutting force will decrease if this occurs. For an ODC increasing the oscillation speed (up to a limit) will provide this positive effect. It should be mentioned that this result is in agreement to the theory explained in 2.1. In the formulas for the cutting force it can be seen that forces drop when the contact area between the rock and the cutter are decreased. However, in chapter 2.1 the volume of rock removed decreases. This is in contradiction to the simulations of the ODC in which the volume of rock removed increases. For the ODC smaller contact area also, creates higher stresses in the bonds which create tensile cracks and pre-damage for the next oscillation cycle. Another contradiction is found by comparing the graphs of section 2.2. The data from experiments shown in section 2.2, suggest that the peak force on the ODC drops. This is not found in the simulations. The reasoning behind this is that the experimental data is probably imprecise. The data already gives an average force. This can be seen in figure 2.10 by taking into account that the drop in force(to almost zero), when the disc looses contact with the rock can not be seen in the figure.

The backward movement of the disc, which can be seen in figure 5.12 together with high peak forces is found to be crucial in order to drop average cutting forces significantly. If backwards movement exist the cutting force can be lowered even more by increasing the oscillation speed. This benefit of force reduction, however seems to be limited, as shown in figure 5.7.

The eccentricity (distance between disc center and oscillation axis) is mainly needed to achieve backwards motion. This eccentricity is therefore to be determined after setting the oscillation and forward velocity of the disc cutter. Further increase of the distance between disc center and oscillation axis will decrease cutting forces even more but only slightly. Increasing this distance will however increase the rock removal rate, because of the larger rotation of the disc. But this will also create larger inertia forces in the cutting system and might therefore be not beneficial in the design of an ODC. However, high eccentricity (0.4) is found to be able to decrease the specific energy and might therefore still be interesting.

5.8. Practical implications

For practical implementation the ODC requires a surface on which it can pull in order to create tensile cracks. Therefore, the tool might be suitable for trenching. The ODC is able to reduce average forces while cutting, this might benefit the support frame of the ODC, which can be build smaller. Therefore, it will be easier to transport and insert the ODC at spots, which are difficult to reach.

The ODC has one other limitation and that is its linear forward velocity. The oscillation speeds needs to increase whenever the forward velocity of the disc increases. In case rock needs to be cut with high velocity, as in for example dredging the ODC requires extremely large oscillation speeds and is therefore not suitable. The high oscillation speeds will create high inertial forces due to the eccentric rotation. The frame that holds the ODC would need to damp out this inertial forces. Therefore, the forward speed of the disc cutter is crucial, when determining the suitability of the ODC. Overall the ODC has its benefits, but this must come at a cost of higher complexity of the mechanical actuation and disc kinematics. More moving parts, will make the mechanical system of the ODC more vulnerable.

6

Conclusions and recommendations

This research started with the purpose of getting a better understanding of oscillated disc cutters. To achieve this several research questions were formulated at the start of this research.

- What are the effects of the kinematic parameters of an oscillatory disc cutter on the cutting forces?
- How can eccentric oscillations help to improve the cutting equipment?

The approach to answer these two questions is to use a discrete element model. In such a model particles are used to simulate rock failure. The method to use DEM with bonded particles for rock cutting is still quite new. Most information regarding this topic is from recent years. Information of oscillated cutting with DEM is not found in literature. Therefore, two more research questions were added to this research.

- Is DEM suitable to simulate oscillatory cutting methods on rock?
- Do the forces found in oscillating disc cutter simulations agree with those from literature?

In the following sections the research questions will be answered. After the conclusions a section with recommendation for future research on this topic will be given.

6.1. Conclusions

The discrete element model gives good agreement with experiments from literature. Similar observations were found. For example, the DEM also found that higher oscillations speeds of the disc reduces average cutting forces significantly. The data however suggest a limit towards this drop of average cutting force. Besides this limit, certain conditions are to be met regarding the kinematics of an ODC in order to reduce average cutting forces. During a cycle the disc can lose contact with the rock. It can be said that the disc moves backwards at this moment. To achieve this the distance between the center of the disk and axis of rotation (eccentricity) together, with the oscillation and the discs linear forward speed must be chosen such, that during an oscillation cycle the disc shortly loses contact with the rock. If the disc does not move backwards during a cycle the reduction of the force average is not found.

To go more in depth on why the ODC needs backward motion (during a cycle) and high oscillations frequencies, the forces and bond breakage are evaluated. If the backward motion exists the forces will divert stronger. The contact area between the rock/assembly and the disc will also decrease, due to the backward motion. At first contact of the rock the force will peak. After this peak the force drops to zero until contact is made again. If the high force peak occurs, lots of bonds fail under tensile failure. In other words a significant number of tensile fractures are initiated in a short time, due to the small contact area and high cutting forces. These fractures are more than for linear cutting simulations. In linear cutting simulations fractures were found to gradually be created during the whole simulation.

The oscillation speed is found to affect the damage of bonds during a cycle. Higher oscillation speeds will create a force peak together with a even smaller contact area. This will eventually create more tensile fractures. Also, faster oscillation means more peaks and therefore more tensile fractures. The increase in oscillation speed is limited. At some point tensile fractures (bond failure) increase less for higher oscillation speeds. The tensile bond failure will not increase further and therefore increasing oscillation speeds will not change much. At this point the ODC will only remove tiny layers of rock during each oscillation cycle.

Eccentricity, which is defined as the distance between the center of the disc and axis of rotation should be chosen, based on the ratio between forward speed and oscillation speed. At low ratios, where backwards movement is not present it is useful to increase eccentricity. This might give backward motion and will increase the force peak during a cycle and thus is beneficial. Large eccentricity can however create more inertia in the system. This inertia needs to be dampened in the support of the cutter, too large eccentricity might therefore not be beneficial in the design of the ODC. However, large eccentricity might still be interesting as it can reduce the specific energy required to cut the rock.

Overall this research gives more insight in the ODC. Especially for designing an ODC it can help in choosing parameters like eccentricity, oscillation frequency and linear forward speed. DEM with bonded particles is found to be effective in order to simulate oscillating cutter behavior. The bonds are able to represent the accumulation of the damage that occurs from oscillating the disc cutter.

For practical application the ODC is suitable for rock cutting applications with low velocities. In case of high cutting velocities as in dredging the oscillation speed needs to be high in order to get the backwards movement, which is required to lower average cutting forces. The ODC can lower average cutting forces and therefore requires a smaller support structure, which is beneficial. Furthermore, the disc of the ODC is quite similar to a chisel. Therefore, since average cutting forces are lower for ODC's it might be possible that the ODC can cut rocks with higher UCS and/or BTS. The cost of this will be that the cutting mechanism is going to be more complex due to the actuation of the disc.

6.2. Recommendations

For future research the following improvements and recommendations are to be considered:

6.2.1. DEM-bonded particle method

Particles are quite large (1mm diameter) in respect to reality (nanometres). The cutting depth during simulations is only 3-4 particles. The effect of smaller particles on the cutting forces is still to be simulated. In order to do this the model needs to change from CPU to GPU based computing. GPU will decrease simulation time significantly (approximately 10 times).

The Hertz-Mindlin model is to be replaced with a linear spring model following the shear and normal stiffness of the bond. Due to the Hertz-Mindlin model, energy is lost when all bonds connected to a particle break. By calibrating the particle Young's modulus this reduction of energy is reduced. The reason why the Hertz-Mindlin contact model is used in this research is that, the linear contact model in EDEM is currently not configured in order to be used in combination with bonded particle models. It is not possible to set the shear and normal stiffness of the linear contact model to be equal to the shear and normal stiffness of the bond, without significantly increasing the computation time.

The cutting tool is rigid. In reality the ODC will likely have some bending within the mechanical construction. Effects of this are to be simulated, especially since kinematics is crucial for an ODC. The small eccentricity of the ODC might be counterfeit by elasticity. This can be done by using a multi-body dynamics coupling.

Assembly strength in this research is kept low UCS (<20MPa). The ODC should also be tested on higher strength rock (>60MPa). The bonded model becomes unsteady in this region and is not able to simulate higher strength rocks. In simulations it is found that typical stress-strain response and cracking patterns, like the shear plane disappear for assemblies with UCS higher than 60MPa. Furthermore, for low strength UCS assemblies used in this research, it is hard to get a UCS/BTS ratio higher than eight. For higher ratios typical fracture patterns in the UCS and BTS simulations are not found.

Simulations differ based on the particle assembly, which are randomly stacked. For UCS and BTS this forces don't seem to change much for different assemblies. But for the cutting simulation the randomness of the stacking influences the simulations results. More simulations are needed to give more insight on the significance of the assembly randomness.

The cutting tool (disc) is infinitely sharp. In reality there is a wearflat on the edge of the disc. This wearflat will probably increase normal forces. Simulations are to be done with a wearflat or bluntness.

The tool (disc) is rotated to test the effect of the clearance angle. However, this also changes the rake angle. More in depth simulations are needed to give more information on the influence of rake/clearance angle. Therefore different disc geometries are to be tested with variation of both angles.

Linear cutting simulations showed an increase in force when speeds were increased. In reality this occurs, but in the simulations this effect was too high. The inertia forces in the simulations are presumably the reason this occurs. Improvements are to be found to counter this occurrence.

6.2.2. Oscillated disc cutter

Mechanical and structural limitations are to be assessed for the ODC. Knowledge is needed on the maximum cutting force the ODC can withstand. The benefit of the ODC might disappear if the tool is able to deform plastically or elastically during cutting.

An economical assessment is needed for the ODC. The reduction of cutting force might be beneficial however, due to the complexity of the cutting tool it might not be economically feasible to use an ODC.

The wear on an ODC is still to be researched. The disc of the ODC can also be made to rotate freely around the disc center axis. It is not clear if this will lower wear rates. This rotation was not

incorporated in the simulations. Besides it is still not clear if the lowering of average cutting forces can reduce wear on an ODC.

Similar to conventional disc cutters, it might be possible to use multiple ODC. Only one ODC is investigated in this research. The effect of multiple interacting ODC is still to be investigated.

It might be possible that the reduction of the force is supported by the cutting force, which differs in direction. A weaker link in the material, might be affected which might help to initiate cracks. This statement is still to be checked, by doing either experiments or simulations.

Bibliography

[1] Deketh H.J.R. Wear of rock cutting tools. Laboratory experiments on the abrasivity of rock. PhD thesis, TU Delft, 1995.

[2] Technogenia. Dredging. URL http://www.technogenia.com/application/dredging/.

[3] van Kesteren W. Numerical simulations of crack bifurcation in the chip forming cutting process in rock. Rock and Ceramics, pages 505–524, 1995.

[4] Verhoef P.N.W. Wear of rock cutting tools : implications for the site investigation of rock dredging projects. Balkema, Rotterdam, 1st edition, 1997. ISBN 9789054104346.

[5] ESCO. Helilok points. URL http://www.escocorp.com/EN/products/Pages/helilok-points.aspx.

[6] Hood M. and Alehossein H. A development in rock cutting technology. International Journal of Rock Mechanics and Mining Sciences, 37(1):297–305, 2000. ISSN 13651609. doi: 10.1016/S1365-1609(99)00107-0.

[7] Kovalyshen Y. Analytical model of oscillatory disc cutting. International Journal of Rock Mechanics and Mining Sciences, 77:378–383, 2015. ISSN 13651609. doi: 10.1016/j.ijrmms.2015.04.015. URL http://dx.doi.org/10.1016/j.ijrmms.2015.04.015.

[8] Karekal S. Oscillating disc cutting technique for hard rock excavation. 47th US Rock Mechanics/Geomechanics Symposium, 2013.

[9] Evans I. The force required to cut coal with blunt wedges. International Journal of Rock Mechanics and Mining Sciences & Geomechanics Abstracts, 2(1):1–12, 1965. ISSN 01489062. doi: 10.1016/0148-9062(65)90018-5.

[10] Nishimatsu Y. The mechanics of rock cutting. 9:261–270, 1972.

[11] Miedema S. A. The Delft sand, clay & rock cutting model. IOS Press BV, Amsterdam, 2nd edition, 2015. ISBN 978-94-6186-249-5. doi: 10.3233.

[12] Dehkhoda S. and Detournay E. Mechanics of actuated disc cutting. Rock Mechanics and Rock Engineering, 50(2):465–483, 2017. ISSN 07232632. doi: 10.1007/s00603-016-1121-y.

[13] Thouless M.D., Evans A.G., Ashby M.F., and Hutchinson J.W. The edge cracking and spalling of brittle plates. Acta Metallurgica, 35:1333–1341, 1987. doi: 10.1016/0001-6160(87)90015-0.

[14] Labra C., Rojek J., and Oñate E. Discrete/Finite Element Modelling of Rock Cutting with a TBM Disc Cutter. Rock Mechanics and Rock Engineering, 50, 2016. doi: 10.1007/s00603-016-1133-7.

[15] Menezes P. Influence of rock mechanical properties and rake angle on the formation of rock fragments during cutting operation. The International Journal of Advanced Manufacturing Technology, 90, 2016. doi: 10.1007/s00170-016-9342-5.

[16] Helmons R. Excavation of hard deposits and rocks, on the cutting of saturated rock. PhD thesis, 2017.

[17] Sivakumar G. and Maji V. Simulation of crack propagation in rocks by XFEM. 2016. doi: 10.2991/rare-16.2016.46.

[18] Mohammadnejad M., Liu H., Dehkhoda S., and Chan A. Numerical Investigation of Dynamic Rock Fragmentation in Mechanical Cutting Using Combined FEM/DEM. 2017.

[19] Nikolic M., Roje-Bonacci T., and Ibrahimbegović A. Overview of the numerical methods for the modelling of rock mechanics problems. Technical Gazette, Scientific-professional Journal of Technical Faculties of University in Osijek, 23:627–637, 2016. doi: 10.17559/TV-20140521084228.

[20] DEM Solutions Ltd. EDEM 2018.

[21] Edinborough University. Courtesy of EDEM technical overview. URL http://demlateralearthpressure.weebly.com/contact-models.html.

[22] Brown N.J. Discrete element modelling of cementitious materials, 2013.

[23] Chen G., Schott D., and Lodewijks G. Tensile test simulation of high-carbon steel by discrete element method. Engineering computations, 33:1224–1245, 2016. doi: 10.1108/EC-03-2015-0064.

[24] Przemieniecki J. Theory of matrix structural analysis. SERBIULA (sistema Librum 2.0), 2019.

[25] Coll A., Ribó R., Pasenau M., Escolano E., Perez J., Melendo A., Monros A., and Gárate J. GiD v.13 reference manual, 2016.

[26] Yenigul N.B. and Alvarez Grima M. Discrete element modeling of low strength rock. 2010. doi: 10.1201/b10551-38.

[27] Potyondy D. and Cundall P.A. A bonded-particle model for rock, 2004.

[28] Rojek J., Oñate E., Labra C., and Kargl H. Discrete element simulation of rock cutting. International Journal of Rock Mechanics and Mining Sciences, 48:996–1010, 2011. doi: 10.1016/j.ijrmms.2011.06.003.

[29] Dehkhoda S. and Detournay E. Rock cutting with an actuated disc: an experimental study. 2018.

[30] Deresiewicz H. and Mindlin R.D. Elastic spheres in contact under varying oblique forces. 1952.

[31] DEM Solutions Ltd. EDEM 2.6 Theory reference guide. 2014.

A

Hertz-Mindlin contact model

Below the formulas for the different components of the Hertz-Mindlin [30] contact model which is available in EDEM are explained [31]. First, the formula for the normal force of the contact model and the corresponding normal damping is shown. Afterwards, the tangential force of the contact model and the corresponding normal damping is shown. Lastly, the rolling friction term applied to the Hertz-Mindlin contact model is shown.

$$F_n = \frac{4}{3} E \sqrt{R} \sigma_n^{\frac{2}{3}} \tag{A.1}$$

where, Fn is the normal force, E is equivalent Young's modulus, R is the equivalent radius, σ_n is the normal overlap

$$F_n^d = -2\sqrt{\frac{5}{6}} \beta * \sqrt{S_n m v_n^{rel}} \tag{A.2}$$

where, F_n^d is the normal damping force, β is the damping coefficient, S_n is the normal stiffness, n^{rel} is the normal component of the relative velocity, m is the equivalent mass

$$F_t = -\sigma_t S_t \tag{A.3}$$

where, Ft is the tangential force, S_t is the tangential stiffness, σ_t is the tangential overlap

$$F_t^d = -2\sqrt{\frac{5}{6}} \beta * \sqrt{S_t m v_t^{rel}} \tag{A.4}$$

where, F_t^d is the tangential damping force, t^{rel} is the tangential component of the relative velocity

The tangential force can't be higher than the Coulomb (static)friction force

The rolling friction is applied by adding a torque to the contact surfaces

$$\tau_r = -\mu_r F_n * R_i \omega_i \tag{A.5}$$

where, τ_r is the rolling friction torque, μ_r is the coefficient of rolling friction, ω_i is the unit angular velocity vector at contact point, R_i is the distance from the contact point to centre of mass

B

Bond failure envelope for different eccentricities

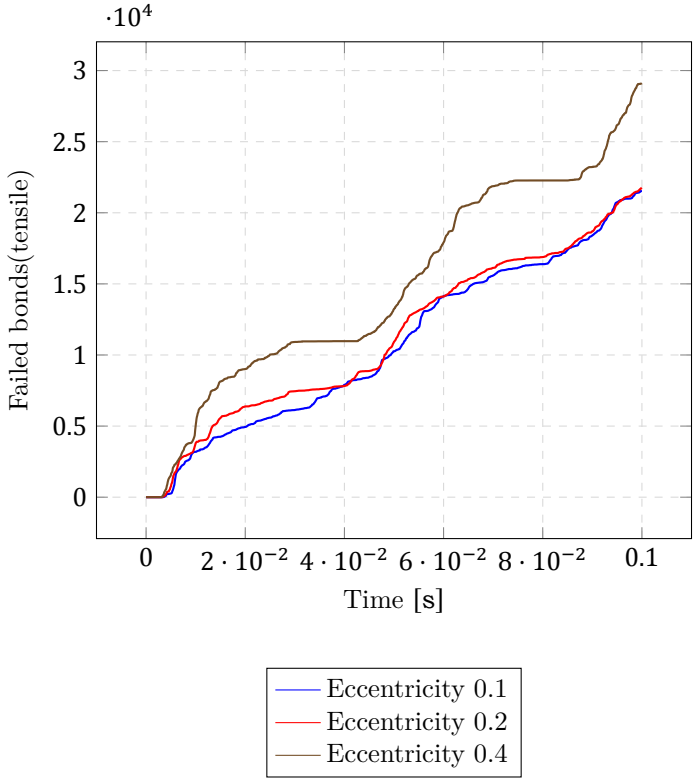

Figure B.1: Tensile bond failure(Shear bond failure is negligible and therefore discarded in the graph), disc radius is 10mm, disc forward speed is 0.5m/s, oscillation speed is 1350 rpm, clearance angle 9 degrees

C

Forces ODC Simulations

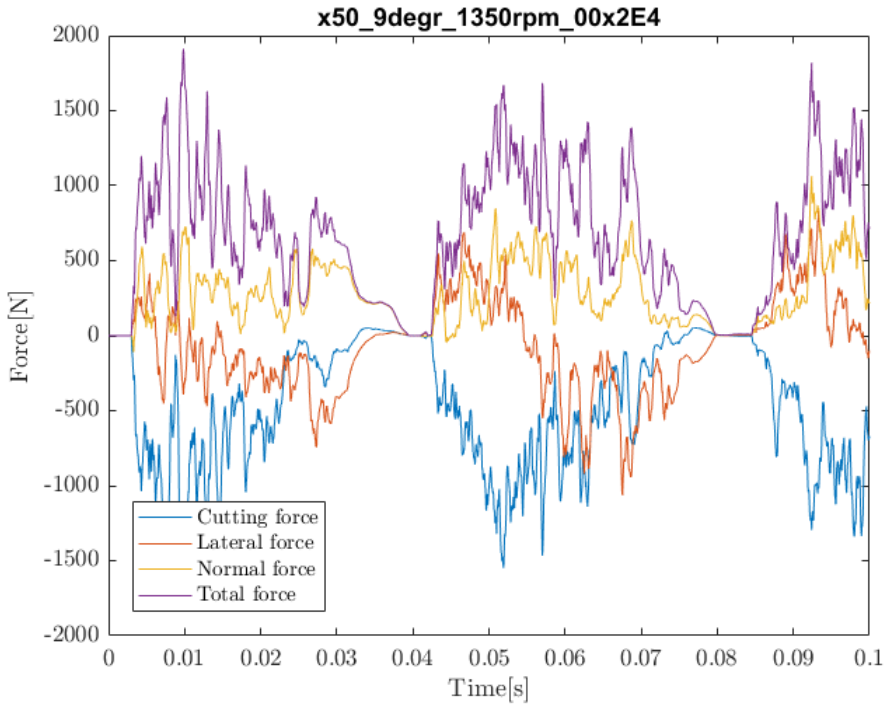

Figure C.1: Disc radius is 10mm, disc forward velocity is 0.5m/s, oscillation speed is 1350 rpm, clearance angle 9 degrees and eccentricity is 0.4

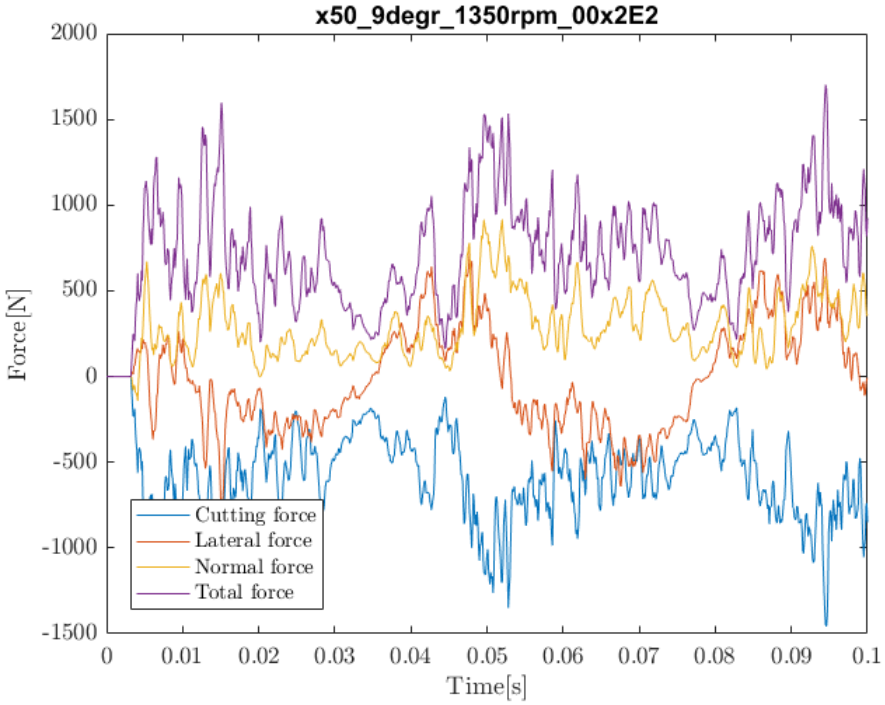

Figure C.2: Disc radius is 10mm, disc forward velocity is 0.5m/s, oscillation speed is 1350 rpm, clearance angle 9 degrees and eccentricity is 0.2

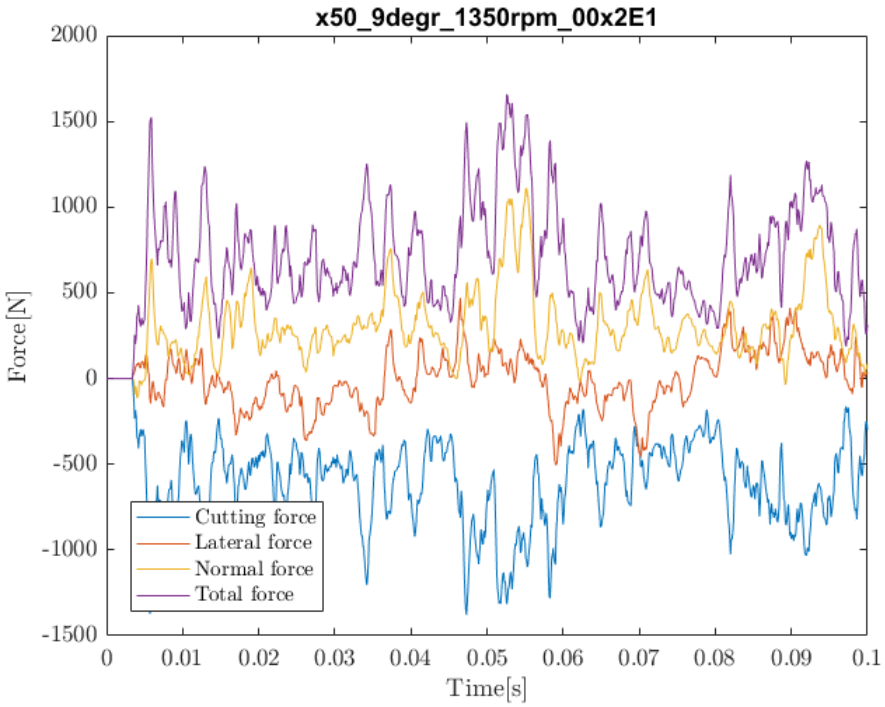

Figure C.3: Disc radius is 10mm, disc forward velocity is 0.5m/s, oscillation speed is 1350 rpm, clearance angle 9 degrees and eccentricity is 0.1

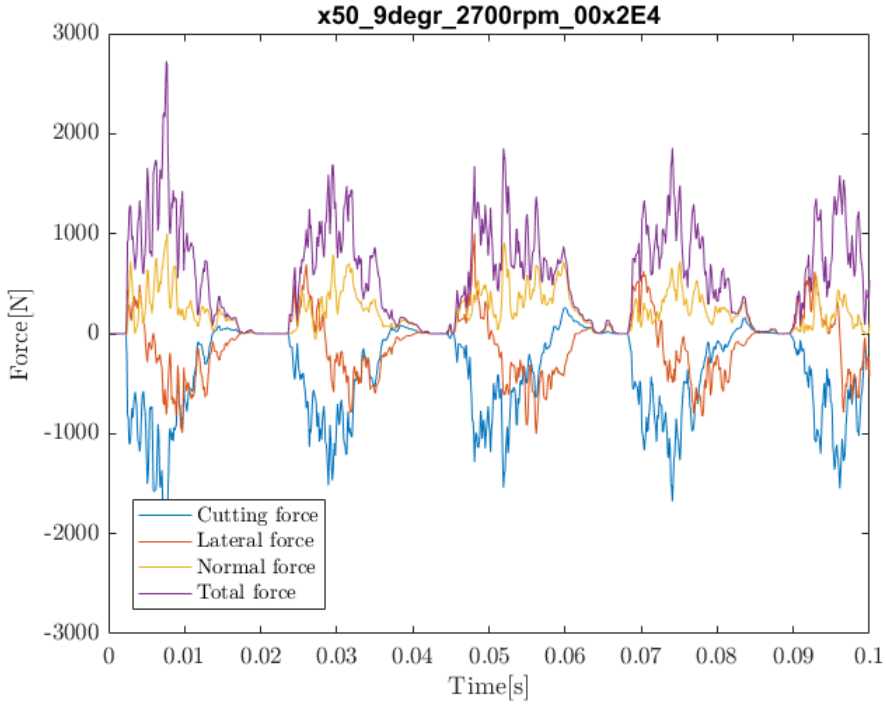

Figure C.4: Disc radius is 10mm, disc forward velocity is 0.5m/s, oscillation speed is 2700 rpm, clearance angle 9 degrees and eccentricity is 0.4

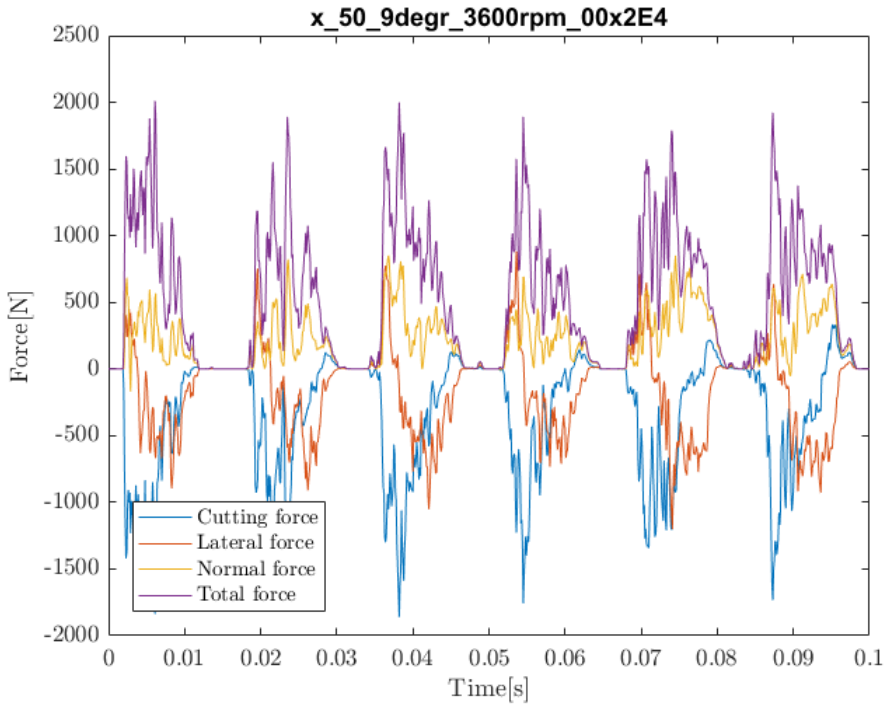

Figure C.5: Disc radius is 10mm, disc forward velocity is 0.5m/s, oscillation speed is 3600 rpm, clearance angle 9 degrees and eccentricity is 0.4

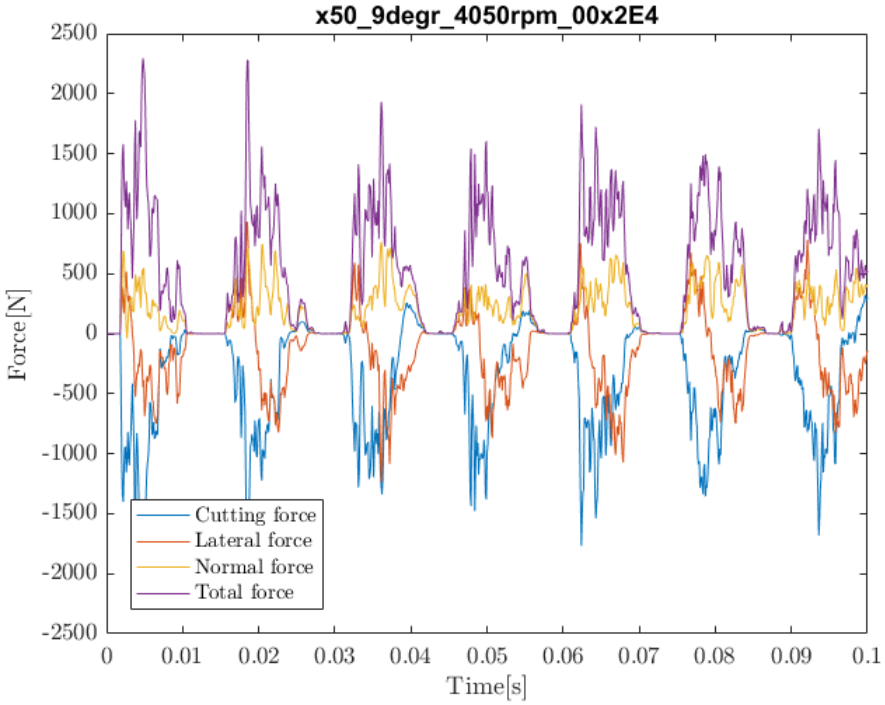

Figure C.6: Disc radius is 10mm, disc forward velocity is 0.5m/s, oscillation speed is 4050 rpm, clearance angle 9 degrees and eccentricity is 0.4

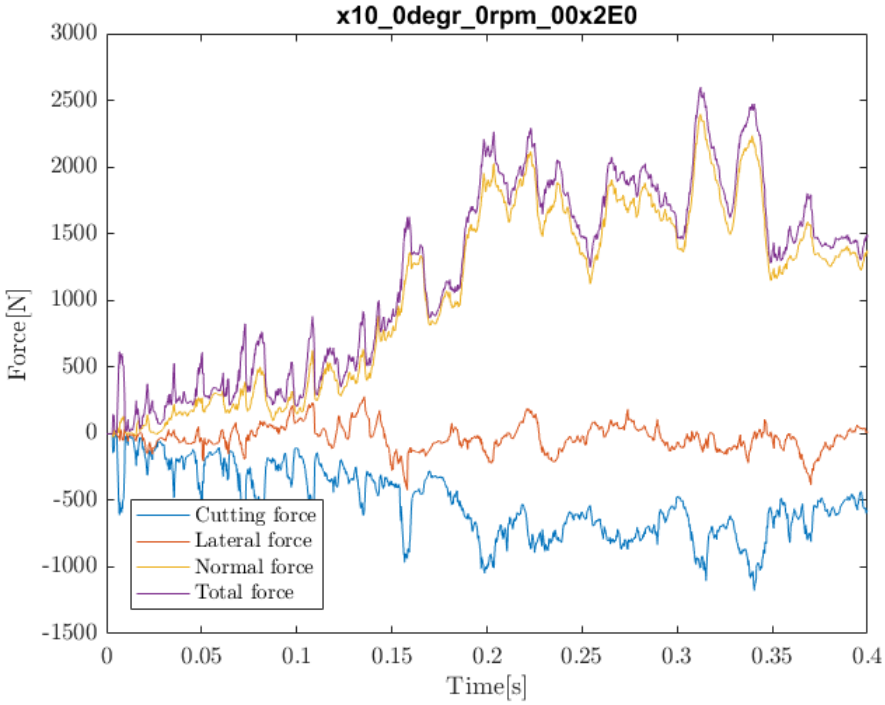

Figure C.7: Disc radius is 10mm, disc forward velocity is 0.1m/s, oscillation speed is 0 rpm, clearance angle 0 degrees and eccentricity is 0.0

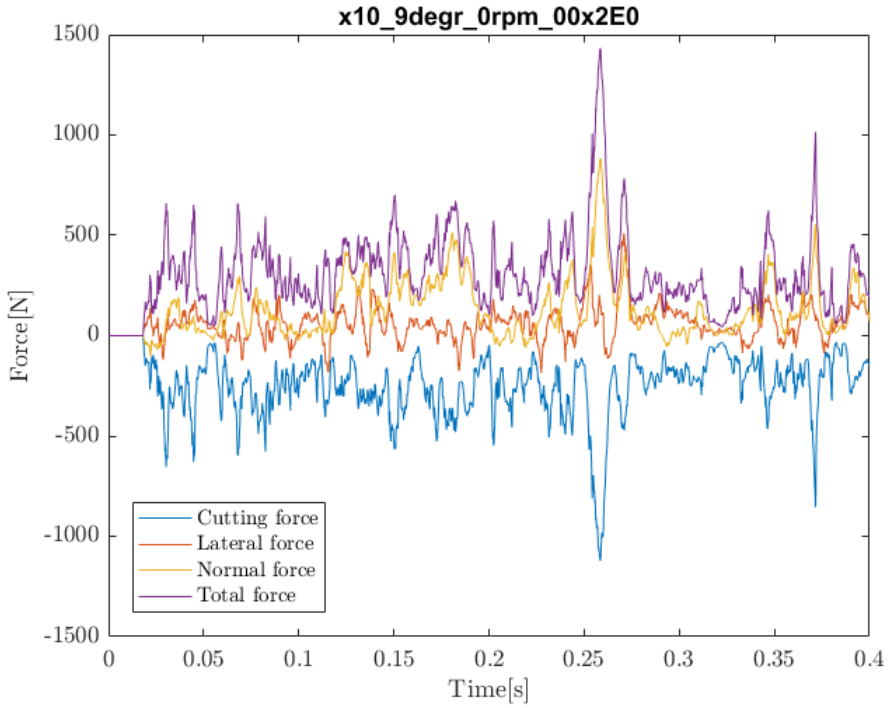

Figure C.8: Disc radius is 10mm, disc forward velocity is 0.1m/s, oscillation speed is 0 rpm, clearance angle 9 degrees and eccentricity is 0.0

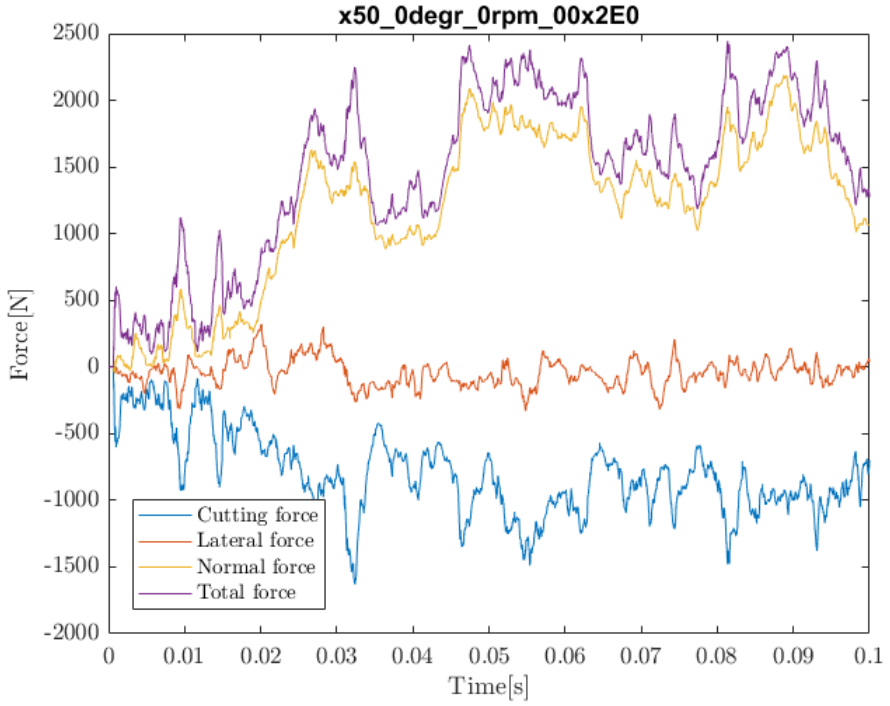

Figure C.9: Disc radius is 10mm, disc forward velocity is 0.5m/s, oscillation speed is 0 rpm, clearance angle 0 degrees and eccentricity is 0.0

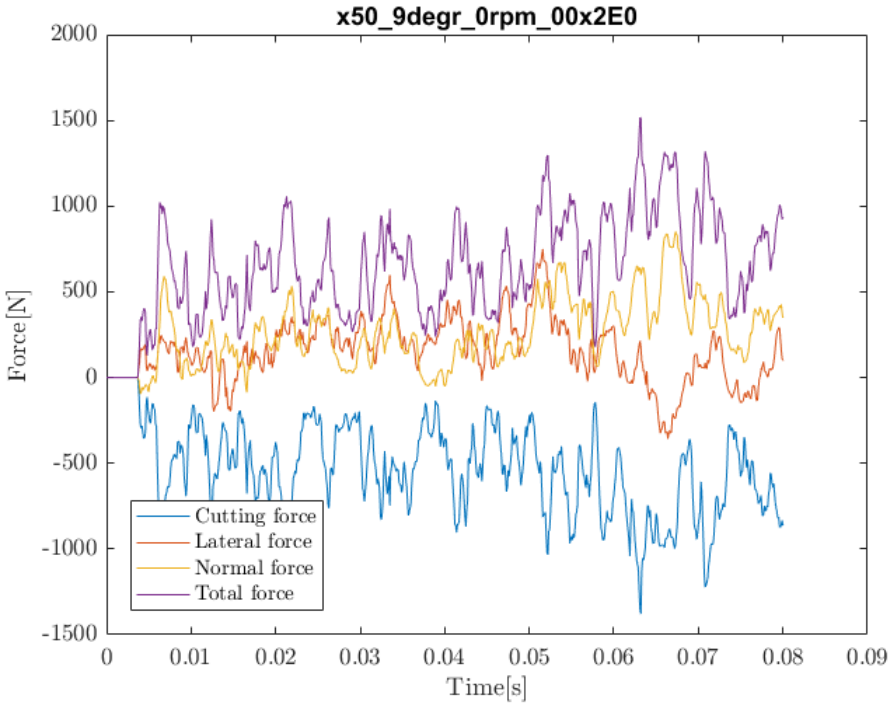

Figure C.10: Disc radius is 10mm, disc forward velocity is 0.5m/s, oscillation speed is 0 rpm, clearance angle 9 degrees and eccentricity is 0.0

D

Comparison of model prediction with experiments, Detournay and Dehkhoda

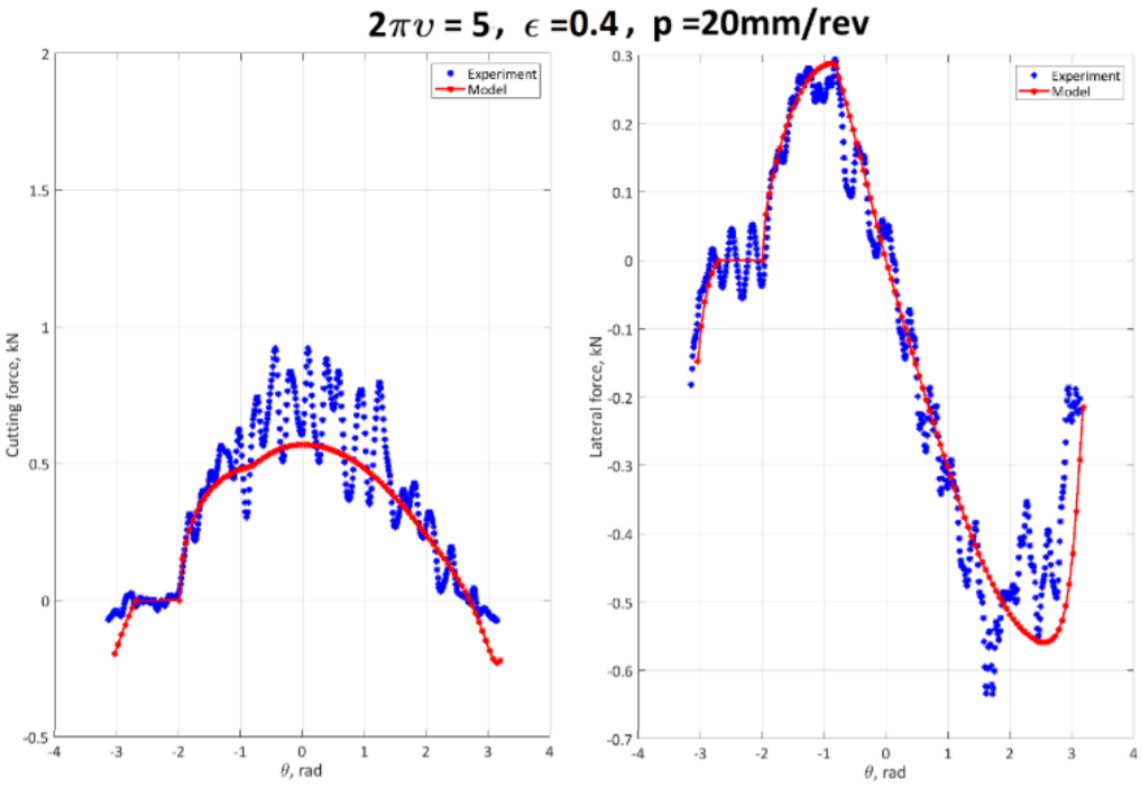

Figure D.1: Comparison of model prediction Detournay and Dehkhoda with experiments [29]

E

Acknowledgements

My work on this thesis started in March 2018 at Royal IHC. At first, the goal of this research was to create a test set-up and perform experimental tests. This gradually shifted into creating a numerical model to simulate an oscillating rock cutting tool (oscillating disc cutter). I am very proud to present you this thesis in which, I hope, to give more insight in the oscillating disc cutter and the suitability of DEM to simulate oscillating cutting tools.

This would not have been possible without the support I received. I first of all would like to thank IHC MTI for giving me the opportunity to graduate and provide the required tools for this research. The supervisors from MTI, I would like to thank for the guidance and feedback during the project meetings. A special thanks to my daily supervisor from the TU Delft, Rudy Helmons, for guiding me during the thesis and helping me gain a better understanding of discrete element modelling for solid granular materials (rock). Also, I want to thank the remaining supervisors for helping me to bring more structure towards the thesis report. Furthermore, I wish to thank the students at IHC MTI and the EDEM group at the TU Delft for the useful discussions and relaxing coffee breaks.

I am very grateful for the support and encouragement I received from my family during my graduation.